TRANSPORT AND MAGNETIC PROPERTIES OF Co-RICH AMORPHOUS FERROMAGNETIC ALLOYS CONTAINING Cr/Mn

By

AMITABH DAS

DEPARTMENT OF PHYSICS

INDIAN INSTITUTE OF TECHNOLOGY KANPUR

MAY, 1992

TRANSPORT AND MAGNETIC PROPERTIES OF Co-RICH AMORPHOUS FERROMAGNETIC ALLOYS CONTAINING Cr/Mn

A Thesis Submitted
In Partial Fulfilment of the Requirements
for the Degree of

DOCTOR OF PHILOSOPHY

By

AMITABH DAS

to the

DEPARTMENT OF PHYSICS

INDIAN INSTITUTE OF TECHNOLOGY KANPUR

MAY, 1992

PHY-1995-D-DAS-TRA

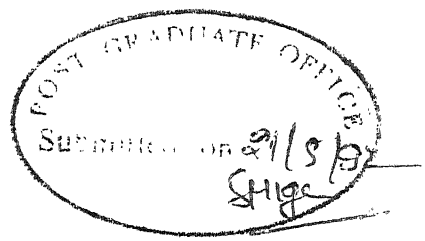

CERTIFICATE

It is certified that the work contained in the thesis entitled "**TRANSPORT AND MAGNETIC PROPERTIES OF Co-RICH AMORPHOUS FERROMAGNETIC ALLOYS CONTAINING Cr/Mn**" by **Amitabh Das** has been carried out under my supervision. This work has not been submitted elsewhere for a degree.

May, 1992

Alak Kumar Majumdar

(Alak Kumar Majumdar)
Professor
Department of Physics
I.I.T., KANPUR, INDIA

Synopsis

Name of Student : AMITABH DAS Roll No. 8520962

Degree for which submitted : Ph.D., Department of Physics

Thesis Title : **TRANSPORT AND MAGNETIC PROPERTIES OF Co-RICH AMORPHOUS FERROMAGNETIC ALLOYS CONTAINING Cr / Mn.**

Thesis Supervisor : Dr. A.K. Majumdar, Professor of Physics, Indian Institute of Technology, Kanpur 208016, India.

Month and year of thesis submission : May 1992

Dc electrical resistivity, magnetoresistance, dc and ac magnetization, ac susceptibility, critical exponents, and crystallization studies have been made on a series of amorphous alloys $Fe_5Co_{50}Ni_{17-x}Cr_xB_{16}Si_{12}$ (x = 0, 5, 10, and 15 designated as A1, A2, A3, and A4), $Fe_5Co_{50}Mn_{17}B_{16}Si_{12}$ (A5), and $Fe_{7.8}Co_{31.2}Ni_{24}Mn_{15}B_{14}Si_8$ (B5) prepared by the melt-quenching technique. The samples are in the form of ribbons and are ferromagnetic with T_C lying between 170 and 400 K. The motivation behind the experiments are to study the following:

Resistivity minimum at low temperatures is a characteristic feature of amorphous alloys irrespective of their magnetic state. It is found that the introduction of Cr or Mn in these alloys shifts the minima from $\cong$ 20 K to $\geq$ 200 K. Earlier, the region below the minima was explained on the basis of either the Kondo model or the two-level states. The temperature dependence of resistivity given by these models is of the same form, -ln T, although the origin of the minima is ascribed to totally different

mechanisms. One is magnetic and the other is structural in nature, respectively. We find that the resistivity, as a function of temperature, does not fit into the -lnT expression satisfactorily. It is now observed that the resistivity minima in many nonmagnetic amorphous alloys with resistivity minima at high temperatures and magnetic alloys with minima at low temperatures are better described by the models based on electron localization and interaction theories. We have made an attempt here to explain the resistivity minima observed at high temperatures (T ≅ 200 K) and in a ferromagnetic system on the basis of these models. We also included magnetic effects.

In the region above the resistivity minima in ferromagnetic systems, it is now widely recognized that the electron-phonon interaction alone, without taking into account the magnetic state of the alloy, does not describe the resistivity behavior. Therefore, additional terms ascribed to magnetic scattering, which are of the form $T^{3/2}$ or T^{2} are to be incorporated. Theoretically, the leading term is $T^{3/2}$ but the experimental results indicate that it can be of either form. With this background we have analyzed the region above the minima.

The ferromagnetic anisotropy of resistance (FAR), obtained from magnetoresistance measurements, is discussed in terms of the two-current conduction model. Introduction of Cr results in a positive high-field slope (1/R dR/dH) at all temperatures. This feature is in contrast to the negative slope normally observed in ferromagnets. The numerical values of the slopes are also compared with the prediction of the model based on electron localization

and interaction effects. Magnetoresistance measurements have also been made on the mixed phase alloys (Mn-containing A5 and B5) to identify the presence of long-range order in these alloys.

Low-field ac susceptibility (χ_{ac}) has been done to study the low-temperature phase of the samples. The presence of Cr and Mn in these alloys gives rise to competing interactions which are essential towards the formation of spin-glass-like phases at low temperatures.

The variation of the magnetic moment, as a function of Cr and Mn concentration, is discussed on the basis of the virtual bound states and the charge transfer model. The modes of thermal demagnetization are analyzed from the M(T) data. Necessity of terms in addition to the $T^{3/2}$, in the form of $T^{5/2}$ or Stoner single-particle excitations, is discussed. The variations of the spin-wave stiffness constant with T_c and Cr concentration are also found.

The influence of disorder, both topological and compositional, is easier to study with amorphous materials. It is found that the topological disorder does not have any significant effect on the exponents. But in the presence of Cr and/or Mn, the critical exponents are different from those predicted by the 3D Heisenberg model, viz., $\gamma \rightarrow 2$, and $\delta \rightarrow 5$. Here we study the effect of Cr on the critical exponents measured by ac and dc magnetization techniques.

Chapter I of the thesis serves as an introduction to the subject. It includes a brief literature survey of the topics of study, the motivation behind the present work, and the basic

theoretical background.

In chapter II, the details of the experimental techniques used are given. The dc electrical resistivity are measured by the standard four-probe method between temperatures 8 and 300 K. The set-up consists of a 7 1/2 digit multimeter, a temperature controller, and a closed-cycle helium refrigerator. The data obtained were stable up to a few parts in 10^{6}. A similar set-up was used for magnetoresistance measurements along with an electromagnet which could provide fields up to 17 kOe. The ac susceptibility measurements between 16 and 300 K were done using a closed-cycle helium refrigerator, a locally made mutual-inductance bridge, and a lock-in amplifier. Suitable coils were made to reduce the effect of the demagnetization factor and they were placed inside the cryostat. The operating frequency was 3.33 kHz and the measuring rms field was 0.1 Oe. For the measurement of critical exponents, since the transition regions were well above 77 K, a separate double-walled glass cryostat was made. The coils were wound coaxially on top of the cryostat and were kept immersed in liquid nitrogen. The temperature was sensed by a copper-constantan thermocouple placed very close to the sample. The data were taken while slowly heating the sample and by this arrangement it was possible to obtain data every 30 mK apart. The dc magnetization measurements between 19 and 300 K were made with a set-up consisting of a closed-cycle helium refrigerator, a vibrating sample magnetometer (VSM), and a temperature controller. The high-temperature magnetization measurements were done using a separate oven assembly along with the VSM in the presence of the

residual field of the electromagnet.

The results and discussion are compiled in chapter III. The absolute values of resistivity of A1 - A4 are ≥ 150 $\mu\Omega$cm and they increase with the increase in Cr. The resistance minimum in A1 is at 15 K which shifts to 200 K and above on substituting Cr or Mn (A2-A5). The depths of the minima are roughly about 1 % . In sample A1, in the region above T_{min}, there is a clear evidence of the magnetic term $\propto T^2$, in addition to the structural term. The coefficients of the structural and the magnetic terms match with the published experimental results on other amorphous ferromagnetic systems. The region below T_{min}, in sample A2-A5, is analyzed on the basis of electron-electron interaction and localization effects. By the method of least-squares fit analysis, we obtained three distinct regions where the conductivity ($\Delta\sigma = \sigma(T)-\sigma(0)$) varies as $T^{1/2}$, T, and $T^{1/2}$ at low, intermediate, and high temperatures, respectively in agreement with the predictions of the theory. The magnetic scattering seems to contribute very little below T_{min}. The numerical values of the density of states at the Fermi level and the diffusion constant are obtained from this analysis and they compare well with the results reported in other systems.

The magnetoresistance (MR) behavior of the samples A1-A5 and B5 exhibits identical results in both the transverse ($\vec{J} \perp \vec{M}$) and the longitudinal ($\vec{J} \parallel \vec{M}$) directions. The ferromagnetic anisotropy of resistance (FAR) is positive and is about an order of magnitude small compared to that of the Fe-B series. A correlation between the magnetization and the FAR is obtained which shows that the FAR

decreases with the average magnetic moment/atom ($\bar{\mu}$). Using the expression of Campbell et al. [$\Delta\rho/\rho = \gamma(\alpha-1)$, where $\alpha = \rho_{\downarrow}/\rho_{\uparrow}$, $\rho_{\uparrow}$ and $\rho_{\downarrow}$ are the residual resistivities for the spin-up and spin-down electrons respectively], the value of α is calculated to be 1 which means $\rho_{\downarrow} \sim \rho_{\uparrow}$. This implies that holes exist in both the spin-up and spin-down bands and this is an indication of a weak ferromagnet. However, this result is not in agreement with the conclusion drawn from the high-field slope measurements. The FAR decreases with increase in temperature and vanishes at the respective T_c's and is understood on the basis of the increase in the thermal fluctuations which compete with the exchange splitting. As a result, the two sub-band occupations tend to equalize resulting in a fall in α. The slopes ($1/\rho\ d\rho/dH$) of A1, A5, and B5 are negative whereas the Cr-containing samples (A2-A4) have positive slope. The slopes of A2-A4 are large and are comparable to those of the other amorphous materials and positive at all temperatures. The MR curves are not strictly linear and are best described by the equation of the form $\Delta\rho/\rho = a + bH + cH^2$. The ratio of $c/b \cong 10^{-2}$. The plot of $\Delta\rho/\rho$ versus T/T_c, at a given field, shows a pronounced peak at their respective T_c's. This result is identical to those of the rare-earth containing amorphous materials and therefore an attempt has been made to understand this observation on the basis of exchange-scattering model by Asomoza, Bhattacharjee and Coqblin. The negative slope in A1, A5, and B5 is understood, in terms of the localized model, to be due to the result of a reduction in the number of magnons as the field is raised. The magnon number also decreases with the

decrease in temperature and therefore in the ferromagnetic regime, the magnitude of the slope is expected to decrease with the lowering of temperature which is in agreement with our observations. An attempt has been made to compare the MR effect of samples A2-A4 with the predictions of the electron-electron interaction and the localization effects in the presence of the spin-orbit coupling. The expressions used in these theories are modified by replacing the applied field H by an effective field $H_{eff} = H_{int} + H$, where H_{int} is the internal field of a ferromagnet and is of the order of 5Ø T. Since $H \ll H_{int}$, the MR expression reduced to give $\Delta\rho/\rho^2 \propto H$. A reasonably good agreement is obtained between the theory and the experiment when this correction is incorporated. This approach, also found to be valid in Fe-Cr-B alloys, could explain the positive MR observed in these alloys.

In samples A5 and B5, the FAR below $\cong$ 6Ø K becomes nearly constant. The magnitude of the slope increases. This behavior is unlike that observed in normal ferromagnets where, as we lower the temperature, the FAR increases and the magnitude of the slope tends to zero. This is interpreted as an indication for the onset of partial breakdown of long-range order, confirmed also from χ_{ac} measurements. However, there éxists long-range order even down to 11 K as the FAR gives a non-zero value. The magnetic phase below 3Ø K resembles the mixed phase as envisaged in the Gabay-Toulouse model where both the long-range order and the spin-glass phase coexist. Signatures of the spin-glass phase are obtained from the low-field dc magnetization and time dependence of magnetization.

The magnetic moment and the T_c decrease identically with the

addition of Cr. The variation of the magnetic moment with the addition of Cr and Mn is discussed on the basis of various models. We find that the rate of change of magnetic moment with Cr concentration $\xi = d\mu/dx \approx -1$. The fall in μ, however, could not be described by the 'virtual bound state' model which gives $\bar{\mu} = \mu - (Z + 10)\, c\mu_B$, where z is the valence difference between the solute and the host. We obtain $z = -9$ whereas actually it is about -3.5. The calculation, based on the charge transfer model, does reproduce the observed average $\bar{\mu}$ (0.5 μ_B/atom). The calculation further yields $\mu_{Cr} = -0.83$, -0.59, and -0.45 for A2, A3, and A4, respectively. We also find that on replacing Ni with Mn, $\bar{\mu}$ increases. Similar calculation yields $\mu_{Mn} = 1.48\ \mu_B$. This result is thought to arise from strong ferromagnetic interaction between Mn and Co which overcomes the Mn-Mn nearest neighbor antiferromagnetic interaction. Spin-wave analysis is extended up to $0.5T_C$. Bloch's $T^{3/2}$ law adequately describes the temperature dependence of the magnetization in Cr-containing samples. The calculated spin-wave stiffness constant, D, decreases with the increase in Cr. In A5 and B5, additional terms in the form of $T^{5/2}$ is found necessary. The results of the fit on including the Stoner single-particle excitations are discussed. The value of D scales with T_C and the ratio $D/T_C \approx 0.27$ meV A^2/K. When the value of D is extrapolated to $T_C = 0$, within experimental error, it is found to pass through the origin. This result is discussed on the basis of the Heisenberg model.

The values of β_{eff}, γ_{eff}, and δ_{eff} for the alloys with x = 5 and 10, in the asymptotic critical region, agree with those of the

other amorphous materials and are consistent with the predictions of the 3D Heisenberg model. In contrast, for the sample with x=15, the effective value of the exponent β (Ø.52) and γ (1.79) are significantly larger while δ (4.45) remains the same. The difference is ascribed to the formation of magnetic clusters with the addition of Cr which leads to the non-divergence of the correlation function at T_c and consequently a different set of exponent values is found. Further, these results strengthen the conclusion that there is no influence of topological disorder on the values of the exponents in the critical region.

The crystallization study shows that the nature of the crystallized phase changes significantly with the replacement of Ni by Cr. The crystallization temperature increases with the addition of Cr. The major phase which crystallizes in A1 is cubic Co. In sample A3, distinct appearance of Co_2Si is observed. In A4, the final phase is paramagnetic and consists mostly of Cr_3Co_5Si and Co_2Si.

In chapter IV, the conclusions are summarized and the scope of future work is discussed.

Acknowledgments

I was not sure, seven years back, when I first resolved to do a Ph.D, about the prospects, the difficulties etc., that I would encounter during/after the course. Hailing from family with an ordinary background and from an equally remote area in this country, the decision to leave a simple but secure job and do this 'elitist' course was formidable and more influenced by my parents wishes. Looking back, now I realize that their wishful thinking at that point of time, has done a world of good for me.

It is a pure chance that I find myself in this institute and much more importantly in the present laboratory. During the stay I have had the opportunity to come across several fine persons, in the form of teachers and friends, whose memories would be close to my heart long long after I leave the boundaries of this campus. In particular,

- my thesis supervisor, an acknowledged good teacher and expert, approachable, very communicative, open to ideas and suggestions, and overall very encouraging. These features, collectively, in my opinion, have gone a long way in instilling confidence and drawing me away from the initial 'pertubative' stage of stay in this campus. His expertise in the current area of study and ever willingness to help on all fronts was largely responsible in the completion of this thesis. My association with him starts at a period when this lab was in a state of transition from liquid helium based experiments to closed-cycle- helium refrigerators. It is coincident that now it is again so, in the process of installation of a new, compact liquid helium plant and switching

back to liquid helium based experiments. I have benefited immensely, to say the least, academically and otherwise being his student and working towards this thesis and other related problems.

All of us, his students, enjoyed every bit at his residence, over imaginatively prepared food and after dinner talk. Both he and Mrs. S. Mazumdar are very fine hosts and I for one always look forward to such occasions.

The initial period was the time when high temperature superconductors had hit the scene. I had toyed with the idea of working in this area for my thesis but finally gave up because of the volume and nature of work going on elsewhere far outpaced ours. During that period working with Prof. K.P. Gupta and Dr. D. Bahadur was very beneficial.

Prof. R.K. Ray and Prof. T.M. Srinivasan gave invaluable suggestions particularly in the fabrication of experimental set up.

I am grateful to Dr. P. Nagy, Hungarian Academy of Science, Budapest, for providing the full batch of samples to carry out this work.

It was a rich experience to share the lab and work with

Dr. A. Banerjee - very confident in everything he was doing, a feature I secretly admired in him.

Dr. A. Mitra - a brief but very productive encounter with him.

Dr. Rita Singhal - my better half, during the course we decided to share the sorrows and joys in life in unison.

And a group of young, intelligent, and very enthusiastic juniors, Swapan Chakroborty, Tapan K. Nath, Gautam Sinha, and N. Sudhakar.

Help was always forthcoming from Mr. D.C. Banerjee and Mr. Ram Prakash Pal in the day to day functioning of the lab.

During the various stages of work I also received full support from the technical personnel in liquid nitrogen plant, physics workshop, and physics office.

A handful of friends Subir Bhowmik, Arun K. Mishra, Aniruddha Mukhopadhyay, S.S.A. Razee, Amit Sircar, and Pinaki Sengupta whose company I will forever relish.

It is an irony that my country invests so much money in basic science research which are and would be of no relevance, in foreseeable future, in meeting the immediate requirements of the country; drinking water, food, medicine, and shelter which millions of my countrymen are deprived of and look upon as a luxury. I am and will forever be grateful to the mute millions for supporting me and my ilks and asking nothing in return.

To

My Parents

CONTENT

LIST OF FIGURES

LIST OF TABLES

CHAPTER I
INTRODUCTION

1.1 Brief Review

A. Electrical Resistivity

The resistivity behavior of metallic glasses is one of the most widely and extensively studied topics. A number of relatively recent review articles in this area summarize the large volume of experimental data [1-4]. The main characteristic features which are representative of the transition metal-metalloid type of alloys are:

(i) High resistivity values (ρ > 100 $\mu\Omega$cm) which implies that the mean free path is of the order of interatomic distance.

(ii) Small temperature coefficient of resistance (TCR = α = $1/\rho$ $d\rho/dT$) at room temperature which changes with composition.

(iii) Resistivity minima at low temperatures.

An analysis by Mooij [5], based on the study of amorphous and crystalline materials, arrived at a correlation between the magnitude of the resistivity and the TCR. It was proposed that if ρ of an alloy exceeds 150 $\mu\Omega$cm, then it would exhibit a negative TCR independent of it being crystalline or amorphous or in liquid state. In the review by Mizutani [1] , the correlation between ρ and α is shown to hold good for high resistivity alloys. Mott [6] suggested that the presence of d-band holes is responsible for the high resistivity and the negative α may arise from the broadening of Fermi level. Nagel [7] argued that the sign of α is independent of the structure factor. Cote and Meisel [3] also reached at a similar conclusion but proved that the sign of α can be solely

determined from the expansion of the Debye-Waller factor and is independent of the position of $2k_F/k_P$, where k_P is the position of the main peak in the structure factor S(k). However, a survey of Mooij's analysis [8] has revealed that the above condition is based upon insufficient number of data points. In effect, there is no single universal value of ρ (which is shown to vary between 30 to 400 $\mu\Omega$cm) and that the correlation between α and ρ is nonuniversal, contrary to the original suggestion of Mooij. It is assumed that the nonuniversality has its origin in electron localization effects which play a major role in determining the sign of the TCR in 3d disordered materials.

Temperature dependence of resistance

It is observed that the low value of α and the high value of ρ are the characteristics of the amorphous phase. In one of the early experiments, reported [9] on metglasses 2826 and 2826A, it is found that a drastic change occurs in the magnitude of both α and ρ upon crystallization. Also, the value of ρ in the crystallized phase is considerably less ($\simeq$ 70 $\mu\Omega$cm) than that in the amorphous phase and the value of α is large, similar to that observed in crystalline materials.

A resistance minimum is invariably observed in these metallic glasses, independent of its magnetic state, often at rather low temperatures ($\sim$ 10 K). The resistivity minimum has been a subject of controversy, especially its possible origin. We would emphasize this later in the text. In the region above the minimum the resistance varies with temperature quadratically at low

temperatures (T < 5Ø K) and linearly near room temperature. The suggested explanations for these common characteristics include the localized spin fluctuations [1Ø], Mott s-d scattering [11] and the generalized Ziman theory [12-15]. The generalized Ziman theory, also known as the diffraction model, has taken into account the scattering of electrons by the ion cores that carry a muffin-tin potential and also the change in the shape of the structure factor S(k) as T is varied [3,16]. All these theories reproduce the experimentally observed [1,17-2Ø] T^2 behavior at low temperatures and linear in T at higher temperatures.

In crystalline ferromagnets the interaction of the conduction electrons with the magnons of the localized spin system at low temperatures gives rise to a T^2 dependence of ρ_{mag} [21-23]. Since most of the alloys were ferromagnetic in the region of temperature where resistivity analysis was done and they supported spin waves, it was expected that an evidence of the electron-magnon scattering might be found. One group of experimental results infers that the magnetic term is proportional to T^2 [24-27] and the other $T^{3/2}$ [28-32]. Though a clear consensus on the exponent of temperature dependence (whether it is 2 or 1.5) of $\rho_{mag}(T)$ has not been arrived at experimentally, nevertheless, these reports show a clear necessity of magnetic terms over and above the electron-phonon term. This result also reveals the general inadequacy of the diffraction model. The magnitude of the T^2 coefficient, observed in amorphous ferromagnets, agrees well with those found in crystalline ferromagnets (Fe, Co, Ni and their alloys) [33-34]. From this agreement it is concluded that the

quenched disorder does not practically influence the coherent electron-magnon scattering contribution to ρ [25]. Further, there are other reports [35] that $\rho_{mag}(T)$ does not contribute at all. Theoretically, a model based on a structurally disordered Heisenberg ferromagnet predicts that the spin-disorder resistivity varies as $T^{3/2}$ [36].

The existence of a term ascribed to ferromagnetic order is very much in evidence from the published experimental results. This term is of the form T^2 or $T^{3/2}$. We study this behavior in one of the alloys having $T_c \simeq 400$ K and $T_{min} \simeq 20$ K in order to find the temperature dependence of the magnetic term. We find a clear necessity of a term of the form T^2 over and above the electron-phonon term as predicted by the diffraction model. We relate the observed T^2 term with the magnetic contribution which is in agreement with some of the experimental results but in contradiction to the theoretically predicted $T^{3/2}$ as the leading magnetic term.

Resistivity Minimum

The interpretation of resistivity minimum in amorphous materials has been a controversy-ridden subject and is of immense interest as to the nature of interactions responsible for this minimum. In the early reports, in the region below the minimum, it was concluded that $\rho(T)$ varies as -lnT. A lnT dependence of ρ is a characteristic signature of Kondo phenomenon [37] observed in dilute magnetic alloys. In terms of Kondo theory, a lnT dependence is a manifestation of the dynamical nature of the magnetic spin

system; in other words, the spin system needs to possess an internal degree of freedom, e.g., spin flipping to produce the lnT anomaly. How can one observe a Kondo anomaly in ferromagnets where, because of the exchange interaction, a long-range order among the spins exist. Meanwhile, Cochrane et al. [38] proposed a theory based on effects derived from the configurational indeterminacy in the atomic arrangement of amorphous alloys. The basic idea behind this theory is that there are two nearly equivalent atomic configurations which a certain number of atoms can take, e.g., represented by a double-well potential. At low temperatures, the atoms or groups of atoms tunnel back and forth between these two minima. This theory also arrives at a temperature dependence of the form $-\ln(T^2 + \Delta^2)$ where Δ is of the order of Ø.1 meV. The two theories, though practically identical in formalism, attribute the minimum to two completely different mechanisms, one to magnetic interaction and the other to structure.

The experimental results were equally confounding and made it very difficult for one to choose one in favor of the other as the following observations would show. (i) The appearance of minimum is associated with the presence of magnetic impurities, i.e., local moments. Very pure a-Pd-Si does not show a minimum. (ii) The position of minimum is dependent on the concentration of impurities. The presence of Cr and/or Mn is known to shift the position of the minimum to as high as room temperature and beyond [27,39-41]. (iii) The range in temperature of the lnT region is independent of the ferromagnetic order. (iv) The application of

magnetic fields as high as 60 kOe does not change the slope of the ρ versus lnT plots [42-43].

Sharen and Tsuei [44] put forward an argument on the basis of Mössbauer effect studies on Fe-Pd-P alloys to explain the possible existence of free spins in ferromagnetic alloys. They found that though the distribution of internal fields P(H) peaked at a high field H_o, it had a long tail below H_o which extended to zero field. In other words, there were a number of spins which experienced zero internal field and thus met the criterion for an orthodox Kondo scattering. Similar suggestions were also made, on the basis of Mössbauer studies, by Chien [45] and Wieser et al. [46]. Grest and Nagel [47] have given a theoretical justification to the existence of the tail extending to negative exchange fields. They have calculated $P(H_{eff})$ which has the properties of amorphous ferromagnets mentioned above including direct exchange, RKKY interaction and the super-exchange between next nearest-neighbor magnetic atoms separated by a metalloid atom. This explanation for the observed lnT dependence has been used by several experimental groups [39]

A new consensus seems to be emerging which suggests that the nearly-free-electron (NFE)-based models and in particular the Ziman model [12], do not appropriately describe the transport phenomena in high resistivity materials. The NFE-based models are good when the mean free path of the electron is large enough compared to the atomic spacing or to k_F^{-1} or when $k_F l \gg 1$, where k_F is the Fermi wave vector and l is the mean free path and where between scatterings, classical trajectories describe the motion.

But when $k_F l \sim 1$, interference of scattered waves from different centers takes place and, as suggested [48,49], the classical equations are inadequate. This, then, leads to the localization of the electronic wave functions [50] and the conductivity is zero at T = 0 K.

In transition metal-containing metallic glasses, resistivities are of the order of 100 $\mu\Omega$cm and greater. The mean free path, calculated from the Drude formula, is of the order of the interatomic distance. In this condition the motion of electrons between scatterings is described as 'diffusive' (diffusing from ion to ion in a random manner) rather than ballistic. This necessitates the use of theories which take into account the interference between the scattered waves, viz., the localization and interaction theories.

Due to short mean free path of the electrons, there arises two effects referred to as 'weak localization' and 'interaction effects'. The detailed theoretical treatment and the references are given in the review articles by Lee and Ramakrishnan [51] and Altshuler and Aronov [52]. This theory predicts that, in three dimensional systems, the correction term to the conductivity would have a temperature dependence of the form $\Delta\sigma$ ($\sigma(T)-\sigma(0)$) $\propto T$, $T < \theta_D/3$ and $\Delta\sigma \propto T^{1/2}$ for $T > \theta_D/3$, where θ_D is the Debye temperature, in the weak localization regime. Due to the interaction effect, at still lower temperatures, $\Delta\sigma$ varies as $T^{1/2}$. This particular form of the temperature dependence in the weak localization regime actually arises due to the inelastic electron-phonon scattering process which in this case enhances the

conductivity.

The temperature dependence of resistivity of a number of magnetic metallic glasses has been explained on the basis of the predictions of this model and is in good agreement with them (for review see [2,53]). Of late, the minimum in resistivity at low temperatures, observed in transition metal-based glasses, is identified with the onset of localization effects. Rapp et al. [54] have reanalyzed the data on a number of TM-M type alloys and concluded that a relation of the type $R = R_o(1-BT^{1/2})$ fits better than the -lnT one. The $-T^{1/2}$ dependence is interpreted in terms of the interaction theories. Similarly, other reports [24,55,56] on magnetic as well as on non-magnetic alloys show that the region below the minimum is well-described in terms of the $-T^{1/2}$ relation. Cochrane and Storm-Olsen [55] have shown that most of the metallic glasses follow the empirical rule

$$\sigma(T) - \sigma(0) = (500 \pm 100)T^{1/2}\ (\Omega m)^{-1}.$$

Thus we observe that controversy really shrouds the origin of the resistance minima which are characteristic features of most metallic glasses. Measurements and interpretations based on localization and interaction theories have only been made on nonmagnetic simple metallic glasses and ferromagnetic ones with low temperature minima. Here, we analyze our data for a series of *ferromagnetic* glasses, where by continuous Cr or Mn substitution, T_{min} could be shifted to higher temperatures. We have made an attempt to explain the results below T_{min} along lines similar to those adopted in the case of nonmagnetic glasses but included magnetic effects as well.

B. Magnetoresistance

The general features of magnetoresistance (MR) of a ferromagnet are:

(i) At low fields, a large anisotropy is found which is due to the result of spin-orbit coupling and s-d scattering [57]. The ferromagnetic anisotropy of resistance, FAR, is defined as $(\rho_{\parallel s}-\rho_{\perp s})/\rho_o$, where ρ_o is the electrical resistivity in zero internal field (H_{int}) and $\rho_{\parallel s}$ and $\rho_{\perp s}$ are the longitudinal and transverse magnetoresistivities extrapolated to $H_{int} = H_{ext} - H_{demag} = 0$. FAR is a measure of this anisotropy and is an inherent property of the alloys studied. It is large at low fields and it decreases with increasing temperature and finally disappears at $T = T_c$.

(ii) The slope of the high-field MR ($1/\rho\ d\rho/dH = d/dH\ (\Delta\rho/\rho)$) is negative, i.e., the resistance decreases with increasing field. At $T \ll T_c$, the magnitude of the slope is nearly zero and it progressively increases as T_c is approached. This behavior is attributed to the electron-magnon scattering. At low temperatures, the number of magnons is less and so there is less electron-magnon scattering and consequently the slope is nearly zero. With the increase in temperature, the number of magnons increases resulting in a negative slope.

Both these features of FAR and the high-field slopes are common to both crystalline and amorphous phases. The magnitudes of both are significantly different in the two phases. The magnitude of FAR averages to about 0.5 % in amorphous materials [58,59]

whereas in crystalline systems it averages between 10-15 % (experimental results cited in [60,61]). Similarly, the slopes in amorphous materials are smaller than those in the corresponding crystalline materials. Room temperature measurements of FAR suggest that it is closely related to the saturation magnetic moment (μ) per transition metal atom at 0 K, i.e., FAR = $A\mu^m$, where A and m are temperature-dependent parameters [62-64]. The value of m is obtained between 1 and 27. However, results of Kaul and Rosenberg [65] show that the above relation does not hold good for $(FeNi)_{80}(P-B)_{20}$ alloys. A correlation between the FAR and the transport characteristics, such as the resistivity at 300 K and the temperature coefficient of resistance (TCR), is found in the case of the low resistivity crystalline and amorphous Fe-Co-Ni-based alloys [66].

The model proposed by Campbell, Fert, and Jaoul (CFJ) [60,61,67], based on the mechanism suggested by Smit [57] on parallel current conduction, finds a more universal acceptance in explaining the concentration and temperature dependence of FAR in dilute Ni-based and Fe-based alloys. In this model, s-electrons are solely responsible for the conduction process and spin-up and spin-down electrons conduct in parallel. They are scattered into either an s-band (ρ_{ss}) or a d-band (ρ_{sd}). It is assumed that $\rho_{sd} > \rho_{ss}$. Due to the exchange splitting the d-band splits into $d_\uparrow$ and $d_\downarrow$-bands. In the presence of spin-orbit coupling a mixing of $d_\uparrow$ and $d_\downarrow$ occurs at the Fermi surface. The FAR is a consequence of $d_\uparrow$-$d_\downarrow$ mixing which is anisotropic because the magnetization direction provides an axis for the spin-orbit perturbation, the

magnitude of which is largely dependent on the ratio of $\rho_{\downarrow}/\rho_{\uparrow}$. This model has also been used to distinguish between strong and weak ferromagnetism [61,65].

This theory, however, is criticized (see for review [68]) for taking a very simple atomic d-state model into account and not the realistic band structure. Also, this model is shown [68] to fail in explaining the dependence of FAR on exchange field H, as $H \rightarrow 0$, in weak ferromagnets. The theories, based on band structures [69,70], produce complex results and do not satisfactorily explain the behavior [65]. A modification of the model by CFJ has been proposed [71] for the case of amorphous metalloid-containing alloys and weak ferromagnets, where ρ_{ss} is estimated to be equal to ρ_{sd}. The derived formula, though semi-quantitatively explains the observed behavior of $\Delta\rho/\rho$ versus x for amorphous alloys, relies on too many simplifications.

We study the FAR of the present series of alloys, as a function of Cr concentration and temperature. The results are discussed in terms of the model based on two-current conduction (TCC).

Contrary to the expected observations in ferromagnets, it is found that certain amorphous magnetic alloys, particularly those containing Cr exhibit a positive high-field slope of the magnetoresistivity $\rho^{-1}d\rho/dH$ [39,58,72-80] in the ferromagnetic regime. The high-field slopes, beyond the technical saturation in both the orientations of magnetization, are positive and linear and within the experimental error are identical in value . An addition of as little as 1 at.% Cr in $Fe_{80}B_{20}$ is found to change

the slope from negative to positive. In the absence of a proper theoretical justification for such a behavior, the experimental results [73,76,78] are discussed qualitatively on the basis of the interpretation of Hake et al. [81], which uses the model of Grest and Nagel [47] on the distribution of effective internal magnetic field $P(H_{eff})$. According to this model, the shape of the $P(H_{eff})$ distribution, which extends to negative exchange field, is not changed on application of an external field and it only translates the distribution to higher fields. The sign of the magnetoresistance depends upon the sign of $dP(H_{eff})/dH$ at $H_{int} = 0$. Thus a positive slope in Cr-containing alloys implies that $dP(H_{eff})/dH$ is positive. However, the experimental results for detecting the sign of $P(H_{eff})$ are difficult to interpret due to uncertainties in the low-field measurements [73,78].

The positive slope in magnetoresistance has also been observed in rare-earth containing amorphous materials, viz., NiGd [82,83] and HoCoB [84,85] and other alloys e.g., FeZr [86,87]. Some of these results are discussed on the basis of coherent scattering exchange model of Asomoza et al. [88] and Bhattacharjee and Coqblin [89]. The principal result of these models is that the slope of the magnetoresistivity is proportional to M^2 at temperatures far away from T_c. Experimental results show that $\Delta R/R$ versus T peaks at T_c. This is explained to arise from the divergence of susceptibility at T_c. An external magnetic field will create substantial alignment and therefore generate a large magnetoresistance.

Explanation of magnetoresistance of non-magnetic glasses on

the models of weak localization and interaction effects has been fairly successful (for review see [2,53]). The magnetic field suppresses the localization effect. The theoretical model by Altshuler et al. [90] predicts a variety of magnetoresistance behavior including both positive and negative magnetoresistances. It is shown that, in the presence of weak spin-orbit scattering, i.e., when $\tau_{so}^{-1} \ll \tau_i^{-1}$, where τ_{so} and τ_i are the relaxation rates for spin-orbit scattering and inelastic scattering respectively, the MR is negative and is proportional to $-H^2$ at low fields and to $-H^{1/2}$ at higher fields. When the spin-orbit scattering is stronger than the inelastic scattering , the MR is positive at low fields and negative at higher fields. The correction to the magnetoconductivity, due to the localization effect, is shown to be equal to $0.918\ H^{1/2}$ mho/cm, where H is in kOe and is valid at very high fields [91]. In the electron interaction picture, the magnetic field produces a difference in energy between the spin-up and spin-down electrons, i.e., the Zeeman spin splitting. This is shown to give a correction to the magnetoconductivity which goes as $H^{1/2}$ at high fields and H^2 at low fields. The contribution from the normal magnetoresistance, arising from the Lorentz force and described by the Kohler's rule $\Delta\rho/\rho = F(H/\rho)$, is estimated to be negligible in comparison to those from the above terms. Experimental evidence of the effect of the spin-orbit coupling and the inelastic scattering has been there in Cu-Zr [92] and Cu-Ti [93] systems among others (for review see [2,53]). The verification of the above results on ferromagnetic systems has not been done extensively. High field ($\leq$ 39 kOe) MR studies on

ferromagnetic Fe-B-C system [94] indicate the existence of $-H^{1/2}$ term, on the basis of χ^2 fit analysis between 5 and 39 kOe, and its coefficient is in quantitative agreement with the theory of Kawabata [91]. However, similar analysis on Fe-Cr-B [39] to explain the change of slope of magnetoresistance from negative to positive, on addition of Cr was not successful.

The positive high-field slope of MR of the Cr-containing alloys in the present study is discussed in terms of the model of Bhattacharjee and Coqblin [89] for rare-earth containing metallic glasses and localization and interaction effects. The models based on the quantum correction effects explain very satisfactorily the positive and negative magnetoresistance in non-ferromagnetic samples. We have made an attempt here to analyze the magnetoresistance behavior of these ferromagnetic samples taking into account the internal magnetic field.

MR is also used as a tool to study the nature of interactions over distances of the order of the mean free path. The slope $\rho^{-1}d\rho/dH$ of a ferromagnet tends to zero as $T/T_c \rightarrow 0$. However, alloys with competing interactions are found to go to a phase where long-range order coexists with the spin-glass phase as predicted by the model of Gabay and Toulouse [95]. The irreversible effects associated with the magnetization behavior of spin-glasses are observed in this phase. MR studies reveal that the slope $\rho^{-1}d\rho/dH$ increases as the system enters a mixed phase [96,97] from a ferromagnetic one. This increase is associated with the increase of random uncorrelated components and breakdown of FM order which results in increase of high-field susceptibility.

We have studied the MR of alloys exhibiting mixed phase characteristics. The FAR and the slope in these alloys show behaviors different from those normally observed in ferromagnetic systems. We have tried to correlate this observation with the onset of collapse of long-range order.

C. Magnetization

To make this write up logical and brief, we restrict to alloys in the ribbon form prepared by melt-quenched techniques and having nominal composition of the type $TM_{80}M_{20}$, where TM and M are the transition metal and the metalloid respectively. The magnetic properties of ferromagnetic glasses have attracted wide attention from both physics and engineering disciplines. The 'soft' magnetic characteristics coupled with the mechanical properties exhibited by these materials are harnessed for a variety of technological applications. It is argued that some of these materials are more efficient as well as economical replacement for the existing conventional crystalline alloys in transformer cores [98]. While the choice of these materials as a viable alternative in industrial and domestic applications is debated upon, the fundamental aspects of magnetism in glasses are fairly well studied. A number of review articles [99-103] discuss the various aspects of the problem.

Broadly speaking all of the various features observed in crystalline systems are manifested in amorphous systems as well viz., existence of magnetic moment, spin-waves, well-defined critical exponents, spin-glass and mixed phases, etc. In all these

observations, the role of structural disorder is very subtle and has been an object of study. The magnetic properties are found to be sometimes more sensitive to the various types of short-range order (SRO) than to the lack of periodicity [100]. The role of various preparation techniques and its effect on the magnetic properties is less than clear [100]. The influence of the structural disorder on the low-temperature average magnetic moment ($\bar{\mu}$) does not appear to exist. A comparison of the experimental results on amorphous and compositionally identical crystalline alloys such as $Co_{75}B_{25}$ [104], $Co_{75}Si_{15}B_{10}$ [105], Fe_3B [106], and Fe_5Si_3 [107] indicates that the magnitude of $\bar{\mu}$ remains practically unchanged. Also, it is observed that upon crystallization of these alloys on heating, the magnetic moment changes by only a few percent [108]. The T_c, however, decreases appreciably as a result of amorphocity. This shows that the T_c is very sensitive to the detailed atomic configuration.

The data on the effect of the metalloid variation [109,110] suggest that the glass-formers (metalloids) can be grouped into two categories: (i) Substitutional (P,Si,Ge) which lowers the mass density appreciably and (ii) Interstitial (B,C) which lowers the density weakly. The members of the latter group suppress μ and T_c more than the former. The addition of metalloid to Co, Ni, and Fe-based metallic glasses brings about a change in the behavior of the magnetic moment in these three alloy systems differently. The magnetic moment of pure Co, deduced from bulk magnetization measurements on Co-metalloid alloys, matches with that of crystalline Co. A small difference appears in the case of Ni-based

alloys while in Fe-based alloys anomalies appear in the variation of T_c on metalloid concentration. While T_c extrapolates to room temperature for amorphous Fe, the magnetic moment changes between Ø and 1 μ_B/Fe at.% (A detailed discussion is given in [1ØØ]).

The variation of the magnetic moment with the substitution of one transition metal by another falls on a curve equivalent to the Slater-Pauling curve for the crystalline Fe, Co, and Ni alloys [111]. It is observed that the well-known triangular shape of the Slater-Pauling curve is maintained, i.e., the right-side has a downward 45° slope and the left-hand side has an upward 45° slope. The difference between the curves for the amorphous and the crystalline alloys is on the right side, i.e., $(Z_{impurity} - Z_{host}) > Ø$, where Z is the chemical valence. The curve, though parallel, is displaced to lower Z in the case of amorphous alloys and is often cited as the displaced Slater-Pauling curve. The initial explanation of this displacement was in terms of the 'charge-transfer' model [1Ø2,112]. The charge-transfer model is actually a special case of the rigid-band model [113] in which the host bands are rigid and the metalloid bands are ignored. The rigid-band model presumes that the d-bands as well as the sp-bands of the alloy components form common bands, invariant under alloying. These common bands are filled according to the chemical valence. For conventional strong magnets it assumes that the spin-up d-band is full. In this approximation, an empirical relation for the variation of the average magnetic moment in an $A_{1-x}B_x$ alloy is written as

$$\mu_{av} = \mu_A^o - x(Z_B - Z_A),$$

where μ_A is the moment of the matrix, Z_B and Z_A are chemical valences of B and A respectively, and x is the concentration. This expression holds good for several binary crystalline alloys and also amorphous alloys which follow the right-hand side, downward sloping portion of the curve. Similarly, the left portion of the curve is described by a relation

$$\mu_{av} = \mu_A^o + x(Z_B - Z_A).$$

Though this theory could explain the variation of the moment in Fe-Ni, Fe-Cr, Co-Cr alloys, subsequent sophisticated experimental techniques showed that the bands were not rigid even for single systems and its "success based on cancelling mistakes" [114]. The above simple expressions are observed to hold for small concentrations of impurities that weakly perturb the periodic potential of the matrix ($|Z| \simeq 1$) [115]. However, this model fails for $|Z| \geq 2$. Experiments on $Co_{80-x}T_xB_{20}$ glasses (T = Fe, Mn, Cr, V) [115] show that Friedel's virtual bound state approximation [116] holds good for Cr and V containing alloys and are able to account for the sharp fall in the moment with the addition of these impurities. The above theory is able to explain the variation of moment on replacing a transition metal with another. However, on replacing the transition metal with metalloid, modifications to the charge-transfer model are suggested to account for the contribution from the s and p bands [114,117].

We study the effect of the variation of Cr, in essentially the pseudobinary alloys $Ni_{1-x}Cr_x$ and $Ni_{1-x}Mn_x$, on the magnetic moment and the T_C. We discuss the fall in the moment of the alloy with the increase in concentration of Cr on the basis of the

charge-transfer model and Friedel's virtual bound state approximation. We also observe that substitution with Mn, in contrast, increases the moment of the alloy. The results are discussed on the basis of the above models.

The temperature dependence of magnetization (M(T)) is explained largely in terms of the spin-wave excitations which, at low temperatures, follow the well-known Bloch equation [118]

$$M(T) = M(0)[\ 1 - BT^{3/2} - CT^{5/2} - \cdots\cdots\cdots\cdots\cdots\cdots].$$

The $T^{3/2}$ term originates from the harmonic (q^2) term and the $T^{5/2}$ term from the (q^4) term in the spin-wave dispersion relation. The above result for long-wavelength spin-waves was first obtained by Bloch [119] utilizing the Heisenberg hamiltonian for spins on a lattice. The $T^{3/2}$ dependence of magnetization is shown to be true even for a continuous medium [120]. At low temperatures, only a few spin-waves are excited and they can be treated as bosons. The number of spin-waves n = phase volume/volume of a unit cell = $(4\pi/3)(Lq)^3/(2\pi\hbar)^3$ is proportional to q^3. But, since $Jq^2 \sim T$, n is proportional to $(T/J)^3$ or $(T/T_C)^{3/2}$. The existence of spin-waves in amorphous materials has been confirmed directly from magnetic inelastic neutron-scattering measurements on $Fe_{75}P_{15}C_{10}$ and $(Fe_{93}Mo_7)_{80}B_{10}P_{10}$ [121,122], Co_4P [123], $Fe_{89}B_{10.5}Si_{0.5}$ and $Fe_{20}Ni_{60}B_{19}P_1$ [124] and $(Fe_xNi_{1-x})_{75}P_{16}B_6Al_3$ [125]. Due to the absence of reciprocal lattice vectors in amorphous solids, all measurements were confined to the small-angle scattering region. In the long-wavelength limit, the spin-waves obey the quadratic dispersion relation of the form

$$E_q = Dq^2,$$

where D is the spin-wave stiffness constant. The values of D, obtained from the magnetization measurement, do not differ from those obtained from neutron-scattering measurements in non-invar metallic glasses [1Ø3]. However, in Fe-rich glasses the difference is found to be as much as a factor of 2 [1Ø3,126], which shows that modes of excitation other than the spin-waves , i.e., Stoner single particle-type excitations also contribute to the demagnetization process.

The temperature dependence of the magnetization is found to follow identical relations in both the crystalline and the amorphous alloys but with the following differences. In amorphous alloys, it is found that the $T^{3/2}$ dependence holds good for a much larger range of temperature ($\geq Ø.5T_c$). The coefficient of the $T^{3/2}$ term is, in general, larger than that of the corresponding crystalline system. Majumdar et al. [127] compares the data of crystalline Fe with a-$Fe_{8O}B_{2O}$ and finds that the coefficient of the latter exceeds by a factor of ~ 5. Since this coefficient of $T^{3/2}$ is related to the stiffness constant, this then implies a smaller value of D. In a phenomenological model, proposed by Simpson [128], it is explained that the increase of this coefficient in amorphous systems is a consequence of simultaneous effect of structural disorder and s-d exchange fluctuations. The $T^{5/2}$ term is associated with the quadratic term of the energy dispersion relation (a different interpretation for this term is given in [123]) and is found to be small compared to the $T^{3/2}$ term in the whole range of analysis [127,129-131]. The ratio of $C_{5/2}/B_{3/2}$ for Ni is of the order 1, whereas for amorphous

ferromagnets, it is only about Ø.3. In crystalline ferromagnets the ratio of C/B provides a measure of the range of magnetic interaction [118,132]. The result of small $C_{5/2}/B_{3/2}$ in amorphous systems suggest that the mean exchange interaction has a shorter range than in crystalline systems, i.e., the exchange interaction does not extend much beyond the nearest neighbors. This also means that the q^4 term provides an insignificant contribution. In general, the experimental results on the magnetization of amorphous alloys are well represented by the $T^{3/2}$ term alone. When the temperature dependence of D is also taken into consideration [133-136], in the low-temperature limit, D(T) is found to vary as

$$D(T) = D_o(1 - D_1T^2 - D_2T^{5/2}).$$

This yields, in addition to the $T^{3/2}$ and $T^{5/2}$ terms due to q^2 and q^4 term in the dispersion relation, a $T^{7/2}$ and/or a T^4 term depending on the temperature dependence of D.

In addition to the spin-wave excitations, Stoner single-particle excitations contribute to the thermal demagnetization which is given in the form [137]

$$\Delta M_{sp} = AT^{\alpha}exp (-\Delta/k_BT)$$

which reduces to the expression [138]

$$\Delta M_{sp} = AT^2 \quad \text{when } \alpha = 2 , \Delta = Ø$$

and

$$\Delta M_{sp} = AT^{3/2}exp (-\Delta/k_BT) \text{ when } \alpha = 3/2 , \Delta \neq Ø$$

for weak and strong ferromagnets, respectively.

Babic et al. [139] find the presence of stoner terms ($\Delta \neq Ø$) together with the spin-wave terms from the magnetization data of $Fe_xNi_{80-x}B_{18}Si_2$ and $Fe_{80}B_{20}$. The values of Δ obtained are between

20 and 60 K.

The influence of Cr and Mn in Fe and Co-rich glasses [139-142] and crystalline materials [143,144] on the magnetization process has received considerable attention. The magnetic moment, Curie temperature, and average hyperfine field of the alloy decrease on addition of Cr and Mn but there exists a difference. While substitution with very little amount of Cr produces a drop in the moment, it is found that in the case of Mn it actually increases. This behavior is found to be common in both Fe and Co-rich glasses. However, recent Mössbauer study on a-Co-Fe-B-Si alloys shows that there exists a striking difference in the hyperfine parameters between Mn doped Fe- and Co-rich alloys [145]. The M(T) study of Fe-Cr-containing glasses show that the $T^{3/2}$ law holds good in these alloys [143,144,146]. Additionally, the presence of Stoner excitations in the form of T^2 is detected. This is found to increase with increase in Cr. The data of Aldred [143] show that the spin-wave stiffness constant, which decreases with increase in concentration of Cr, has a temperature dependence of the form T^2 and is found to decrease with increase in Cr concentration.

We study the effect of Cr and Mn on the temperature dependence of magnetization. If the thermal demagnetization is only through the $T^{3/2}$ term or additional terms due to anharmonic terms in the spin-wave dispersion relation, temperature dependence of spin-wave stiffness constant and/or Stoner single particle excitations are required to explain the results. The dependence of spin-wave stiffness constant on T_c is also investigated.

The magnetic phase diagrams established for alloys $(Fe_{1-x}Mn_x)_{75}P_{16}B_6Al_3$ [147,148] and $(Fe_{1-x}Mn_x)_{77}Si_{10}B_{13}$ (where M = V,Cr,Mn,Ni) [149] show the existence of a spin-glass-like phase at low temperatures in these alloys. The alloys, on cooling, undergo a paramagnetic (PM) to ferromagnetic (FM) transition and on further cooling, at a characteristic temperature (T_{SG}), the ferromagnetic order disappears and the resulting phase exhibits features associated with the classical spin-glass system. Those alloys which exhibit this double transition are also known as reentrant spin-glass systems (RSG). This type of behavior has been observed in a wide variety of materials such as polycrystalline metallic alloys $Fe_{1-x}Cr_x$ [150], Fe_xAu_{1-x} [151], Mn_xNi_{1-x} [152], and $Fe_{80-x}Ni_xCr_{20}$ [153] and amorphous metallic alloys $(Fe_xNi_{1-x})_{80}P_{14}B_6$ [154] and $(Fe_xNi_{1-x})_{78}Si_9B_{13}$ [155], crystalline semiconductors $Eu_xSr_{1-x}S$ [156], EuS_xSe_{1-x} [157] and $Eu_{1-x}Gd_xS$ [158] and insulators $KMn_xZn_{1-x}F_3$ [159] and $CdCr_{2-x}In_{2-2x}S_4$ [160]. The nature of transitions is studied through a number of experimental techniques including ac susceptibility, dc magnetization, thermoremanent magnetization, hysteresis loop, magnetic viscosity, pressure dependence of low-field ac susceptibility, temperature dependence of ferromagnetic resonance line width, Mössbauer spectroscopy, small angle neutron scattering [101], frequency dependence of the ac susceptibility [160], etc.

There are two types of problems associated with the low-temperature reentrant transition which are most debatable.
(1) The nature of transition ,i.e., whether it is at all a phase transition or not, the order of transition, the critical exponents

associated with the transition [148], etc.

(2) The ground state of the low-temperature phase of the ferromagnetic metallic glasses which are reentrant, i.e., whether it is a pure spin-glass phase with no long-range order or in this phase both spin-glass order and long-range order coexist.

Edward and Anderson [161] first showed the existence of the low-temperature spin-glass phase. Their study was based upon classical Heisenberg hamiltonian with exchange interactions varying randomly over a Gaussian distribution centered at zero. They predicted that, below a certain critical temperature, the system would have a magnetically ordered state in which the spin directions at any site are frozen, even though on the average, there would be no spatial correlation. Sherrington and Kirkpatric [162] later showed the existence of both the spin-glass phase and the ferromagnetic phase by considering an Ising model in which the spins are coupled by infinite-ranged random interactions independently distributed with a Gaussian probability density with a non-zero mean. This model also studies the influence of an external field H on magnetic susceptibility. The evidence for the existence of a mixed phase, apart from the para, ferro, and spin-glass phases, was shown by Gabay-Toulouse [95]. The mixed phase is characterized by the coexistence of a spontaneous longitudinal magnetization and a spin-glass ordering of the transverse components of the spins.

Experimentally it has been found difficult to study the mixed phase region. It is found that this phase is very susceptible to the application of an external dc magnetic field, and a field as

low as 1Ø Oe, is found to either suppress this phase or shifts the critical temperature very appreciably to further lower temperatures [146,147].

D. Critical Exponents

The nature of phase transition in disordered materials has been an area of study which has attracted considerable attention, both in the theoretical and the experimental fronts [163]. Theoretical understanding is divided on the issue of the role of disorder. Fisher [164] has shown that, in systems with annealed disorder, the critical indices are not influenced by the disorder if the specific heat exponent $\alpha < Ø$. Based on phenomenological arguments, Harris [165] has put forward a criterion: if the specific heat exponent $\alpha < Ø$ for an ordered system, the critical exponents would remain unchanged in the presence of weak, spatially random disorder. Renormalization group theory-based calculations [166,167] also arrive at the same conclusion. There are, however, other theoretical calculations [168] which contradict the above conclusion and suggest that the critical indices of the system with $\alpha < Ø$ will depend on the amount of quenched disorder present. A new set of fixed points is suggested when the systems are close to the critical concentration, x_c, for the appearance of long-range ferromagnetic order. In the limit $x \rightarrow x_c$, the numerical values of the indices are $\alpha=-1$, $\beta=Ø.5$, $\gamma=2.Ø$, and $\delta=5$ for the exponents of specific heat, magnetization, susceptibility, and isothermal magnetization respectively.

It has been shown [169] by careful experimentation and data

analysis that the value of the exponent γ agrees exactly with the theoretically-predicted value for 3D Heisenberg system [170] in the asymptotic critical regime (ACR), if proper corrections are made to the experimentally measured value of γ. The correction parameters have their origin in the higher order derivatives of the Gibb's potential. A survey of experimental results supports the view that the phase transition in amorphous materials is not influenced by the topological disorder and behave in the same manner as homogeneous crystalline systems. The influence of disorder is mainly at temperatures beyond the true critical region, i.e., in the intermediate region between the mean-field and the ACR, where $\gamma(T)$ describes a nonmonotonic behavior (for review see [171]).

Experimental results on amorphous systems containing Cr or Mn, around the critical concentration x_c, however, are different [147,172]. It is found that as $x \rightarrow x_c$ in these alloys, $\beta \rightarrow 0.5, \gamma \rightarrow 2$, and $\delta \rightarrow 5$. Specific heat measurements [173] near the T_c of Cr-containing glasses indicate a smeared transition with negligible height of the peak. The temperature derivative of the resistivity also shows a broad transition region. These results point to the formation of magnetic clusters with distribution of T_c's which results in the deviations of the critical exponents from those of the homogeneous systems.

E. High-temperature magnetization

Amorphous materials, being unstable, are susceptible to heat treatment and undergo crystallization on heating above their

respective crystallization temperatures. The crystallization process in amorphous materials is widely studied to find out the nature of the various crystallized phases, the thermal stability of the material, and the effect of additives in the form of transition metal and/or metalloid on the crystallization process. The published results indicate that the addition of Cr and V in Fe-rich alloys raises the crystallization temperature and hence the thermal stability [174,175]. Here we study the effect of Cr substitution on the crystallization process of FeCoNiBSi system. This alloy system is very close in composition to the alloys known for vanishingly small linear saturation magnetostriction coefficient [176]. These samples exhibit resistance minima at relatively high temperatures [27] and the magnetoresistance measurements at $T < T_c$ indicate a positive high-field slope [79]. The dc magnetization measurements below room temperature indicate progressive decrease of magnetic moment, T_c and spin-wave stiffness constant following the addition of Cr. The role of magnetism in these studies will be better understood if the evolution of the magnetic phases could be traced through the amorphous as well as the crystallized states. For this purpose the change in magnetization of the sample is studied as a function of temperature above 300 K. Then x-ray analysis is done at room temperature on those very pieces of samples to determine the final crystallized phase(s) and finally correlate the results of the two measurements.

1.2 Theory

A. Temperature dependence of electrical resistivity

1. $T > T_{min}$:

The resistivity of an amorphous material containing transition metal is expressed, in the diffraction model, as [177]

$$\rho = \frac{30\ \pi^2\ \hbar^3}{m\ e^2\ k_F^2\ E_F\ \Omega} \sin^2 [\ \eta_2(E_F)\ ]\ S_T(2k_F), \qquad (1.1)$$

where k_F and E_F are the Fermi wave vector and energy, respectively, and Ω is the atomic volume. $\eta_2(E_F)$ is the d-wave phase shift describing the scattering of the conduction electrons of energy E_F by the ion cores which carry a muffin-tin potential. The temperature dependence of ρ is determined by the structure factor which is written as [7]

$$S_T(K) \cong 1 + [\ S_E(K) - 1\ ] \exp(\ -2\ W_K(T)\ ), \qquad (1.2)$$

where $S_E(K)$ is the equilibrium structure factor. $\exp(-2W_K(T))$ is the Debye-Waller factor with $W_K(0)$, in the Debye approximation, is given by [178]

$$W_K(T) = W_K(0) + 4\ W_K(0) \left[\frac{T}{\theta_D} \right]^2 \int_0^{\theta_D/T} \frac{z\ dz}{e^z - 1}\ , \qquad (1.3)$$

$$\text{where } W_K(0) = 3\hbar^2k^2\ /\ 8Mk_B\theta_D\ , \qquad (1.4)$$

M is the atomic mass, k is the wave vector and k_B is the Boltzmann constant. In the high and low temperature limits, $W_K(T)$ reduces to [7]

$$W_K(T) = W(0) + 4\ W(0)\ \frac{\pi^2}{6} \left[\frac{T}{\theta_D} \right]^2, \quad \text{for } T \ll \theta_D \qquad (1.5)$$

$$W_K(\emptyset) = 4\, W(\emptyset) \left[\frac{T}{\theta_D} \right] , \qquad \text{for } T > \theta_D . \qquad (1.6)$$

Incorporating Eqs. (1.2), (1.5), and (1.6) in (1.1), one gets

$$r(T) = R(T)/R(300K) = a + b\, T^2 \qquad \text{for } T < \theta_D , \qquad (1.7)$$

$$r(T) = R(T)/R(300K) = c + d\, T \qquad \text{for } T > \theta_D . \qquad (1.8)$$

Cote and Meisel [3] has obtained similar asymptotic temperature dependence while taking into account the difference between the resistivity static structure factor and the X-ray static factor.

In the case of amorphous ferromagnetic materials Richter et al. [36] have shown that for $T \ll T_C$, the total magnetic resistivity at low T varies as

$$\frac{\rho_{mag}(T)}{\rho_{mag}(\emptyset)} = a + b\, T^{3/2} + c\, T^2 .$$

In the above equation the $T^{3/2}$ term, which vanishes for crystalline ferromagnets, results from the partial cancellation of two competing terms. (a) A ($-T^{3/2}$) term originates from purely elastic scattering where electrons are scattered by randomly distributed temperature-dependent local moments and (b) A $T^{3/2}$ term arises from the incoherent momentum nonconserving electron-magnon scattering process. The positive contribution overcompensates the negative one. The T^2 term is due to the coherent spin-wave scattering. According to the estimate of Richter et al., the $T^{3/2}$ term dominates the low-temperature behavior, and its coefficient b is 2 orders of magnitude larger than that of the T^2 term.

2. $T < T_{min}$:

In the normal metallic regime, the dc conductivity is given by the Drude formula, as obtained from the Boltzmann transport equation,

$$\sigma_B = ne^2\tau/m, \qquad (1.9)$$

which can also be written as

$$\sigma_B = \frac{S_F e^2 l}{12\pi^3 h}, \qquad (1.10)$$

where τ is the relaxation time, m is the effective mass, n is the number of electrons per unit volume, l is the mean free path, and S_F is the area of the spherical Fermi surface. This result is correct if the values of τ or l are the result of inelastic collisions, such as electron-phonon processes. This is also correct for the T^2 dependence observed for electron-electron collisions. But if τ is the result of scattering by impurities, as in an alloy at low temperatures or by disorder in an amorphous material, then corrections to the above formula apply [51]. These correction terms arise due to the presence of disorder which modifies the electron-electron interaction and also enhances the electron localization process. They are known as (a) interaction and (b) localization effects.

A physical picture of a seemingly complex mathematical argument is given by Dugdale [179]. The concept of localization is based upon the fact that, when the mean free path of conduction electrons is of the order of interatomic distance, the electrons do not travel in classical trajectories ; rather they travel by diffusing from site to site. This results in a mutual interference

between waves scattered from nearby ions and leads to a phase coherence between the scattered partial waves. As a result, there exists a finite probability for an electron to return to the origin and hence get localized. This may be understood by considering the diffusive motion of an electron in 2D where the randomly distributed impurities scatter it elastically (thereby conserving energy but changing the direction of the momentum). One considers a closed path for the scattering events by which an electron may return to the origin at O (Fig. 1.1). Classically the probability of returning to the origin is given by $P_c = 1/4\pi Dt$, where D is the diffusion constant of the electron and is made up of equal contributions from each of the paths followed (clockwise or anticlockwise as indicated by arrows). However, if the electron is treated as a quantum particle, these two partial waves can be considered to propagate around the path shown in Fig. 1.1. The two partial waves come back at the origin in phase with the same amplitude. The amplitude at the origin therefore add coherently. This yields a resultant probability for return to the origin of $P_q = 1/2\pi Dt$ or twice that of the classical diffusion process [180]. At any other point, except the origin, the partial waves are incoherent and therefore only their intensities add, giving a net probability little different from that expected of classically. The quantum interference thus results in an enhanced probability for the electron to remain at the origin, i.e., to be localized. There are processes which destroy this phase coherence and reduce the additional resistivity. Two such processes are inelastic scattering and the effect of magnetic field.

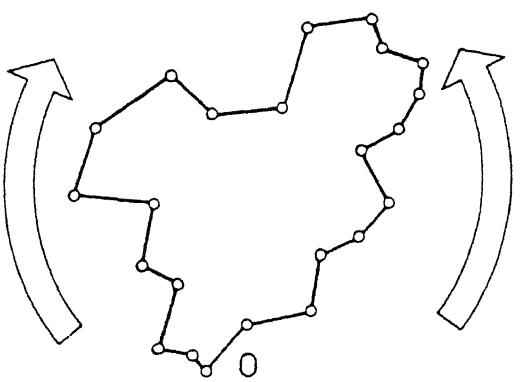

Fig. 1.1 Closed path of an electron moving diffusively under the influence of the elastic scattering from ions. The waves can travel clockwise or anticlockwise round the path as indicated by the arrows.

Scaling theories of localization [181] and the quantum interference effect lead to modifications of Eq.(1.9) in the presence of multiple elastic scattering and is represented by

$$\sigma_3 = \sigma_B \left[1 - \frac{3}{(k_F l_e)^2} \left\{ 1 - \frac{l_e}{L} \right\} \right], \qquad (1.11)$$

in three dimensions, where σ_B is the conductivity given by the Boltzmann formula, l_e is the elastic electron mean free path, and L is either the size of the specimen at finite temperatures or is equal to the inelastic diffusion length L_i. Howson [182] had shown that, by taking into consideration the temperature dependence of σ_B, the temperature-dependent part of Eq. (1.11) can be written as

$$\Delta\sigma(T) = \frac{1}{\pi^2} \frac{e^2}{\hbar} \left[\frac{1}{L_i(T)} - \frac{(k_F l_e)^2}{3} \frac{1}{l_i(T)} \right], \qquad (1.12)$$

The first term gives a non-metallic positive contribution for $d(\Delta\sigma)/dT$, while the second term will give a metallic negative contribution . The non-metallic contribution is important at low temperatures, but as the temperature is increased $d\sigma/dT$ will change sign, i.e., a resistivity minimum will occur. In high-resistivity metallic glasses, the non-metallic temperature dependence may exist up to the crystallization temperature. In this case, neglecting the second term in Eq. (1.12), one gets

$$\Delta\sigma(T) = \frac{1}{\pi^2} \frac{e^2}{\hbar} \frac{1}{L_i(T)}. \qquad (1.13)$$

$L_i^2 = 0.51_i(T)1_e$, where 1_e and 1_i are the elastic and the inelastic mean free paths for electron-phonon scattering. $1_i(T) \propto T^{-1}$ for $T > \theta_D$ and $\propto T^{-2}$ for $T < \theta_D$ from the usual electron-phonon scattering. This leads to

$$\Delta\sigma \propto T \text{ for } T < \theta_D , \tag{1.14}$$

$$\Delta\sigma \propto T^{1/2} \text{ for } T > \theta_D . \tag{1.15}$$

The interaction effect is different from the localization process in the sense that the interaction effect arises from the interaction of one conduction electron with another in the presence of the multiple elastic scattering whereas in the localization process it involves only single electrons. The effect of electron-electron interaction in crystalline systems is of minor importance as compared to amorphous systems or in general metallic systems where the mean free path is short. It was first shown by Altshuler and Aronov [183] that the interaction effect at zero temperature produces a cusp in the density of states (N(E)) at the Fermi level E_F. The change in (N(E)) from the value without interaction is given by [183]

$$\delta N(E) = (2\pi\hbar D1)^{-1} \left[1 + 1 \left\{ \frac{|E - E_F|}{\hbar D} \right\}^{1/2} \right]. \tag{1.16}$$

This is significant for only small values of σ and thus of D. This leads to changes in σ, given by

$$\sigma(T) = \sigma(0) + \delta\sigma ,$$

$$\text{where } \delta\sigma = \frac{1.3}{\sqrt{2}} \frac{e^2}{4\pi^2\hbar} \left(\frac{4}{3} - \frac{3}{2} F_\sigma \right) \left(\frac{k_B T}{\hbar D} \right)^{1/2}, \tag{1.17}$$

where D is the diffusion constant and F_σ is the screening factor

for the Coulomb interaction.

B. Temperature dependence of Magnetization

Experimental evidences on amorphous ferromagnetic materials suggest that long-wavelength spin-wave excitations follow the same dispersion relation as in the crystalline ferromagnets, namely

$$\varepsilon(q) = g\,\mu_B\,H_{int} + D\,q^2 + E\,q^4 + \ldots\ldots\,, \qquad (1.18)$$

where $g\,\mu_B\,H_{int} << D\,q^2$ denotes an energy gap in the presence of an effective internal field H_{int} arising from the applied field, the anisotropy field, and the spin-wave demagnetizing field. D is the spin-wave stiffness constant and E is the constant of proportionality for the q^4 term.

At low temperatures, the change in magnetization (in emu/gm) due to spin-wave excitations, according to the Heisenberg model, is given by [118,132]

$$\frac{\Delta M(T)}{M(\emptyset)} = \frac{M(T) - M(\emptyset)}{M(\emptyset)} = BZ(3/2,T_g/T)\;T^{3/2} + CZ(5/2,T_g/T)\;T^{5/2} \qquad (1.19)$$

$$= B_{3/2}Z(3/2,T_g/T)\;(T/T_C)^{3/2} + C_{5/2}Z(5/2,T_g/T)(T/T_C)^{5/2} \qquad (1.20)$$

where T_g is the gap temperature given by $g\mu_B H_{int}/k_B$. The internal field H_{int} is determined from the relation

$$H_{int} = H_{applied} - 4\,\pi\,N\,M(\emptyset) + H_A, \qquad (1.21)$$

where N is the demagnetization factor and H_A is the anisotropy field. The function $Z(3/2,T_g/T)$ and $Z(5/2,T_g/T)$ are defined as [132]

$$Z\left[\frac{3}{2}, \frac{Tg}{T}\right] = \frac{1}{2.612} \sum_{n=1}^{\infty} n^{-3/2} \exp\left[-\frac{n\,Tg}{T}\right]$$

$$\approx \frac{1}{2.612}\left\{-3.54\,(T_g/T)^{1/2} + 2.612 + 1.46\,(T_g/T) - 0.104\,(T_g/T)^2 + \ldots\ldots\right\}. \qquad (1.22)$$

and

$$Z\left[\frac{5}{2}, \frac{Tg}{T}\right] = \frac{1}{1.341} \sum_{n=1}^{\infty} n^{-5/2} \exp\left[-\frac{n\,Tg}{T}\right]$$

$$\approx \frac{1}{1.341}\left\{-2.36\,(T_g/T)^{3/2} + 1.341 - 2.61\,(T_g/T) - 0.730\,(T_g/T)^2 + \ldots\ldots\right\}. \qquad (1.23)$$

The coefficients B and C are related to the spin-wave stiffness constant D and the average mean-square range $\langle r^2 \rangle$ of the exchange interaction by

$$D\ (= D(0)) = \frac{k_B}{4\pi}\left[\frac{2.612\ g\ \mu_B}{M(0)\ \rho\ B}\right]^{2/3} \qquad (1.24)$$

and

$$\langle r^2 \rangle = 1.948\left[\frac{16}{3\ k_B}\right]\frac{C\ D}{B}\ , \qquad (1.25)$$

where ρ is the density. In the above relation the ratio of the coefficients C/B gives the range of interaction. If $\bar{a}$ is the most probable nearest neighbor distance of the alloys, the range of exchange interaction in units of $\bar{a}$ is

$$n = \langle r^2 \rangle^{1/2} / \bar{a}\ . \qquad (1.26)$$

The $T^{3/2}$ term in Eq. (1.19) has its origin in the harmonic (q^2)

term in the spin-wave dispersion relation and the $T^{5/2}$ in the anharmonic (q^4) term. The above relations assume that D is temperature independent. When the number of magnons excited are large, interactions between them (magnon - magnon) leads to a $T^{5/2}$ term in D in the localized model [184,185]. The interaction between spin-waves and itinerant electrons leads to a T^2 term and magnon - magnon leads to a $T^{5/2}$ term in the itinerant electron model [137,186].

Thus in the low-temperature limit

$$D = D(\emptyset) \left(1 - D_1 T^2 - D_2 T^{5/2} \right). \qquad (1.27)$$

When Eq. (1.27) is substituted in Eq. (1.19) it gives

$$\frac{\Delta M(T)}{M(\emptyset)} = A T^{3/2} \left(1 - D_1 T^2 - D_2 T^{5/2} \right)^{-3/2} Z\left[\frac{3}{2}, \frac{Tg}{T} \right] + B Z\left[\frac{5}{2}, \frac{Tg}{T} \right] T^{5/2} . \qquad (1.28)$$

A binomial expansion of the first term gives a $T^{7/2}$ and/or a T^4 term. Thus the deviation from the $T^{3/2}$ dependence may show up as a $T^{5/2}$ term due to the anharmonic term (q^4) in the spin-wave dispersion relation, and a $T^{7/2}$ and/or a T^4 term depending on the temperature dependence of D.

Besides the spin-wave excitations there exists Stoner single-particle excitations which also contribute to the low-temperature demagnetization of a ferromagnet. According to the approach of itinerant electron or band ferromagnet, the paramagnetic densities of states for spin-up and spin-down electrons are displaced in energy with respect to each other. This displacement is assumed to be proportional to the spontaneous

magnetization and in the low-temperature limit, the decrease in magnetization with temperature is the result of excitation of electrons from the spin-up to spin-down bands. The general expression for the single particle excitation is given by

$$\left[\frac{\Delta M}{M(\emptyset)} \right]_{SP} = A\, T^{\alpha} \exp\left(- \frac{\Delta}{k_B T} \right), \qquad (1.29)$$

where Δ is the energy gap between the top of the full sub-band and the Fermi level. This expression reduces to

$$\left[\frac{\Delta M}{M(\emptyset)} \right] = A\, T^{2}, \qquad \text{where } \alpha = 2,\ \Delta = \emptyset \qquad (1.30)$$

for weak ferromagnets, where holes exist in both the sub-bands as in the case of Fe, for example, and

$$\left[\frac{\Delta M}{M(\emptyset)} \right]_{SP} = B\, T^{3/2} \exp\left(- \frac{\Delta}{k_B T} \right), \text{ where } \alpha = 3/2,\ \Delta \neq \emptyset \qquad (1.31)$$

for strong ferromagnets, where one of the sub-bands is completely filled and holes exist in only the minority band as in the case of Co and Ni, for example. At low temperatures, when deviation from saturation magnetization at Ø K is small, the excitations from the spin-wave and single-particle are nearly independent and the thermal demagnetization is given by the sum of the terms arising from both the contributions, i.e.,

$$\Delta M = [\, \Delta M \,]_{SW} + [\, \Delta M \,]_{SP} . \qquad (1.32)$$

C. Magnetoresistance

For three-dimensional systems and in the presence of spin-orbit scattering, the magnetoresistance due to localization effects is [90,92]

$$\frac{\Delta\rho}{\rho} = \frac{\rho(H) - \rho(0)}{\rho(0)} = \alpha \left(\rho\, e^2 / 2\, \pi^2\, \hbar \right) \times \left[\frac{1}{2}\, f_3\!\left(\frac{H}{H_i} \right) - \frac{3}{2}\, f_3\!\left(\frac{H}{H_{so}} \right) \right], \qquad (1.33)$$

where $H_i = \left(\frac{\hbar}{4\, e\, D} \right) \tau_i^{-1}$,

$H_{so} = H_i + H'_{so}$ and

$H'_{so} = \left(\hbar / 2\, e\, D \right) \tau_{so}^{-1}$,

where τ_i^{-1} is, to a first approximation, the inelastic relaxation rate. τ_{so}^{-1} is the relaxation rate for the spin-orbit scattering. The prefactor α is ≈ 1. The function $f_3(x)$ is represented by the following relations at small and large values of x :

$f_3(x) \simeq x^{3/2} / 48$ for $x \ll 1$ and

$f_3(x) \simeq 0.605$ for $x \gg 1$.

For weak spin-orbit scattering, i.e., $\tau_{so}^{-1} \ll \tau_i^{-1}$ and $H_{so} \simeq H_i$, the magnetoresistance is negative with

$$\frac{\Delta\rho}{\rho} \simeq -\alpha\, \rho \left(e^2 / 96\, \pi^2\, \hbar \right) \left(\frac{e}{\hbar} \right)^{1/2} \left(H^2 / H_i^{3/2} \right) \quad \text{for } H \ll H_i, \qquad (1.34)$$

$$\frac{\Delta\rho}{\rho} \simeq -\rho \left(0.605\, e^2 / 2\, \pi^2\, \hbar \right) \left(\frac{e\, H}{\hbar} \right)^{1/2} \quad \text{for } H \gg H_i. \qquad (1.35)$$

When the spin-orbit scattering is stronger than the inelastic scattering, i.e., $H_{so} \gg H_i$, then the magnetoresistance is given by

$$\frac{\Delta\rho}{\rho} \simeq \alpha\, \rho \left(e^2 / 192\, \pi^2\, \hbar \right) \left(\frac{e}{\hbar} \right)^{1/2} \left(H^2 / H_i^{3/2} \right) \quad \text{for } H \ll H_i, \qquad (1.36)$$

$$\frac{\Delta\rho}{\rho} \simeq \alpha\,\rho\,(\ 0.605\ e^2\ /\ 4\ \pi^2\ \hbar\ )\left[\frac{e\ H}{\hbar}\right]^{1/2}$$

$$\text{for } H_i \ll H \ll H_{so}, \qquad (1.37)$$

$$\frac{\Delta\rho}{\rho} \simeq -\alpha\,\rho\,(\ 0.605\ e^2\ /\ 2\ \pi^2\ \hbar\ )\left[\frac{e\ H}{\hbar}\right]^{1/2}$$

$$\text{for } H \gg H_{so}. \qquad (1.38)$$

The above theoretical results hold good for non-interacting electrons and exhibit both positive and negative magnetoresistance depending on the spin-orbit coupling.

When the electron-electron interaction effect is taken into account, there are additional contributions to MR due to spin-splitting and spin-orbit interaction. According to Lee and Ramakrishnan [51], the MR due to spin-splitting of the spin-up and spin-down bands is written as

$$\frac{\Delta\rho}{\rho} = (\ e^2\ \tilde{F}\ /\ 4\ \pi^2\ \hbar\ )\left[\frac{k\ T}{2\ \hbar\ D}\right]^{1/2} g_3(\ g\ \mu_B\ H\ /\ k_B\ T\ ), \qquad (1.39)$$

where $\tilde{F}$ is an interaction constant. The low- and high-field limits of $g_3(h)$ are

$$g_3(h) = \sqrt{h} - 1.3 \qquad \text{for } h \gg 1\ , \qquad (1.40)$$

$$g_3(h) = 0.053\ h^2 \qquad \text{for } h \ll 1\ . \qquad (1.41)$$

The spin-orbit contribution is [90]

$$\frac{\Delta\rho}{\rho} = g(T)\ \rho\ (\ e^2\ /\ 2\ \pi^2\ \hbar\ )\left[\frac{e\ H}{\hbar}\right]^{1/2} \Phi_3\left[\frac{2\ D\ e\ H}{\pi\ k_B\ T}\right], \qquad (1.42)$$

where g(T) is an interaction parameter.

$$\Phi_3(h) = 1.90 \qquad \text{for } h \gg 1\ , \qquad (1.43)$$

$$\Phi_3(h) = 0.33\ x^{3/2} \qquad \text{for } h \ll 1\ . \qquad (1.44)$$

To a first approximation these are additive.

CHAPTER II
EXPERIMENTAL

The samples (as-received) for the present study are in the form of ribbons, of typical width ~ 1 mm and thickness ~ Ø.ØØ3Ø mm. They were prepared by the method of melt-quenching. The amorphous nature of the samples were checked by performing X-ray measurements using a X-ray diffractometer (Rich and Seifert Isodebyeflex 2ØØ2 diffractometer) with a Cu target (K_{α} = 1.54 Å). It shows a broad peak at low angles. This is observed, in general, in all metallic glasses and is ascribed to the short-range order. The pattern did not show any other observable peak, confirming the absence of crystalline phase(s).

Dc electrical resistivity measurements between 8 and 3ØØ K were done using the four-probe method. The typical lengths of the samples used in these measurements were of ~ 2.5 cm. The electrical contacts with the samples were made by soldering thin phosphor-bronze wires. Zn-Cd non-superconducting solder material with zinc chloride flux and a low-wattage (1Ø W) soldering iron were used for the purpose. While soldering, sufficient care was taken to make each contact within a very short time to prevent any crystallization, at the point of contact, as far as possible. The sample was placed on the top of the cold head of a closed-cycle helium refrigerator (CTI and RMC). It was necessary to establish a good thermal contact between the sample and the cold head, since no exchange gas was there in the sample zone and the sample was cooled only by the conduction process. At the same time it was also essential to have a good electrical insulation for the

sample. To achieve these dual needs, a cigarette paper was first put on the top of the cold head using GE varnish (Oxford Instruments). The sample was placed on top of the paper and varnish was applied. Then it was pressed firmly and was left to dry in air. Similar precaution was also taken to thermally anchor all the wires leading to the sample. The current and voltage wires were connected to a digital voltmeter (1Ø71, Datron) which measures the four-wire resistance directly and has a 7 1/2 place resolution at 1Ø ohm full scale. The measuring current was 1Ø mA. A precalibrated Si diode (LakeShore) was placed very near to the sample to monitor the temperature. The temperature was held constant within Ø.2 K using a temperature controller (DRC-82C, LakeShore).

The magnetoresistance between 11 and 3ØØ K was measured in fields up to 16.5 kOe, provided by an electromagnet (V-38ØØ, Varian) with 15" pole pieces. The cryotip, when placed in the magnetic field, virtually stopped functioning when the field exceeded 12 kOe. The field above which the cryotip stopped working depended upon the proximity of the cold head to the pole pieces. Thus we required to fix an extra attachment on the cold head and still ensured that the sample, in both transverse and longitudinal orientations, was exposed to a uniform magnetic field. At the same time it kept the cold head sufficiently away from the magnetic field for it to function at fields as high as 16.5 kOe. This extra attachment consisted of a 2 inch OFHC (Oxygen free high conductivity) copper tube soldered at both ends by a 1 inch diameter copper disc of thickness 2 mm. This was fixed rigidly to

the original base (for fixing the sample) by nuts and bolts. Indium foils were placed in the intervening space. This resulted in an increase in the lowest attainable temperature from 8 to 11 K. The magnetic field was always in the plane of the ribbon. A dc current of 100 mA from a constant current source (6177C, HP) was passed through the sample. The voltage was measured by the 7 1/2 digit voltmeter. A precalibrated Si diode and carbon glass resistance thermometer (CGR-1-1000, LakeShore) were used to monitor and control the temperature along with the temperature controller (DRC-93C, LakeShore). The CGR thermometer was used because of its low magnetoresistance (-0.2% at 10 K and 2.5 Tesla). At a given temperature the field was fixed at every 1/2 kOe and the data were recorded. The temperature was held constant within 0.2 K during the period of measurement (0 and 16.5 kOe) which was about 20 minutes. Using this set-up we were able to detect changes in resistance of a few parts in 10^6.

The dc magnetization measurements were done between 20 and 300 K in magnetic fields up to 16 kOe. For this purpose, a closed-cycle helium refrigerator (RMC), suitably modified by the manufacturer to fit with the vibrating sample magnetometer (155, PAR) assembly, alongwith the electromagnet was used. The magnetometer was calibrated with the help of a standard Ni sample after the usual saddle point adjustments. The use of the cryotip in conjunction with the VSM, however, created two major difficulties. (1) In this system there is either a OFHC Cu or a Cu-Be tube inside which the sample vibrates. Low-pressure He exchange gas is used in the sample zone. As the temperature is

lowered, the conductivity of Cu rises and there is sufficient shielding of the signal due to eddy currents. To overcome this a modification to the existing set-up was suggested and incorporated by Banerjee [187]. This reduced the shielding significantly but does not remove it completely. Due to this shielding at low fields and below 80 K, the data are not reliable. We find reasonable results between 20 and 300 K for samples having large moments such as in ferromagnets in magnetic fields greater than 2-3 kOe. This prevents us from reporting the much required low-field dc magnetization data on some of the samples. (2) The magnetometer reading shows a large noise when the cryotip is switched on, particularly at temperatures < 100 K. Thus, it is experimentally difficult to measure small changes in magnetization for spin-wave analysis or the behavior of M as a function of H beyond saturation in amorphous ferromagnets. Therefore, for obtaining M(T) data we switch off the cryotip at the lowest temperature and then measure M as a function of temperature as the temperature is increased. Initially the change of temperature is very rapid and therefore the data below 30 K can not be analyzed. A 100 ohm precalibrated platinum resistance thermometer is kept very close to the sample. This ensures high accuracy in the measurement of temperature. The magnetization data, for critical exponents analysis, were also taken in the same way. M(T) was measured at different fixed fields.

Ac-susceptibility was done to identify the low-temperature phases of the samples and obtain the critical exponents. Since the T_c's of the samples were above 77 K, a separate coil assembly was

made which was immersed in liquid nitrogen, and a suitable glass cryostat made to measure the susceptibility as a function of temperature.

The basic principle of an ac susceptibility measurement is that when a magnetic sample is introduced in a primary coil, due to the change in mutual inductance, a change in voltage appears at the secondary which is proportional to the susceptibility of the sample. This change in voltage may be very small in comparison with the voltage existing without the sample. It is necessary to minimize the signal without the sample to detect small changes. This is done by: (1) Adding another secondary coil, away from the first, wound in the opposite direction, i.e., the two secondary coils are in phase opposition and the output voltage without the sample is zero. Now, if the sample is introduced in one of the coils, the off-balance signal can be measured with greater reliability. (2) Adding another coil to null the initial voltage is possible if the two coils are exactly similar, which may be experimentally difficult to achieve. Therefore, a mutual inductance bridge [188] is used which is able to null both the in-phase and the quadrature signals up to a very sensitive scale ($\sim$ 1 μv). Here we use both these procedures to null the voltage.

The primary and the secondary coils are wound coaxially on a perspex tube of outer diameter 1.46 cm. The two secondaries are wound first. Each are of length Ø.1 cm and 15Ø turns wound from 38 SWG copper wires. The two secondaries are separated from each other by 7.2 cms. The primary is wound on top of this and is of length 26 cms having 1Ø5Ø turns made from 3Ø SWG copper wire.

Another coil was wound coaxially on top of this to produce dc fields. The whole coil system was covered with a metglass to screen the horizontal component of the earth's magnetic field. The whole coil-assembly was kept immersed in liquid nitrogen during the measurement period. The off-balance signal was measured by a two-phase lock-in amplifier (52Ø8, PAR) operating at 333 Hz. The rms field generated was Ø.5 Oe. Four pieces of samples of length 4 cms each were tied to the thin Cu sample holder to obtain the maximum sensitivity. In the sample zone He exchange gas was kept at a very small pressure. One end of the Copper-Constantan thermocouple was soldered at the middle of the sample holder, the output of which was detected by a nanovoltmeter (148, Kiethley). The sample was heated slowly by giving a small current to the heater. Near the transition temperature the heating rate was minimized to about 1 mK/s. By this method we could obtain reproducible , near equilibrium data every 3Ø mK apart.

For the low-temperature measurements similar coil but of smaller length and diameter was used due to the restricted space available inside the cryotip. The secondary coil was about Ø.1 cm in length and the primary 15 cm. The operating frequency of the lock-in amplifier was 3.33 kHz, and the measuring rms field was Ø.1 Oe. External coaxial dc fields (Ø to 6Ø Oe) were produced by a coil placed outside the cryostat. The temperature was measured by a copper-constantan thermocouple.

High-temperature magnetization measurements were done by using a vibrating sample magnetometer (155,PAR). Several pieces of the metallic glasses of length 2-3 mm each were loaded in the

sample holder with the magnetic field in the plane of the ribbon. The output from the magnetometer was directly recorded by an X-Y recorder. A high-temperature oven assembly, in conjunction with the VSM, enabled us to make measurements above 300 K. These measurements were done in the presence of the residual field (30 Oe) of a 9-inch (V-7200, Varian) electromagnet. The sample was heated in the temperature range of 300 to 990 K. A chromel-alumel thermocouple was used to measure the temperature with an accuracy of $\approx$ 1 K. The typical heating rate used in the experiment was 5 K/min, but near the transition temperature, the rate was lowered to 2 K/min. X-ray diffraction at room temperature was taken on the crystallized samples after the thermomagnetic study.

CHAPTER III
RESULTS AND DISCUSSION

3.1 Electrical Resistivity

The samples studied are a) $Fe_5Co_{50}Ni_{17-x}Cr_xB_{16}Si_{12}$ (x = Ø, 5, 1Ø, and 15 designated as A1, A2, A3, and A4 respectively) and b) $Fe_5Co_{50}Mn_{17}B_{16}Si_{12}$ (A5). The ferromagnetic transition temperatures, obtained from χ_{ac} measurements, are between 18Ø and 4ØØ K. T_c decreases with the increase of Cr due to its antiferromagnetic interaction. All the samples except the one containing Mn are ferromagnetic, at least, down to 18 K. The Mn-containing sample has reentrant behavior below 3Ø K. All the samples indicate a resistance minimum. The corresponding T_{min}, which is ≈ 15 K for x=Ø, shifts to ≈ 2ØØ K on addition of Cr/Mn. Figures 3.1 and 3.2 show the normalized resistance r (= R(T) / R(3ØØ K)) versus temperature T. There is no indication of a second minimum at the lower temperatures as observed in other Cr-containing amorphous alloys. (Olivier et al. [39], Rao et al. [41]). The resistivity minima are fairly broad and the percentage change in resistance (ΔR/R) between T_{min} and 8K is ≈ 1% for the Cr-containing samples and 4% for the Mn-containing sample. There is no obvious discontinuity in the resistivity plot near their respective T_c's which almost always lie in the region around the broad minima. The room temperature resistivity of these samples increases with the addition of Cr/Mn. The values of the temperature coefficient of resistance α (= 1/R (dR/dT)) at 3ØØ K are rather small. Table 3.1 summarizes the values of T_c, T_{min}, ρ(3ØØ K), α(3ØØ K) and ΔR/R.

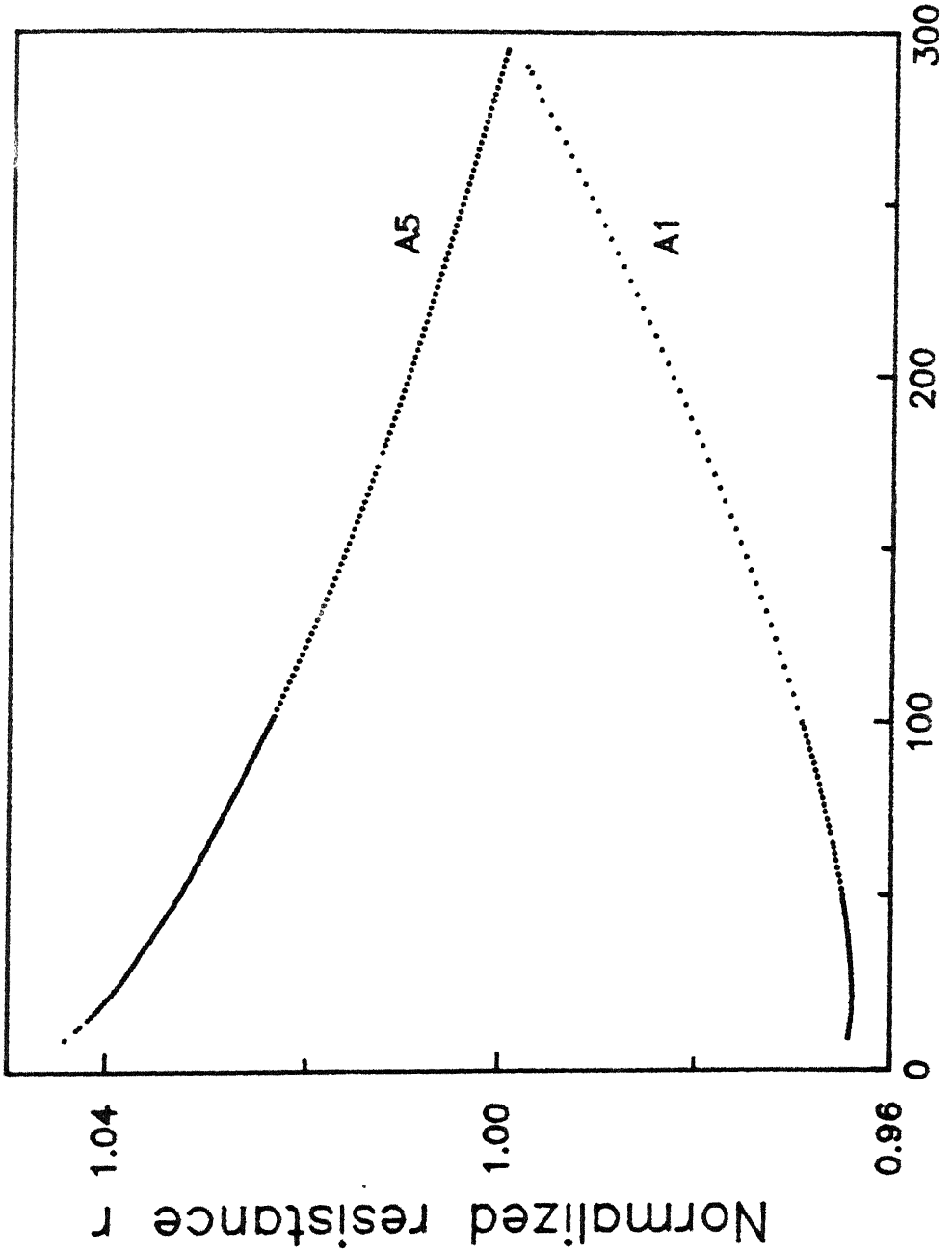

Fig. 3.1 Temperature dependence of the normalized resistivity r = R(T)/R(300 K) for samples A1 ($Fe_5Co_{50}Ni_{17}B_{16}Si_{12}$) and A5 ($Fe_5Co_{50}Mn_{17}B_{16}Si_{12}$).

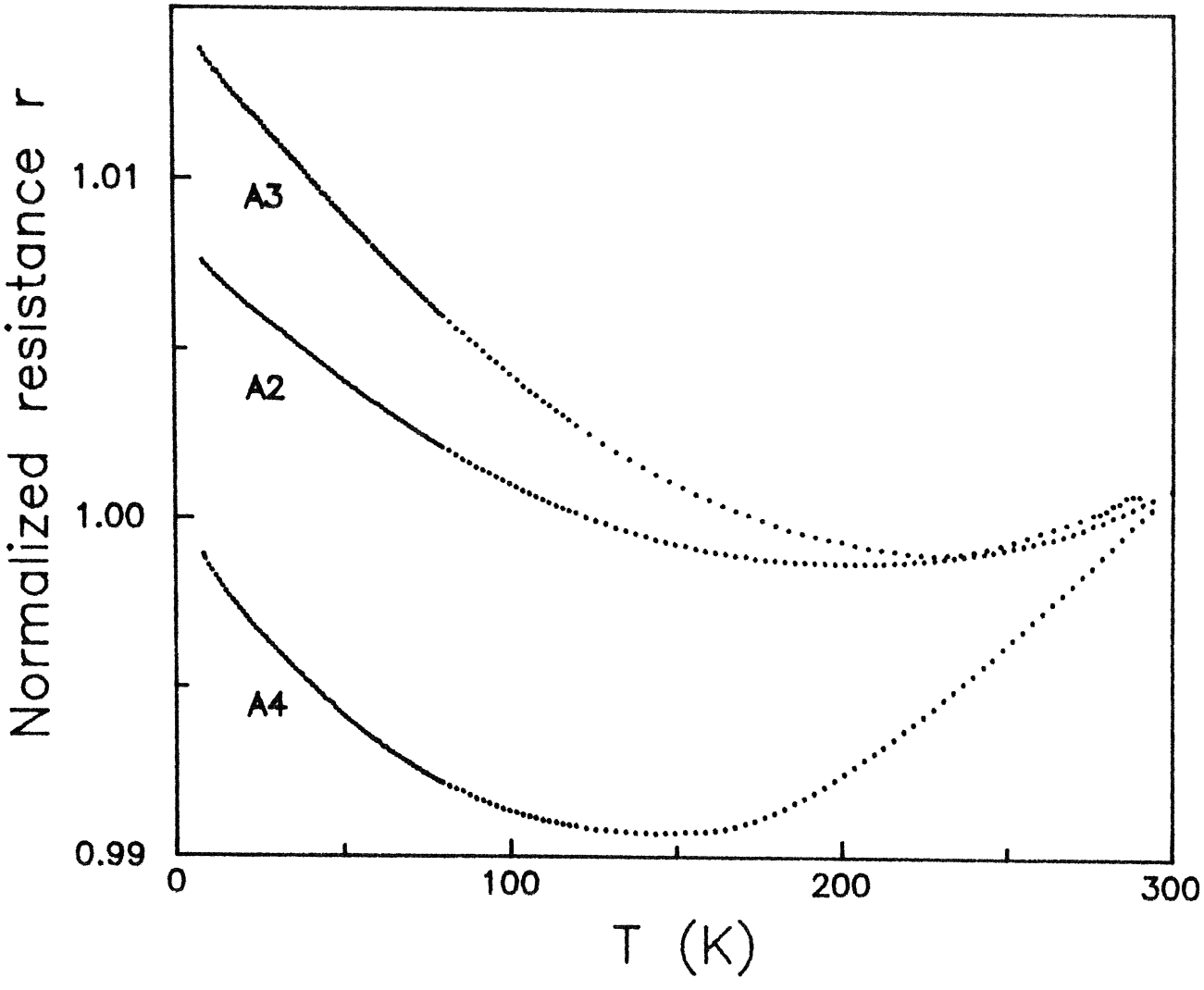

Fig. 3.2 Temperature dependence of the normalized resistivity r = R(T)/R(300 K) for samples A2, A3, and A4 ($Fe_5Co_{50}Ni_{17-x}Cr_xB_{16}Si_{12}$, x = 5, 10, and 15).

Table 3.1

Composition, Curie temperature (T_c), temperature at resistivity minimum (T_{min}), room temperature resistivity (ρ), temperature coefficient of resistance (α) and percentage change in resistance between T_{min} and 8 K, of $Fe_5Co_{50}Ni_{17-x}Cr_xB_{16}Si_{12}$ ($0 \leq x \leq 15$) and $Fe_5Co_{50}Mn_{17}B_{16}Si_{12}$.

Sample	Composition	T_c (K)	T_{min} (K)	ρ (300 K) ($\mu\Omega$ cm)	$\alpha = 1/R\ (dR/dT)$ (10^{-5} K^{-1}) at 300 K	$\Delta R/R$ (%)
A1	x = 0	395	20	150	1.7	-
A2	x = 5	267	200	162	4.4	0.90
A3	x = 10	222	228	162	4.8	1.50
A4	x = 15	174	144	220	9.5	0.83
A5	Mn_{17}	300	>300	254	-10.2	4.40

In the discussion that follows the choice of the temperature regions and the equations to be fitted have been influenced by the χ^2 values obtained from a nonlinear least-squares fitting programme.

A. $T > T_{min}$

The data of sample A1 (x=Ø) between 3Ø and 8Ø K could be fitted well to Eq.(1.7). The value of $\chi^2 = 2.5 \times 10^{-10}$ (Table 3.2) is very close to the experimental resolution in r(T). The fit between 3Ø and 8Ø K with a $T^{3/2}$ term in addition to the T^2 term gave an unphysical negative coefficient for the $T^{3/2}$ term. This observation is at variance with the results of Kettler and Rosenberg [29] and Singhal and Majumdar [31] who find that their results are better described by a positive $T^{3/2}$ magnetic term over and above the structural T^2 term of Eq.(1.7). However, this result is in agreement with that of Kaul et al. [16] who observed that the low-temperature resistivity in amorphous magnetic materials could be described by a T^2 term alone coming from both the magnetic and the structural contributions. The coefficient of the T^2 term (5.8×10^{-7} K^{-2}) of sample A1 (Table 3.2) agrees well with that reported by Kaul et al. [16] on $Fe_{80}B_{20}$ ($\simeq 5.5 \times 10^{-7}$ K^{-2}) showing similar behavior of Co- and Fe-rich samples. Thummes et al. [24] obtained a much larger coefficient of the T^2 ($\simeq 30 \times 10^{-7}$ K^{-2}) term in a Ni-rich series. They argue that on alloying with Ni there is a significant contribution to the d-band conductivity. This is supported by the evidence that the density of states ($N(E_F)$) that they obtain (4.5 (atom eV)$^{-1}$) is $\simeq$ 1Ø times higher

Table 3.2

Fit of sample A1 in the region $T > T_{min}$: Equations, temperature range, coefficients and χ^2 values.

Fit of r to	*Range of T (K)*	*b* ‡	*c* (K^{-2} or $K^{-3/2}$)	χ^2 † (10^{-10})
$a + b T^2$	30 - 80	5.8×10^{-7}	-	2.5
$a + b T$	200 - 300	1.7×10^{-4}		73.0
$a + b T + c T^2$	200 - 300	1.1×10^{-4}	1.3×10^{-7}	4.2
$a + b T + c T^{3/2}$	200 - 300	4.0×10^{-5}	5.5×10^{-6}	4.0

† $\chi^2 = 1/N \sum_{i=1}^{N} (Y_i(\text{fit}) - Y_i(\text{data}))^2 / (Y(\text{mean}))^2$.

‡ *Units of b are* K^{-1}, K^{-2} *for T, and* T^2 *terms respectively.*

than that of the s-band. Our analysis on Cr ($x \neq 0$) substituted samples shows that $N(E_F)$ in these alloys are roughly 1 (atom eV)$^{-1}$. We assume the same value of N(E) for alloy A1 ($x = 0$). The smaller value of $N(E_F)$ for our alloys, compared with those of Thummes et al. [24], justifies the relatively smaller coefficient of the T^2 term.

In the temperature region 200 K < T <300 K, the data are fitted to an expression of the type

$$r(T) = p + q\,T + s\,T^{2}\,. \qquad (3.1)$$

The χ^2 value improves by about a factor of 20 (Table 3.2) when fitted to this expression as against the one of Eq.(1.8). The additional T^2 term is ascribed solely to the magnetic scattering at high temperatures whereas it is indistinguishable from the structural T^2 term at low temperatures. It is difficult to choose between a $T^{3/2}$ and a T^2 term to be added to the T term in Eq. (3.1) at high temperatures, purely on the basis of χ^2 values (Table 3.2) which show equally good fit for both. However, since the $T^{3/2}$ was discarded in the low-temperature fit, we believe it is the T^2 term which describes the magnetic contribution. The necessity of the T^2 term , we find, extends to $T \simeq 0.75\ T_c$ and the coefficient of this term ($s = 1.3 \times 10^{-7}\ K^{-2}$) is even higher than those reported with analyses done only up to $0.5\ T_c$ [16,31]. At temperatures even beyond T_c, the T^2 term ($s = 0.77 \times 10^{-7}\ K^{-2}$), in addition to the linear term in T ($q = 5.1 \times 10^{-5}\ K^{-1}$), is clearly observed in the case of sample A4 (T_c = 174 K) in the region 240 K < T <300 K. The existence of a magnetic term at $T > T_c$ and which is increasing even beyond T_c and saturating at $T \simeq 2$

T_c, has been shown and discussed by Kettler and Rosenberg [29] for a FeNi system. The value of θ_D for sample A1 is obtained from the coefficients of the high-and low-temperature fits to Eqs. (3.1) and (1.7), respectively. The relation for θ_D, taking into account the additional T^2 term in the high temperature fit, is [16]

$$\theta_D = \frac{\pi^2}{6}\left[\frac{q}{b - s}\right] \quad .$$

From this we obtain a realistic value for θ_D = 402 K.

B. $T < T_{min}$

We have used $\sigma(T)$ in the discussion which follows, as opposed to $\Delta\sigma(T) = \sigma(T)-\sigma(0)$ used elsewhere [189]. The value of $\sigma(0)$ (the extrapolated value of $\sigma(T)$ to 0 K) in our case does not remain the same when extrapolated from different regions of temperature. This result is different from that of Howson and Greig [189] who obtained $\sigma(0)$ to be the same, within experimental error, when extrapolated from different regions of temperature. Thus $\sigma(0)$ in our case is a temperature region-dependent parameter which however does not in anyway influence our analysis and conclusions. As a matter of fact, we find that the choice of $\sigma(0)$ hardly affects the coefficients of T and $\sqrt{T}$ terms of Eqs. (1.14) and (1.15) respectively.

In the temperature region between 8 K (the lowest attainable here) and 20 K, for all the samples (A2 - A5) the data could be fitted to $\sigma(T) = a + b\sqrt{T}$ as given by Eq. (1.17). The coefficients and the χ^2 values are summarized in Table 3.3.

Table 3.3

Fit to $\sigma(T) = \sigma(0) + a\sqrt{T}$ below T_{min} (8 - 20 K) : Samples, coefficients, density of states $N(E_F)$, diffusion constant (D) and χ^2 values.

Sample	$\sigma(0)$ (10^5) $(\Omega\ m)^{-1}$	a (10^2) $(\Omega\ m)^{-1}\ K^{-1/2}$	$N(E)$ $(atom\ eV)^{-1}$	D (10^{-5}) $m^2\ s^{-1}$	χ^2 (10^{-10})
A2	6.11987	4.30	0.95	4.0	1.7
A3	6.07921	5.54	1.50	2.4	4.6
A4	4.54092	4.86	0.89	3.2	2.0
A5	3.75518	10.09	3.20	0.7	3.3

The coefficient of $\sqrt{T}$ ((400 - 1000) $(\Omega\ m)^{-1}\ K^{-1/2}$) is in good agreement (inspite of a narrow range of temperature used here) with the near universal value of 600 $(\Omega\ m)^{-1}\ K^{-1/2}$ obtained by Cochrane and Strom-Olsen [56] and Rapp et al. [54], based on an analysis of a large class of non-magnetic as well as magnetic materials. Similar values have also been quoted by Thummes et al. [24] and Olivier et al. [39] on ferromagnetic materials. The diffusion constant D, obtained from the slope of $\sigma(T)$ plot and Eq. (1.17), keeping $\tilde{F}_\sigma = 0$, is in the range (0.7 - 4.0) $\times 10^{-5}$ m^2/s for all the four samples (Table 3.3). Within themselves they however do not show any concentration dependence. The values are

similar to those obtained by Olivier et al. [39] ($\simeq 3 \times 10^{-5}$ m^2/s) and Thummes et al. [24] ($\simeq 1.3 \times 10^{-5}$ m^2/s). Consequently, the value of the density of states, calculated using the Einstein relation $D = (\rho(0)\, e^2\, N(E_F))^{-1}$, is $N(E_F) \simeq 1$ (atom eV)$^{-1}$ for Cr-containing samples and $\simeq 3.2$ (atom eV)$^{-1}$ for the sample with Mn (Table 3.3).

In explaining the nonuniversality of the Mooij correlation Tsuei [8] has suggested that electron localization plays a significant role in determining the sign and magnitude of TCR (temperature coefficient of resistivity) at temperatures even as high as room temperature. Howson and Greig [190] have analyzed the data of a few non-magnetic samples (CuTi, CuHf, CuZr), which show resistance minima at high temperatures, between 30 K and 300 K and have observed the temperature dependence as given in Eqs.(1.14) and (1.15). In our case the samples A2, A3, and A4 have the disadvantage that this analysis could not be carried over a large range of temperature because of resistivity minima occurring around 200 K only. However, sample A5 is free from such restrictions; it has a $T_{min} > 300$ K and also a $T_c = 300$ K. Therefore more emphasis has been given on the analysis of the data of sample A5.

The region between 55 and 90 K of A5 shows a linear temperature dependence as given by Eq.(1.14). In the region between 100 and 300 K a $\sqrt{T}$ behavior, as given by Eq.(1.15), is found. The coefficients and the χ^2 values of the fit are summarized in Table 3.4.

Table 3.4

Fit in the intermediate and high temperature regions below T_{min} : Samples, equations, temperature range, coefficients and χ^2 values.

Sample	*Fit of* σ *to*	*Range of T* (K)	*a* (10^5 $(\Omega m)^{-1}$)	*b* ($(\Omega m\ K)^{-1}$) or ($(\Omega m^{-1} K^{-1/2}$)	χ^2 (10^{-10})
A2	a + b T	25 - 50	6.12961	48.5	0.6
	a + b $\sqrt{T}$	55 - 100	6.10802	648.2	2.7
A3	a + b T	25 - 50	6.09075	662.6	3.3
	a + b $\sqrt{T}$	55 - 110	6.05332	989.4	2.6
A4	a + b T	20 - 40	4.55333	47.8	4.7
	a + b $\sqrt{T}$	45 - 70	4.53924	528.0	5.5
A5	a + b T	55 - 90	3.79457	66.9	3.2
	a + b $\sqrt{T}$	100 - 300	3.73304	1276.0	7.5

The χ^2 values obtained are comparable to the experimental accuracy indicating excellent fit. Figure 3.3 shows the plot of $\ln\Delta\sigma$ against lnT. In ln-ln *plots* the use of $\Delta\sigma$ is essential for finding the exponent of T. The three regions, corresponding to $\sqrt{T}$ at low temperature, T in the intermediate region and again $\sqrt{T}$ at high temperature, are amply evident from the figure. In calculating $\Delta\sigma$ ($\sigma(T) - \sigma(\emptyset)$), $\sigma(\emptyset)$ is obtained from the respective regions of fit (Table 3.4). The same procedure is followed for samples A2-A4 and the resulting plots, similar to that of sample A5, albeit in a contracted temperature scale, are shown for A2 and A3 in Fig. 3.4, and the best-fitted coefficients and the χ^2 values are included in Table 3.4. In both Figs. 3.3 and 3.4 the data points in the region intermediate between two regions of fit are not included. Similar plots are reported for the non-magnetic amorphous systems in $\sqrt{T}$ and T regions at low and intermediate temperatures. Here we are able to clearly demonstrate all the *three* regions on a single figure hitherto only theoretically predicted. It is interesting to note here that the electron-phonon scattering mechanism had led Meisel and Cote [191] to formulate the diffraction model and explain the familiar temperature dependence above T_{min} , $\rho \propto T^2$ at $T < \theta_D$ and $\rho \propto T$ at $T > \theta_D$. In this model the electron-phonon scattering increases the resistivity, or in other words, decreases the conductivity as a function of temperature, as it should be for normal metallic systems. In the localization theory the *same* inelastic electron-phonon scattering is used to explain the reduction of resistivity from its elastic collision-assisted value at T=Ø. Assuming the elastic mean free path length $l_e \simeq 3$Å (Tsuei)

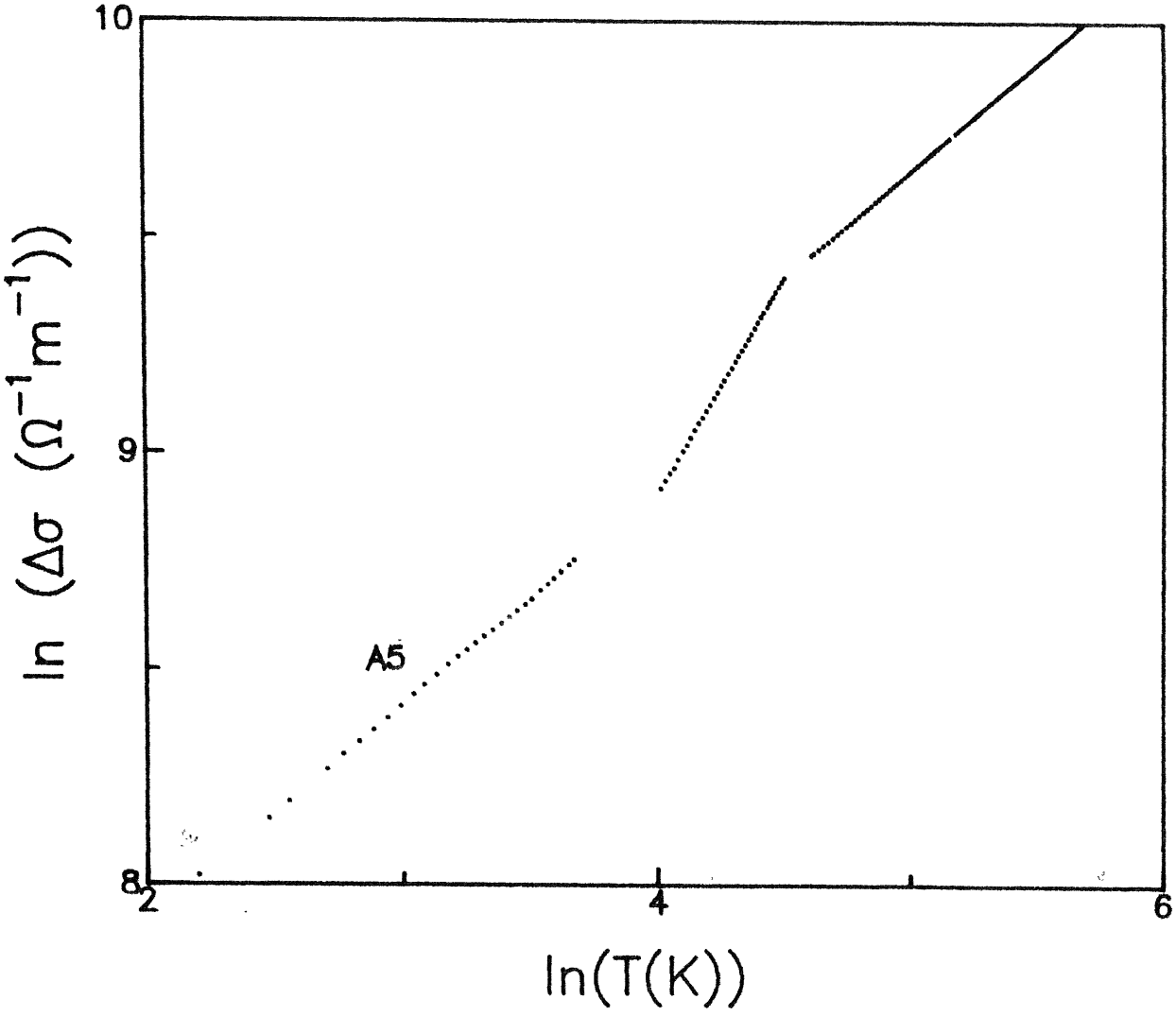

Fig. 3.3 Plot of $\ln\Delta\sigma$ versus $\ln T$ for sample A5 ($Fe_5Co_{50}Mn_{17}B_{16}Si_{12}$) showing three distinct regions of $\sqrt{T}$, T, and $\sqrt{T}$ dependences in agreement with the predictions of interaction and localization theories. The points in the overlap region are omitted.

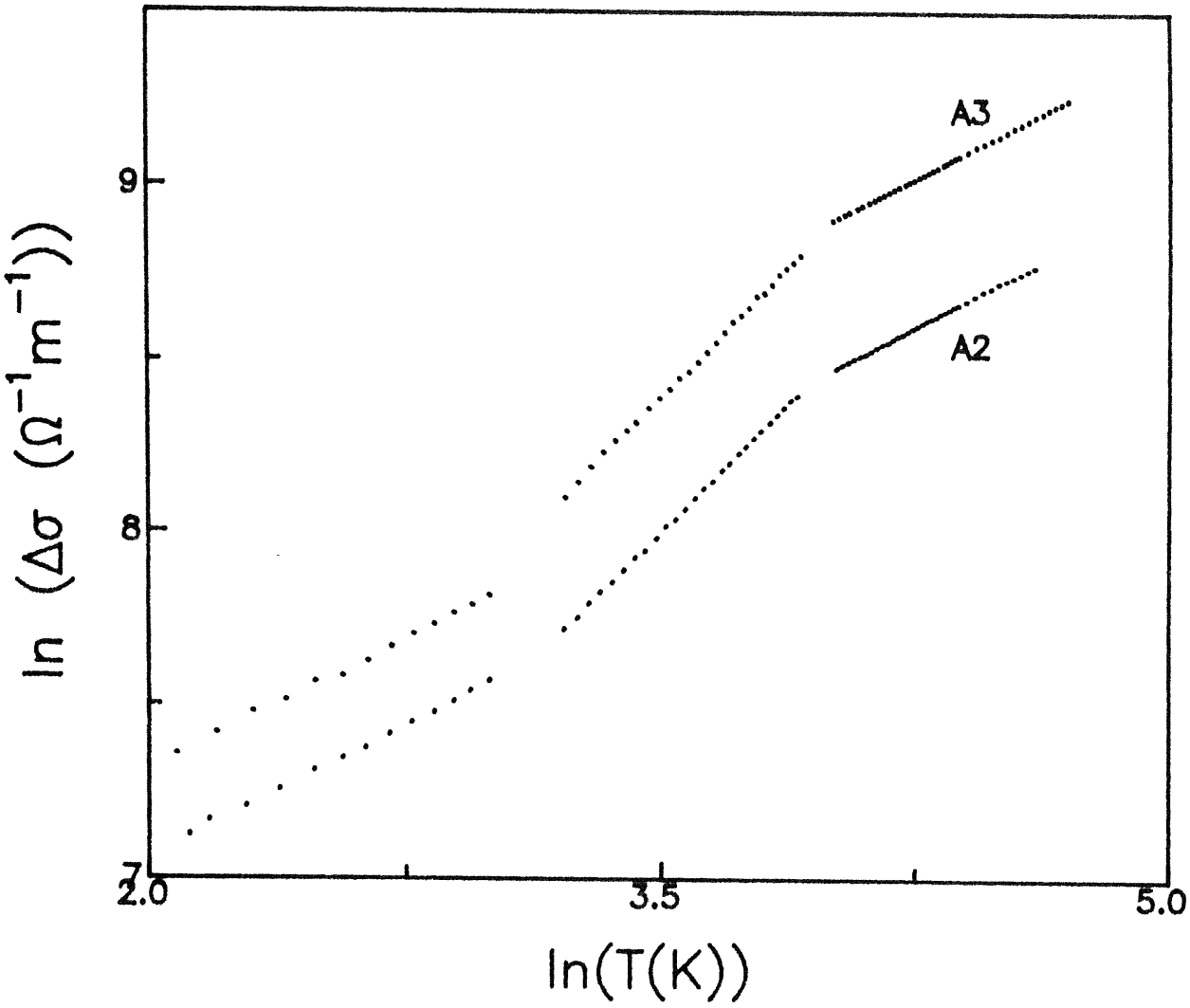

Fig. 3.4 Plot of $\ln\Delta\sigma$ versus lnT for samples A2 and A3 ($Fe_5Co_{50}Ni_{17-x}Cr_xB_{16}Si_{12}$, x = 5 and 10) showing three distinct regions of $\sqrt{T}$, T and $\sqrt{T}$ dependences in agreement with the predictions of interaction and localization theories. The points in the overlap region are omitted.

[8], we obtain from Eq.(1.13) and the slope of the $\Delta\sigma(T)$ curve for A5, the value of the inelastic mean free path length to be 9×10^{-4} m T^{-2} in the range 55-90 K and 2.5×10^{-6} m T^{-1} in the range 100-300 K. These values are similar to those of 7.7×10^{-4} m T^{-2} for $T < \theta_D/3$ and 1.8×10^{-6} m T^{-1} for $T > \theta_D/3$ reported in the case of non-magnetic $Cu_{50}Ti_{50}$ (Howson) [182].

The present samples being ferromagnetic, we have made an attempt to find if contributions to resistivity arising from spin disorder, which gives an inelastic term, could be detected. Our method of analysis is as follows. In the region between 55 and 90 K the localization theory predicts that

$$r(T) - r(0) = - a T \quad , \tag{3.2}$$

where $r(T) = R(T)/R(300\ K)$. In the presence of magnetic scattering the mean free path would be modified as

$$l_{eff}^{-1}(T) = l_i^{-1}(T) + l_m^{-1}(T) \quad , \tag{3.3}$$

where $l_m^{-1}(T)$ is the reciprocal mean free path attributed to magnetic scattering. Replacing l_i by l_{eff} in Eq.(1.13) and noting that $l_m^{-1}(T) \propto T^{3/2}$, we get for $T < T_C$

$$(r(T) - r(0))^2 = a T^2 + b T^{3/2} \quad \text{for} \quad T < \theta_D \tag{3.4}$$

and

$$(r(T) - r(0))^2 = a T + b T^{3/2} \quad \text{for} \quad T > \theta_D . \tag{3.5}$$

The above two relations are on the assumption that $T^{3/2}$ will be the dominant magnetic scattering term as predicted by Richter et al. [36]. However, we observe that in A1 the inclusion of the $T^{3/2}$ term did not give any meaningful result. A T^2 term was essential in addition to the linear term at higher temperatures. The T^2 term is identified as the contribution from the magnetic scattering

which is indistinguishable from the T^2 term due to structural contribution in the low temperature region. If this is so, then $l_m^{-1}(T) \propto T^2$, which gives

$$(r(T) - r(0))^2 = a T^2 \qquad \text{for} \quad T < \theta_D \qquad (3.6)$$

and

$$(r(T) - r(0))^2 = a T + b T^2 \qquad \text{for} \quad T > \theta_D . \qquad (3.7)$$

On fitting the data to Eqs. (3.4)-(3.7) we find that the $T^{3/2}$ *terms* in Eqs. (3.4) and (3.5) are smaller by a factor of 1000 than the T^2 and T terms. In Eq. (3.6) the magnetic term is indistinguishable from the structural term. For $T > \theta_D$ (Eq.(3.7)), the magnetic T^2 term is smaller again by a factor of 1000 in comparison to the T term. The values of χ^2 also have not improved on addition of the magnetic term, be it $T^{3/2}$ or T^2. Thus we conclude that the magnetic term, if present, is very small and does not influence the above analysis in terms of the localization theory.

3.2 Magnetoresistance (MR)

We first describe and explain the results obtained for samples A1 - A5 and B5 and then try to correlate them with the various existing theoretical models and other experimental observations.

In Fig. 3.5 we have plotted the magnetoresistance $\Delta\rho/\rho$ (= $(\rho(H) - \rho(50\ Oe))/\rho(50\ Oe)$) of sample A1 at several temperatures between room temperature and 11 K. The choice of $\rho(50\ Oe)$ instead of $\rho(0)$ is for two reasons; (1) It was difficult to measure $\rho(T,0)$ at each temperature as it required taking the cryostat out of the

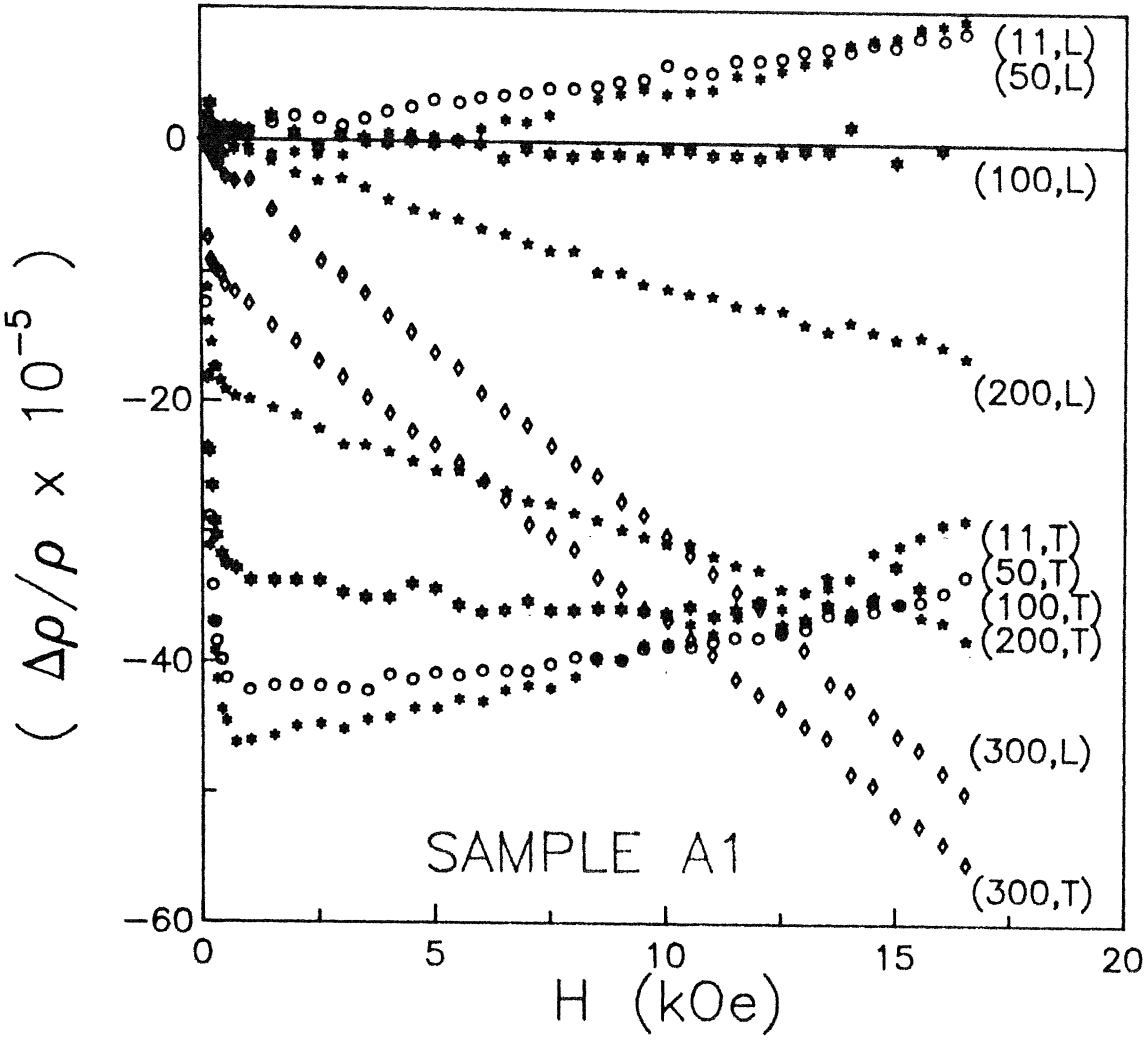

Fig. 3.5 Magnetoresistance ($\Delta\rho/\rho$) versus external magnetic field at several constant temperatures for both longitudinal (L) and transverse (T) orientations for sample A1 ($Fe_5Co_{50}Ni_{17}B_{16}Si_{12}$).

magnet pole pieces at each temperature which posed serious experimental difficulties with the existing set-up. (2) The magnetoresistance (MR) of these samples is very small and so would introduce negligible error in calculation and comparison of their magnitudes with those of others. In both the longitudinal ($J \parallel M$) and transverse ($J \perp M$) directions the MR is negative except for temperatures below 50 K where in the longitudinal case the MR becomes positive. At low fields, in the longitudinal direction, the sharp rise in MR observed in ferromagnets and associated with the domain rotation, is visibly absent. This feature is, however, present in the transverse direction. Therefore, $(\Delta\rho_{\parallel} / \rho)_{H=0} \simeq 0$, and the ferromagnetic anisotropy of resistance FAR ($= \Delta\rho_{\parallel_S}/\rho - \Delta\rho_{\perp_S}/\rho$) practically arises from the extrapolated transverse magnetoresistance. The demagnetization field is calculated in both the orientations and it is negligibly small and, therefore, while calculating the FAR we extrapolate the high-field curve to $H_{applied} = 0$, whereas it would have been more appropriate to extrapolate it to $H_{internal} = 0$. The high-field slopes ($1/R \ dR/dH$), in both the orientations, are approximately the same. The slope at room temperature is negative and large ($\sim -3 \times 10^{-8}$ $gauss^{-1}$) and is comparable to those of other crystalline as well as amorphous ferromagnets [58]. The slope shows a strong temperature dependence as the temperature is lowered. It becomes $\simeq 0$ at around 100 K and below this temperature the slope is positive. The slopes, except at 300 K, are small as compared to Cr-containing samples and therefore the dispersion in the data apparently appears to be large.

In Figs. 3.6-3.8 we show the plot of $\Delta\rho/\rho$ vs H for samples A2, A3, and A4. These three samples, among themselves, behave in a similar manner. Both in the longitudinal as well as in the transverse directions the high-field slopes are positive. They are nearly identical in both the orientations. This particular feature of positive slope has been observed in other Cr- or Mo - containing samples [39,58]. However, in contrast to the previous measurements, we find that in these samples the curves are not linear but has a quadratic component as well. Above T_c, the curves are highly quadratic. We determine both these coefficients from a least-squares fit analysis. The magnetoresistance increases with the increase in temperature up to T_c. Above T_c, the magnetoresistance falls. The behavior above T_c is nearly quadratic and as we go further away from T_c, the MR continues to fall. As in A1, in the longitudinal direction, at low fields the sharp rise in the MR is not observed. From the MR measurements one may obtain an estimate of the direction of the magnetization with respect to the ribbon axis. Assuming that the magnetization lies in the plane of the ribbon, the angle θ that it makes with respect to the ribbon axis is obtained from the relation

$$\cot^2\theta = - \frac{\Delta\rho_\perp / \rho}{\Delta\rho_\parallel / \rho} \quad .$$

Since $\Delta\rho_\parallel/\rho \simeq 0$ for samples A1- A4, we obtain $\theta \simeq 0$. This shows that the magnetization vector **M** is in the direction parallel to the ribbon axis. Direct measurements of domain structure by Bitter technique [192] and neutron depolarization method [193] reveal that alloys, having nearly zero magnetostriction, have long

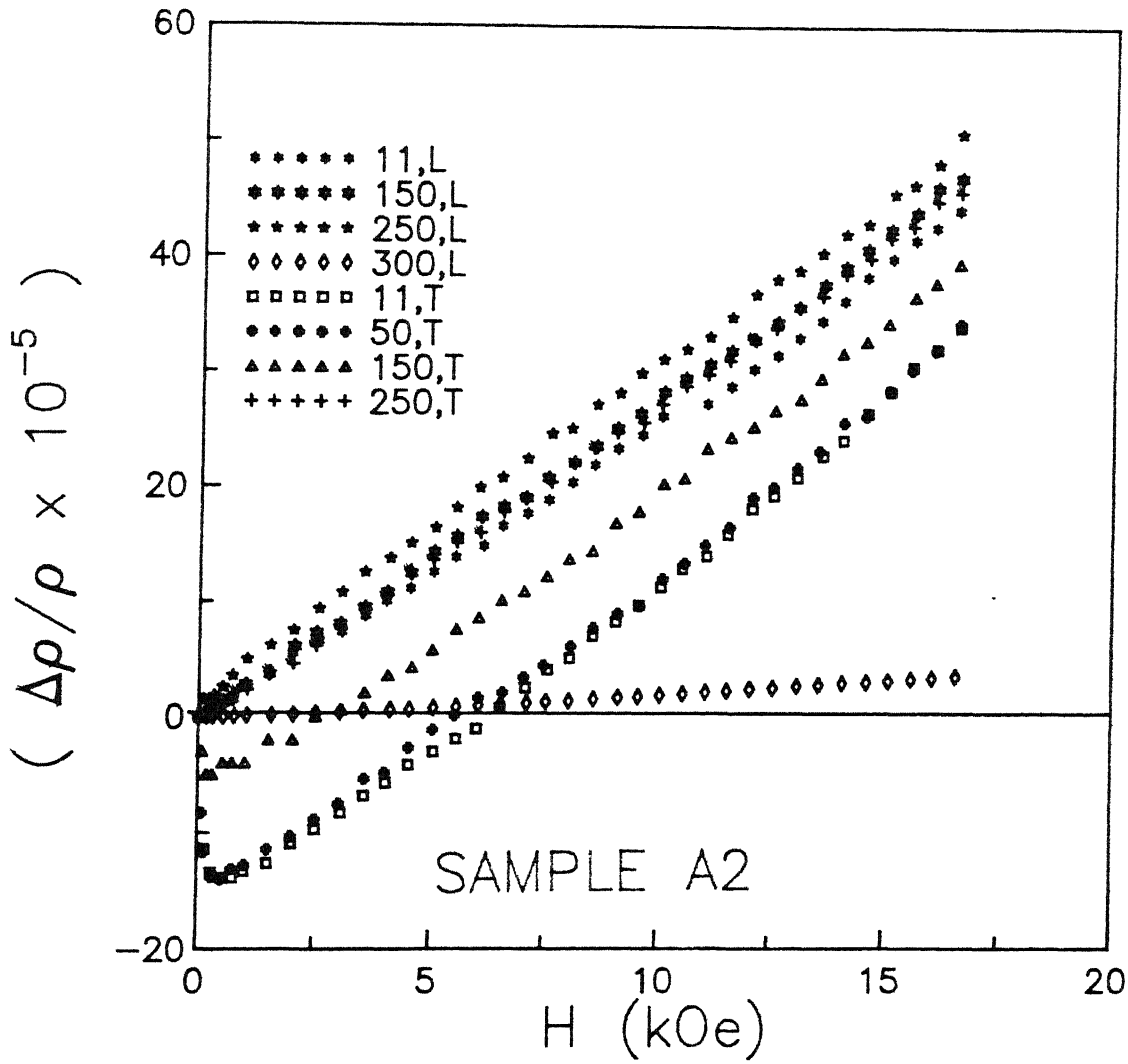

Fig. 3.6 Magnetoresistance ($\Delta\rho/\rho$) versus external magnetic field at several constant temperatures for both longitudinal (L) and transverse (T) orientations for sample A2 ($Fe_5Co_{50}Ni_{12}Cr_5B_{16}Si_{12}$).

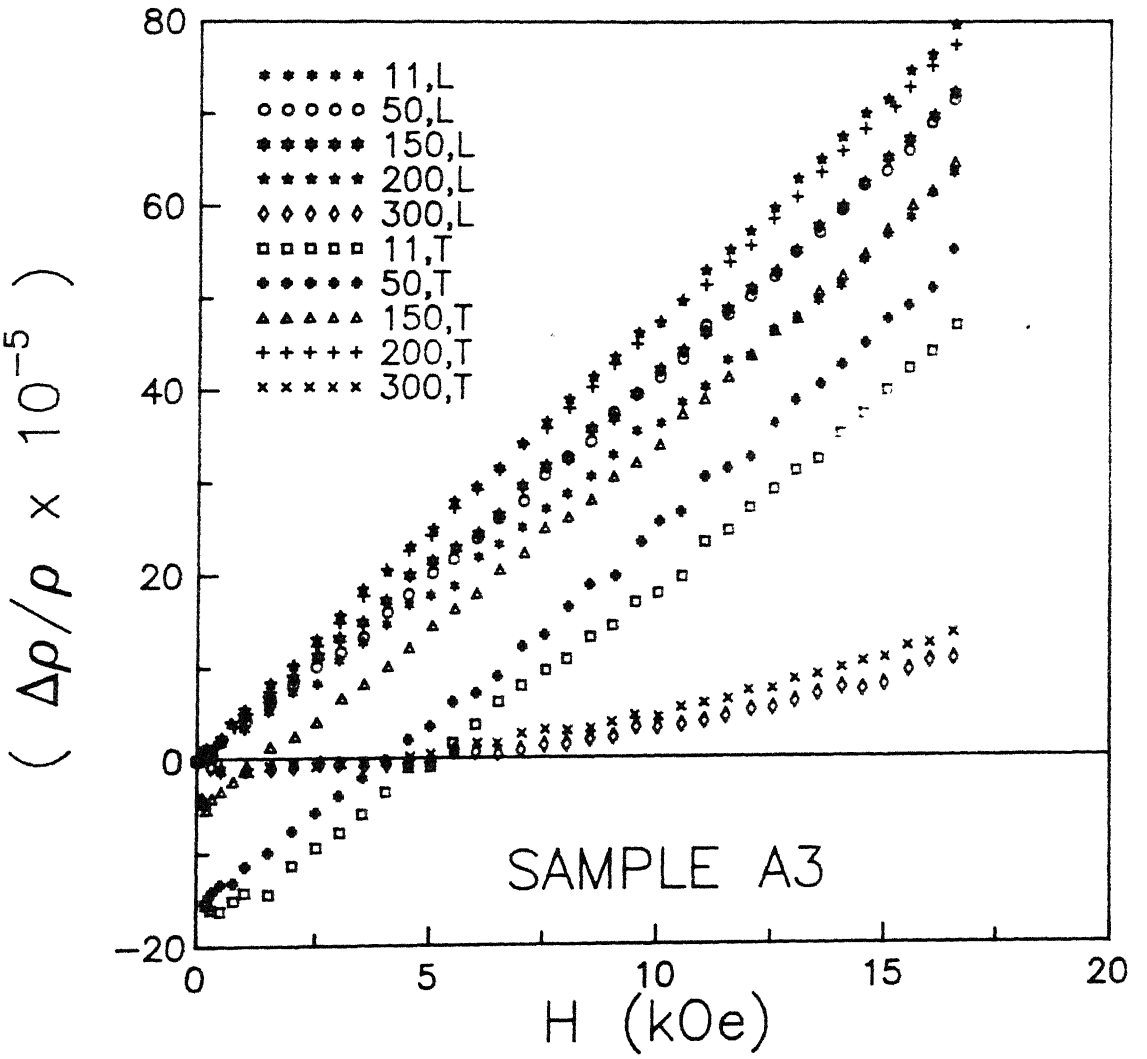

Fig. 3.7 Magnetoresistance ($\Delta\rho/\rho$) versus external magnetic field at several constant temperatures for both longitudinal (L) and transverse (T) orientations for sample A3 ($Fe_5Co_{50}Ni_7Cr_{10}B_{16}Si_{12}$).

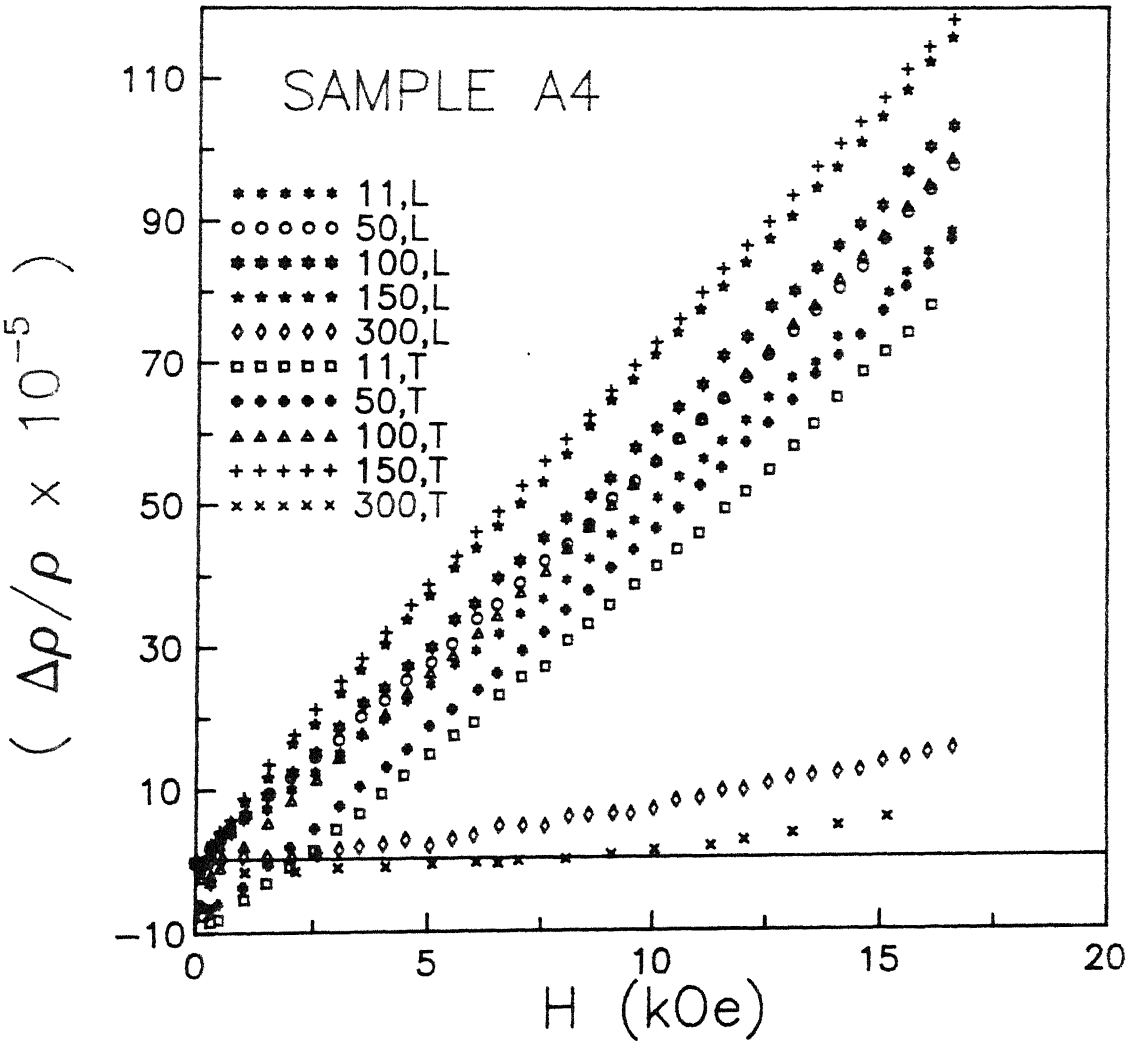

Fig. 3.8 Magnetoresistance ($\Delta\rho/\rho$) versus external magnetic field at several constant temperatures for both longitudinal (L) and transverse (T) orientations for sample A4 ($Fe_5Co_{50}Ni_2Cr_{15}B_{16}Si_{12}$).

straight 180° walls parallel to the ribbon axis and zones with magnetization perpendicular to the ribbon plane are absent. The present alloys have compositions almost identical with the reported [179] nearly zero-magnetostriction alloys. In the light of this picture our MR measurements confirm the absence of magnetization domains in the direction perpendicular to the ribbon axis, and therefore, the absence of anisotropy in the longitudinal direction. This observation also add to the long-held view that the 'anomalous' behavior observed in ferromagnetic materials at low fields is associated with the domain rotation, and the FAR is a consequence and a measure of the intrinsic magnetization of the samples.

In Figs. (3.9) and (3.10) MR is plotted as a function of H for samples A5 and B5 respectively. For A5 the longitudinal MR is positive and the transverse one is negative. The high-field slope is negative for both. Both the shape and the value of the MR show a strong temperature dependence. The absolute value of the slope is small ($\sim 1 \times 10^{-8}$ Oe^{-1}) at the lowest temperature in comparison to other samples of the series. The slope approaches 0 as $T \rightarrow T_c$. In fact, it becomes nearly zero at $T \simeq T_c/2$. At around T $\sim$ 250 K (not shown in Fig. 3.9) it has a positive slope. The low-field magnetization data of this sample shows that at low temperatures the sample show characteristics of reentrant spin glasses (RSG). The MR results corroborate the magnetization studies (as shown below) at low temperatures, but the temperature dependence of the slope in the ferromagnetic regime is different from that expected in a ferromagnet. In the case of

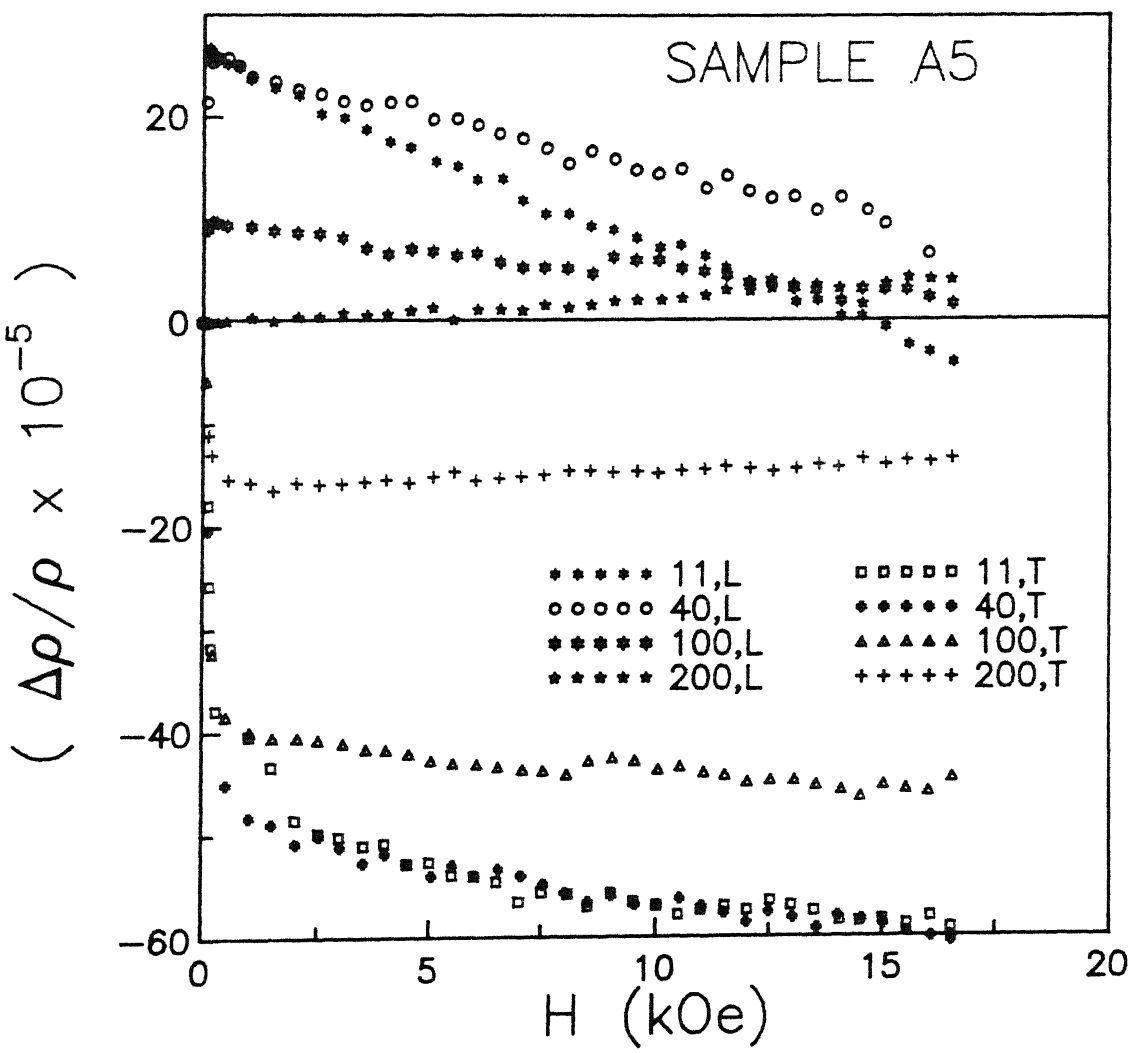

Fig. 3.9 Magnetoresistance ($\Delta\rho/\rho$) versus external magnetic field at several constant temperatures for both longitudinal (L) and transverse (T) orientations for sample A5 ($Fe_5Co_{50}Mn_{17}B_{16}Si_{12}$).

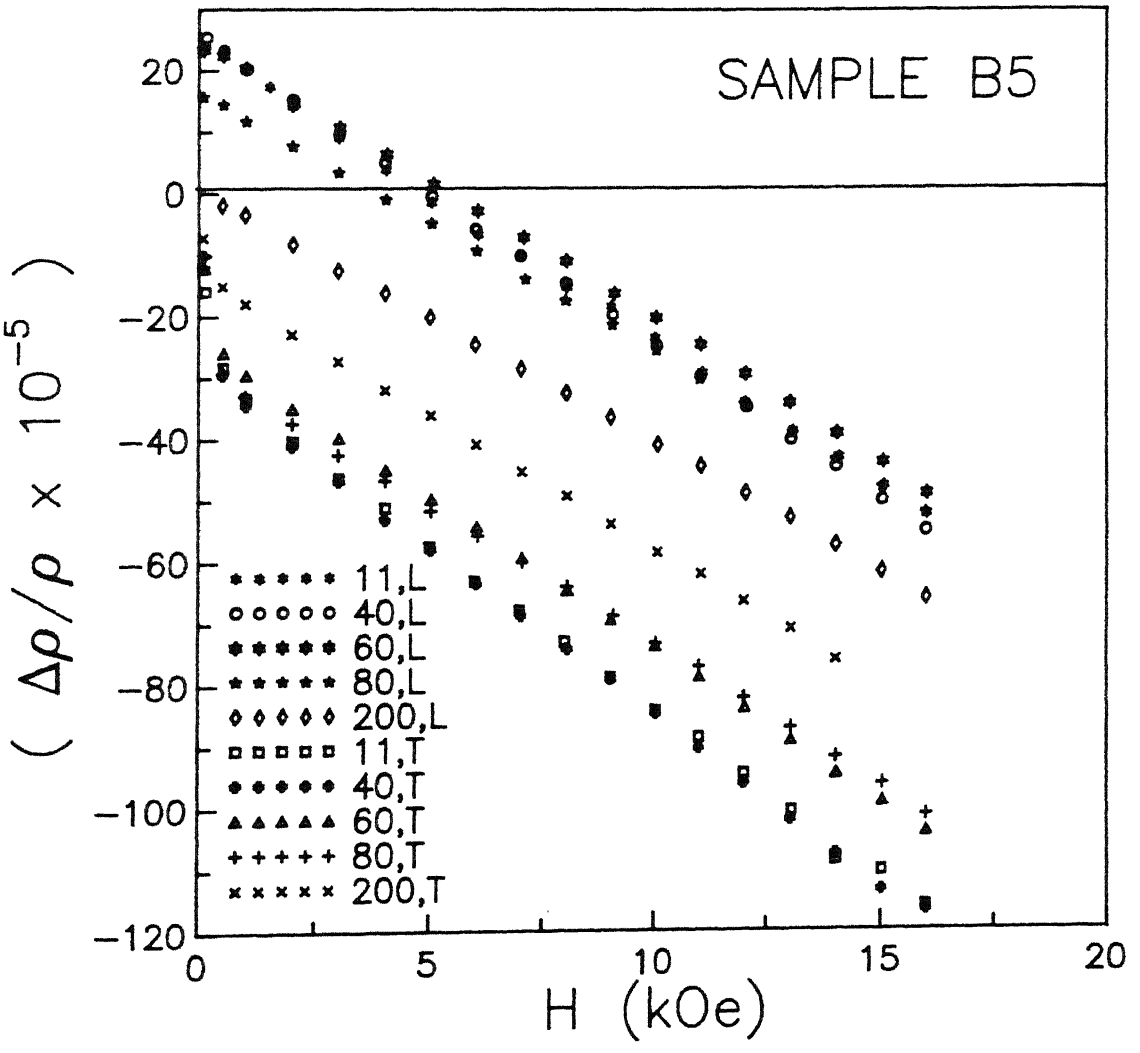

Fig. 3.10 Magnetoresistance ($\Delta\rho/\rho$) versus external magnetic field at several constant temperatures for both longitudinal (L) and transverse (T) orientations for sample B5 ($Fe_{7.8}Co_{31.2}Ni_{24}Mn_{15}(BSi)_{22}$).

ferromagnets the negative slope is nearly zero at low temperatures and its magnitude increases as T_c is approached. The increase in the magnitude of the slope is related to the increase in susceptibility. In this sample the slope tends to zero and then becomes positive as $T \rightarrow T_c$.

In sample B5 the negative high-field slopes are large, due to which the positive MR cuts the field-axis and becomes negative as the field is increased (Fig. 3.10). Similar to A5, the low -temperature phase of this sample is not a pure ferromagnetic phase. The magnitude of the high-field slope decreases as the temperature is increased. It reaches a constant value and on further increase of temperature the magnitude of the slope increases as expected from a sample undergoing a RSG → FM → PM phase transformations as the temperature is increased (discussed later).

Ferromagnetic Anisotropy of Resistance (FAR)

In general, the FAR of these samples are an order of magnitude smaller (≤ 0.05%) than those reported for the FeB glasses [31,58,64]. This may be related to the values of saturation magnetization in the two series of samples. The saturation magnetizations of the present samples are smaller by about a factor of 10 than those of the FeB samples. A comparison made by Yamasaki et al. [59] on $Fe_{84}B_{16}$ and $Co_{83}B_{17}$ alloys shows that the FAR at 0 K of $Fe_{84}B_{16}$ (0.73%) is larger than that of $Co_{83}B_{17}$ (0.11%).

It is found that the substitution of Cr, W, or Ni in Fe-B-Si

alloys lowers the FAR [62,194]. Of the three, Cr is found to lower the FAR value most drastically. The decrease is more pronounced when Fe is substituted by Ti, V, Cr, and Mn than in the cases of Co- and Ni-based metallic glasses [194]. The variation of the FAR follows a pattern similar to that of the magnetic moment. This suggests a correlation between the magnetic moment and the FAR. A plot of ln $\Delta\rho/\rho$ (FAR) versus ln $\bar{\mu}$ yields a straight line whose slope (m) and intercept (A) are temperature-dependent parameters. We find that with the substitution of Cr, the FAR at 11 K decreases from about Ø.Ø5 % to Ø.Ø1 %. Substitution of Mn in place of Ni (A5) increases the FAR at the lowest temperature which also correlates with the magnetization data where it is observed that substitution of Mn raises $\bar{\mu}$ whereas Cr lowers it. In Fig. 3.11 we show a plot of log ($\Delta\rho/\rho$) vs log $\bar{\mu}$. It shows that $\Delta\rho/\rho$ decreases with $\bar{\mu}$ and roughly falls on a straight line. We obtain a value of m $\simeq$ 8. The values of m range between 1 and 27 [62-64]. Kaul [65] had earlier pointed out that this value of m varies significantly with the sample composition and temperature and is of little significance. Nevertheless, there exists a definite correlation between the saturation magnetic moment and the FAR and maybe there is some other equation which expresses it better than the very simplistic expression used above.

The model proposed by Campbell et al. [6Ø,61] studies the effect of magnetization on the FAR. Calculations, based on this model, yield the following expressions for FAR at low temperatures [195]:

$$\frac{\Delta\rho}{\rho} = \gamma\ (\ \alpha - 1\ ) + 3\ \beta\ \frac{\alpha}{\alpha + 1} \quad , \tag{3.8}$$

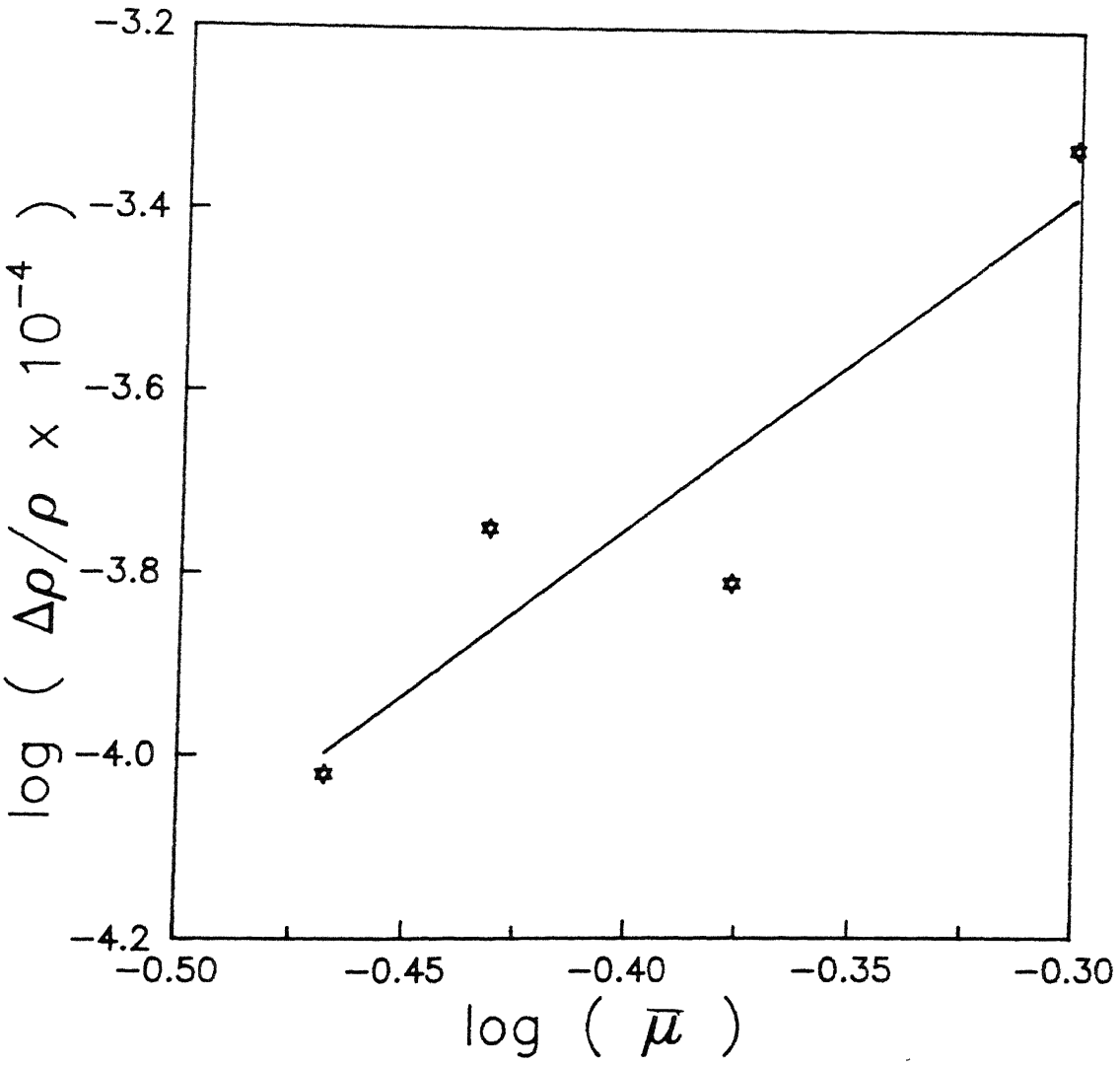

Fig. 3.11 Plot of log(FAR) versus log($\bar{\mu}$).

$$\alpha = \frac{\rho_{\downarrow}^{o}}{\rho_{\uparrow}^{o}} \quad , \tag{3.9}$$

$$\beta = \frac{-7}{90} \left[\frac{\lambda'}{\Delta} \right]^2 \left(1 - 4 \cos^2 \eta_2^{\uparrow} \right) \sin^2 \eta_2^{\uparrow} \quad , \tag{3.10}$$

and $$\gamma = \frac{3}{4} \left[\frac{\lambda}{H_{ex}} \right]^2 \quad . \tag{3.11}$$

$\rho_{\uparrow}^{o}$ and $\rho_{\downarrow}^{o}$ are the residual resistivities for the spin-up and spin-down electrons respectively, λ' is the local spin-orbit coupling constant, Δ is the virtual bound state width, $\eta_2^{\uparrow}$ is the l = 2 phase-shift. λ is the average value of the spin-orbit coupling constant in the d-band, and H_{ex} is the exchange energy that splits the $d_{\uparrow}$ and $d_{\downarrow}$ bands. For the present series of alloys, $\lambda' \ll \Delta$, and therefore β can be neglected, and the value of γ estimated from a number of experimental data [195], is taken as $\simeq$ Ø.Ø1. Therefore Eq. (3.8) can be rewritten in the form

$$\frac{\Delta\rho}{\rho} = \gamma \left(\alpha - 1 \right) \quad . \tag{3.12}$$

The above equation has been used as a criterion for determining whether a given alloy is 'weak' or a 'strong' ferromagnet. A weak ferromagnet has holes in both the $d_{\uparrow}$ and $d_{\downarrow}$ bands, while a strong ferromagnet has holes only in the $d_{\downarrow}$ band. Therefore, a weak ferromagnet will have $\rho_{\downarrow}^{o} \simeq \rho_{\uparrow}^{o}$, since s-d scattering is permitted for both directions of spin, but a strong ferromagnet will have $\rho_{\downarrow}^{o} \gg \rho_{\uparrow}^{o}$, because s-d scattering dominates in the spin-down band but is forbidden for the spin-up band, as there are no $d_{\uparrow}$ electrons at the Fermi surface. Thus for strong ferromagnets $\Delta\rho/\rho$ will be large. In known strong ferromagnetic systems (crystalline NiCo), $\Delta\rho/\rho$ can be as high as 15 %.

We calculate the value of $\rho^{o}_{\uparrow}$ and $\rho^{o}_{\downarrow}$ from the above set of equations to see if, in the above context, the present samples can be described as weak or strong ferromagnets. From Eqs. (3.9) and (3.10) we get the following relations:

$$\rho^{o}_{\downarrow}(x) = \rho^{o}(x)\left[\gamma^{-1}\left[\frac{\Delta\rho}{\rho}(x)\right] + 2\right] \quad , \qquad (3.13)$$

and $$\rho^{o}_{\uparrow}(x) = \rho^{o}_{\downarrow}(x)\left[\gamma^{-1}\left[\frac{\Delta\rho}{\rho}(x)\right] + 1\right]^{-1} \quad , \qquad (3.14)$$

where $$\rho^{o}(x) = \frac{\rho^{o}_{\uparrow}\,\rho^{o}_{\downarrow}}{(\rho^{o}_{\uparrow} + \rho^{o}_{\downarrow})} = \frac{\rho^{o}_{\downarrow}}{(1+\alpha)} \qquad (3.15)$$

and ρ^{o} is the value of the residual resistivity at 11 K. We choose three samples at the extreme ends of composition, viz., A1, A4, and A5. The results are tabulated below.

	ρ^{o} ($\mu\Omega$ cm)	$\rho^{o}_{\downarrow}$ ($\mu\Omega$ cm)	$\rho^{o}_{\uparrow}$ ($\mu\Omega$ cm)	$\alpha = \frac{\rho^{o}_{\downarrow}}{\rho^{o}_{\uparrow}}$	$\Delta\rho/\rho$ ($\times 10^{-5}$)
A1	144	295	281	1.05	48
A4	220	442	438	1.01	10
A5	244	505	471	1.07	75

If we follow the above criterion for identifying them as weak or strong ferromagnets, then the absolute values of $\Delta\rho/\rho$ being small, and the values of $\alpha \simeq 1$ indicate that these samples are weak ferromagnets. The value of α does not exhibit any change with the replacement of Ni by either Cr or Mn. It remains at a value $\simeq 1$ which implies that $\rho^{o}_{\downarrow} \simeq \rho^{o}_{\uparrow}$, i.e., holes exist in both the spin-up and spin-down bands. However, this description does not agree with

the conclusion drawn from other observations. Sample A1, till the lowest temperatures, remains a pure ferromagnet as the χ_{ac} and dc magnetization results show. The magnitude of the high-field slope $1/\rho\ d\rho/dH$ of this sample is large at room temperature and it progressively decreases as the temperature is lowered. It nearly becomes zero at $T \simeq 100$ K, below which it is weakly positive. If it would have been a weak ferromagnet, then at low temperatures, we would have observed a large susceptibility together with a large value of $-1/\rho\ d\rho/dH$. We do not observe both these features. Kaul and Rosenberg [65] concluded from the MR studies on $Fe_xNi_{80-x}B_{20}$ alloys that the Ni-rich alloys are weak ferromagnets. They observed a large χ_{hf} value for these alloys. But the MR results do not show the expected large negative high-field slope. This behavior, they suggest, arises from the large positive contribution to the MR due to Lorentz force, which obscures the real MR behavior. The present results can be similarly viewed. The positive contribution to $1/\rho\ d\rho/dH$ at $T \leq 50$ K can be associated with the Lorentz force. This actually makes the real MR behavior look different. On the basis of these arguments, similar to $Fe_xNi_{80-x}B_{20}$ alloys, these alloys may also be viewed as weak ferromagnets. We are not extending the above argument to sample A4 and A5, as sample A4 shows a large positive $1/\rho\ d\rho/dH$ at all temperatures and the low temperature phase of A5 is not a pure ferromagnetic one.

The Ferromagnetic Anisotropy of Resistance and the High-Field slope - Temperature dependence

In Fig. 3.12(a) we plot the FAR vs T/T_c of samples A1 - A4. The FAR is zero at T_c for theses samples. The MR above T_c is positive in both the orientations, very small, and shows a Kohler-like quadratic behavior. Below T_c, the FAR develops indicating the presence of spin-orbit coupling and exchange-field at this temperature. The FAR increases with decrease in temperature. The growth is much larger in A1 than in A2, A3, and A4. The decrease in FAR with increasing temperature can be understood in a semiquantitative manner using Eq. (3.11). At low temperatures the spin-up and spin-down bands are exchange-split and one of the bands is completely filled and therefore $\rho^{\downarrow}$ is large, i.e., α is large, which implies a large FAR. As the temperature increases thermal fluctuations compete with exchange splitting. This tends to equalization of the two sub-band occupations. This results in a fall in α and hence FAR. Bohnke et al. [196] observed that the FAR exhibits a $T^{3/2}$ temperature dependence. The present results, however, do not show such a temperature dependence. Figure 3.12(b) shows the plot of the high-field slope ($1/\rho\ d\rho/dH$) vs T/T_c for samples A1-A4. The slope of A1 decreases with increasing T/T_c. The magnitude of the slope is large and comparable to those of the other amorphous ferromagnetic samples. The negative MR observed after saturation has been explained on the basis of localized as well as band models [65]. In the former model, this effect is caused by the reduction in electron-magnon scattering as the field increases.

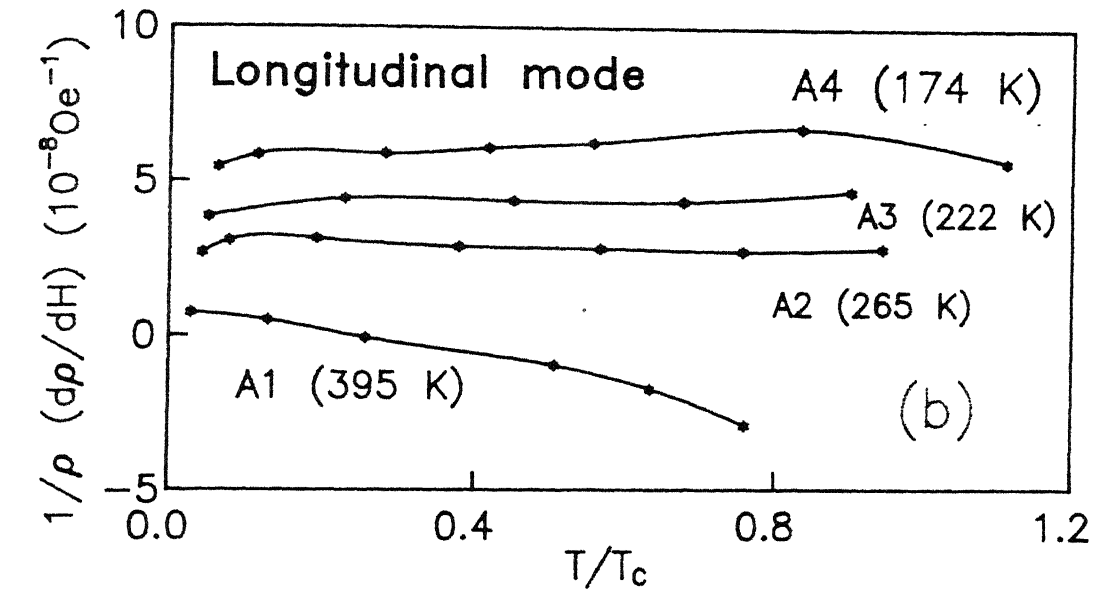

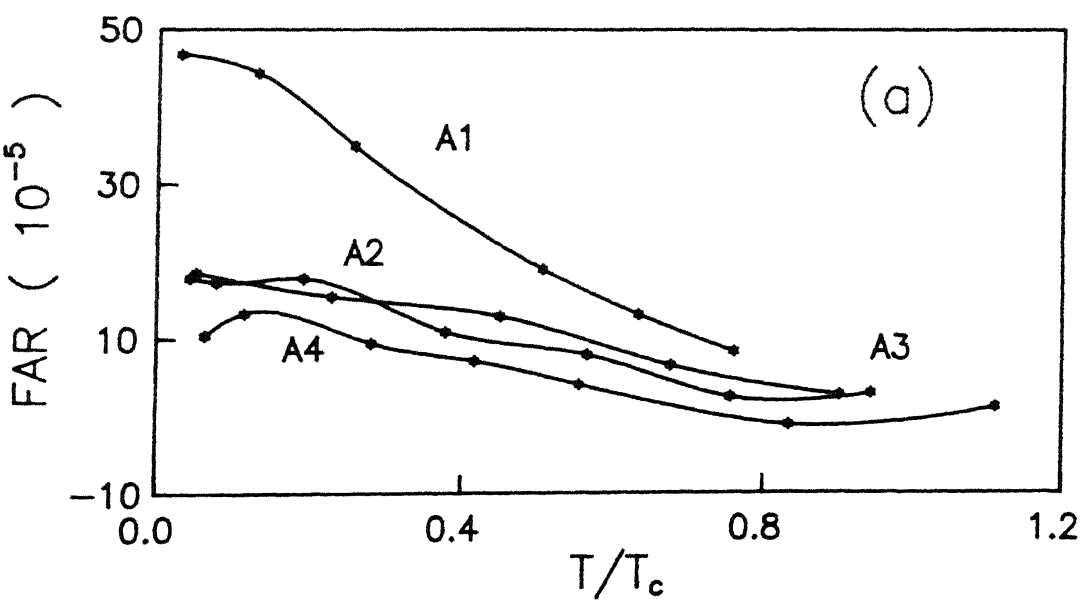

Fig. 3.12 (a) Variation of FAR with T/T_C of A1, A2, A3, and A4 ($Fe_5Co_{50}Ni_{17-x}Cr_xB_{16}Si_{12}$, x = 5, 10, and 15).
(b) Variation of $1/\rho\ d\rho/dH$ with T/T_C of A1, A2, A3, and A4 in the longitudinal mode. The [illegible] brackets are their respective

Both temperature and magnetic field affect the magnon number. At low temperatures, the number of magnons is small and therefore the high-field slope that one observes is generally low. As the temperature increases the magnon number increases and therefore the slope increases. However, this argument is contested by Rajaram et al. [78]. They estimate the number of spin-waves reduced in an external magnetic field of 40 kOe and find that it is 28%, 38%, and 70% at temperatures of 100, 50, and 10 K respectively. This means that the number of spin-waves reduced is the largest at the lowest temperature and therefore the high-field slope in the MR should be largest at the lowest temperature. This is in contrast to the previous argument and also the general experimental observations. In the band model the negative slope is related to the slow increase of magnetization above saturation.

The values of the slope for samples containing Cr are large and comparable to that of Al in magnitude but are of opposite sign. The curve beyond the saturation is not strictly linear and has a small quadratic contribution. We fit the high-field part of the MR data to an equation of the form

$$\frac{\Delta\rho}{\rho} = a + b\,H + c\,H^2.$$

Such non-linear behavior in MR has been observed in $Fe_{80-x}Cr_xB_{20}$ for $x \geq 20$ alloys [39]. It is observed that in alloys with $x \geq 20$, the MR varies non-linearly with the field and show a strong temperature dependence. It consists of a positive term showing a weak temperature dependence and a negative term with a strong temperature dependence. However, the observations in the present

set of alloys are different from this in the sense that the coefficients of both the linear and the non-linear terms show temperature dependence. The coefficient of the H^2 term is smaller than that of the linear term by a factor of 100. b increases with increasing temperature and is maximum around T_c. It has a very weak temperature dependence but near T_c it increase very sharply. This effect is observed in all the three Cr-containing samples. The magnitude of b at any given temperature increases with the increase in Cr concentration. This result, i.e., increase in $1/\rho$ $d\rho/dH$ with Cr concentration, is in good agreement with the observation of Wang et al. [72] on Fe-Cr-B system. They observe that $1/\rho$ $d\rho/dH$ increases while the saturation magnetization decreases with the increase in Cr concentration. The decrease of saturation magnetization is related to the increase of antiferromagnetic Fe-Cr pairs. Therefore, the increase in the positive high-field slope is closely dependent on the antiferromagnetic interaction between Fe and Cr. Since c is very small compared to b, the high-field slope may be identified with the linear term alone in our case. Then a similar conclusion may be drawn from the present observation that the increase in Cr content increases the antiferromagnetic coupling between Co and Cr. The quadratic term, similarly, has a pronounced minimum at around the respective T_c's. This also increases with the increase in the concentration of Cr. However, since the coefficient of the quadratic term is small, the errors introduced are relatively large. The above observation is summarized in Figs. 3.13 and 3.14. Fig. 3.13 shows the variation of b versus T/T_c for samples A2-A4

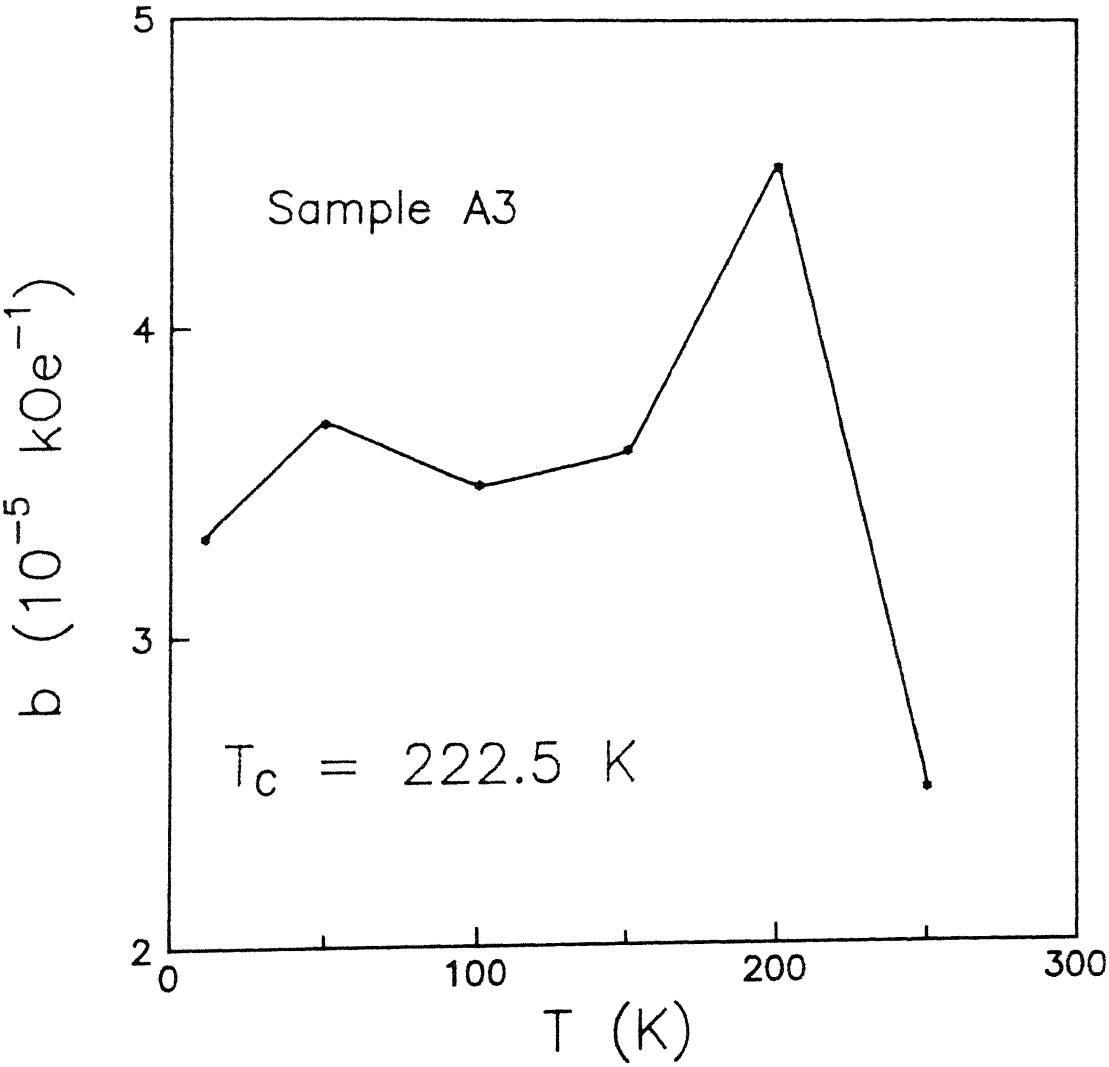

Fig. 3.13 Variation of the coefficient of linear term (b) of Eq. ($\Delta\rho_\perp/\rho = a + bH + cH^2$) with T for sample A3 ($Fe_5Co_{50}Ni_7Cr_{10}B_{16}Si_{12}$).

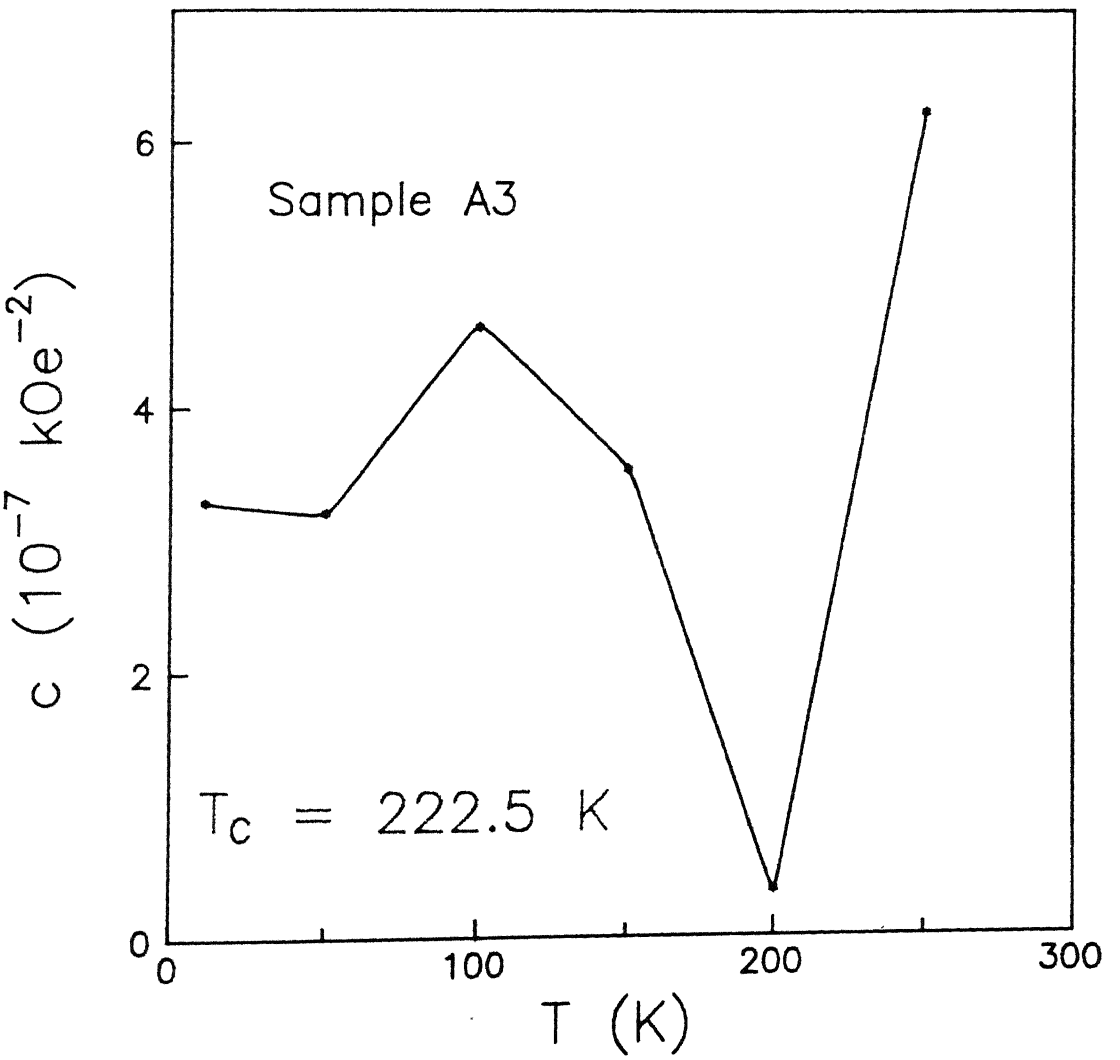

Fig. 3.14 Variation of the coefficient of quadratic term (c) of Eq. ($\Delta\rho_\perp/\rho = a + bH + cH^2$) with T for sample A3 ($Fe_5Co_{50}Ni_7Cr_{10}B_{16}Si_{12}$).

and Fig. 3.14 shows c versus T/T_c of the same samples. The figures show that the coefficient b exhibits a maximum and c a minimum at the respective T_c's. This points out a strong effect of the magnetization on the MR behavior of these samples. At $T \gg T_c$, the H^2 dependence may be associated with the same type of behavior observed in non-magnetic samples. The magnitude of c, in the paramagnetic region, progressively decreases as we go away from T_c. This may result if short-range order does not vanish totally at T_c and persists at temperatures sufficiently away from T_c. The Curie-Weiss type of behavior in these materials is also found to hold at temperatures far away from T_c, indicating the existence of short-range order well above T_c.

In Fig. 3.15 we show the plot of $\Delta\rho_\perp/\rho$ at H = 10 kOe vs T/T_c of samples A2 - A4. It shows : (1) $\Delta\rho_\perp/\rho$ at given temperature increases with increase in concentration of Cr. (2) A peak at $T/T_c \simeq 0.9$ which is most pronounced for sample A4. There is no data point exactly at T_c and therefore the peak shown may be slightly shifted away from T_c. The value of $\Delta\rho_\perp/\rho$ falls sharply at $T>T_c$. This behavior is similar to that found in the rare-earth containing amorphous alloys but is very different from the Fe-Cr-B alloys [72], eg., Fe-Zr [86,87]. In this alloy, the MR is found to be positive and it shows a peak at $T \approx T_c$. In the Fe-Cr-B alloys $\Delta\rho_\perp/\rho$ progressively decreases with the increase in Cr concentration. The positive values of the MR of these alloys are explained by the coherent exchange-scattering model of Asomoza et al. [88] and Bhattacharjee and Coqblin [89]. These theoretical models predict a contribution to the resistance which depends upon

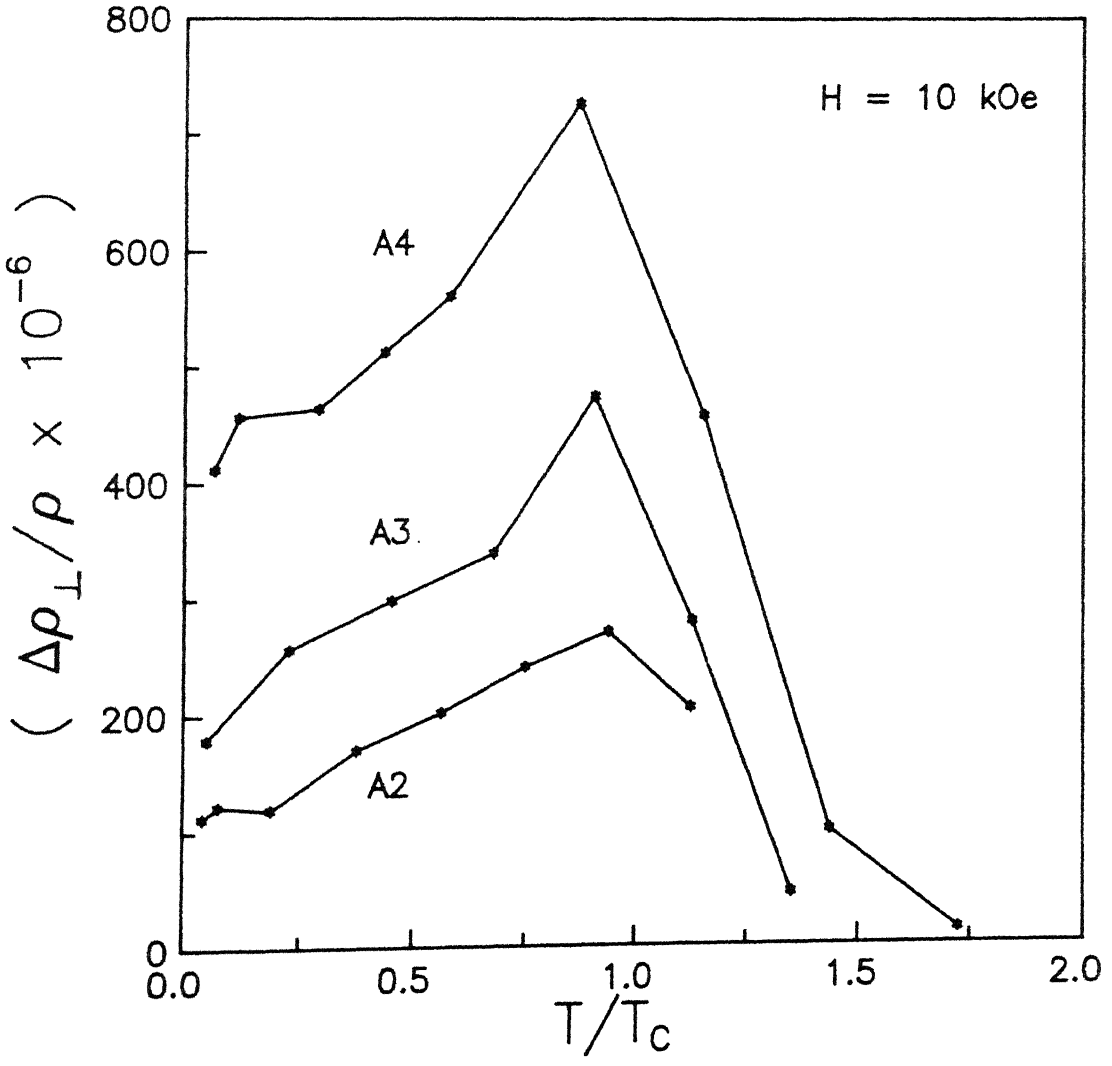

Fig. 3.15 Plot of $\Delta\rho_{\perp}/\rho$ versus T/T_C of samples A2, A3 and A4 ($Fe_5Co_{50}Ni_{17-x}Cr_xB_{16}Si_{12}$, x = 5, 10, and 15).

the coherent exchange scattering from spins separated by distances less than the electronic mean free path. This effect is due to the interference of electrons scattered from spatially separated exchange fields of the magnetic moments and is sensitive to the spin-spin correlation function of the scattering moments. This model predicts the form of the resistance as

$$\rho \propto \sum_{R \neq R'} \exp\ (\ i(2k_F)\ .\ (R - R')\ )\ \langle S_R . S_{R'} \rangle \quad ,$$

where k_F is the Fermi vector, S_R and $S_{R'}$ are the spin vectors of the magnetic moments situated at R and R'. When the susceptibility χ is small, the term $\langle S_R . S_{R'} \rangle$ is approximately equal to M^2. The exponential term in the above equation is identified with the partial structure factor of the magnetic ions. This model, thus, predicts that the MR should be proportional to the square of the magnetization for temperatures much greater than or less than T_c. It can be of either positive or negative sign depending on the sign of the partial structure factor. In Fig. 3.16 we show that the proportionality holds good for the present samples where we plot $\Delta\rho/\rho$ vs M^2 for A4 at two temperatures, one greater than and the other less than T_c. The peak in $\Delta\rho_\perp/\rho$ at T_c (Fig. 3.15) is due to the increase in susceptibility at $T \approx T_c$. A qualitative explanation to our observations is thus given in terms of the above model. In the absence of concrete theoretical studies on this type of MR behavior, it is difficult to draw more conclusions. Our interpretations are also limited by the inability to measure M vs H at different temperatures accurately,

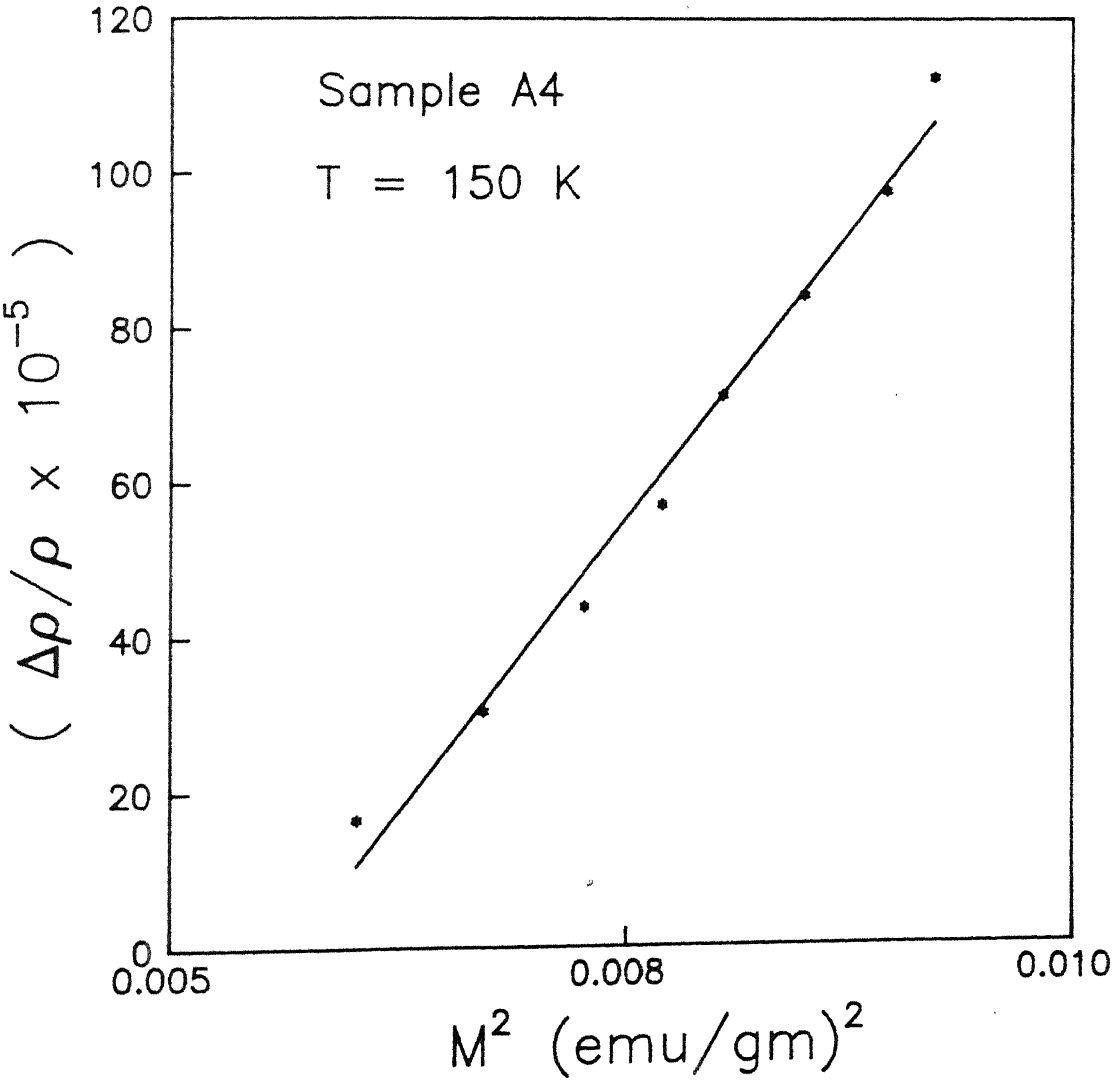

Fig. 3.16 (a) Plot of $\Delta\rho/\rho$ versus M^2 of sample A4 ($Fe_5Co_{50}Ni_2Cr_{15}B_{16}Si_{12}$) at T = 150 K, for the transverse mode.

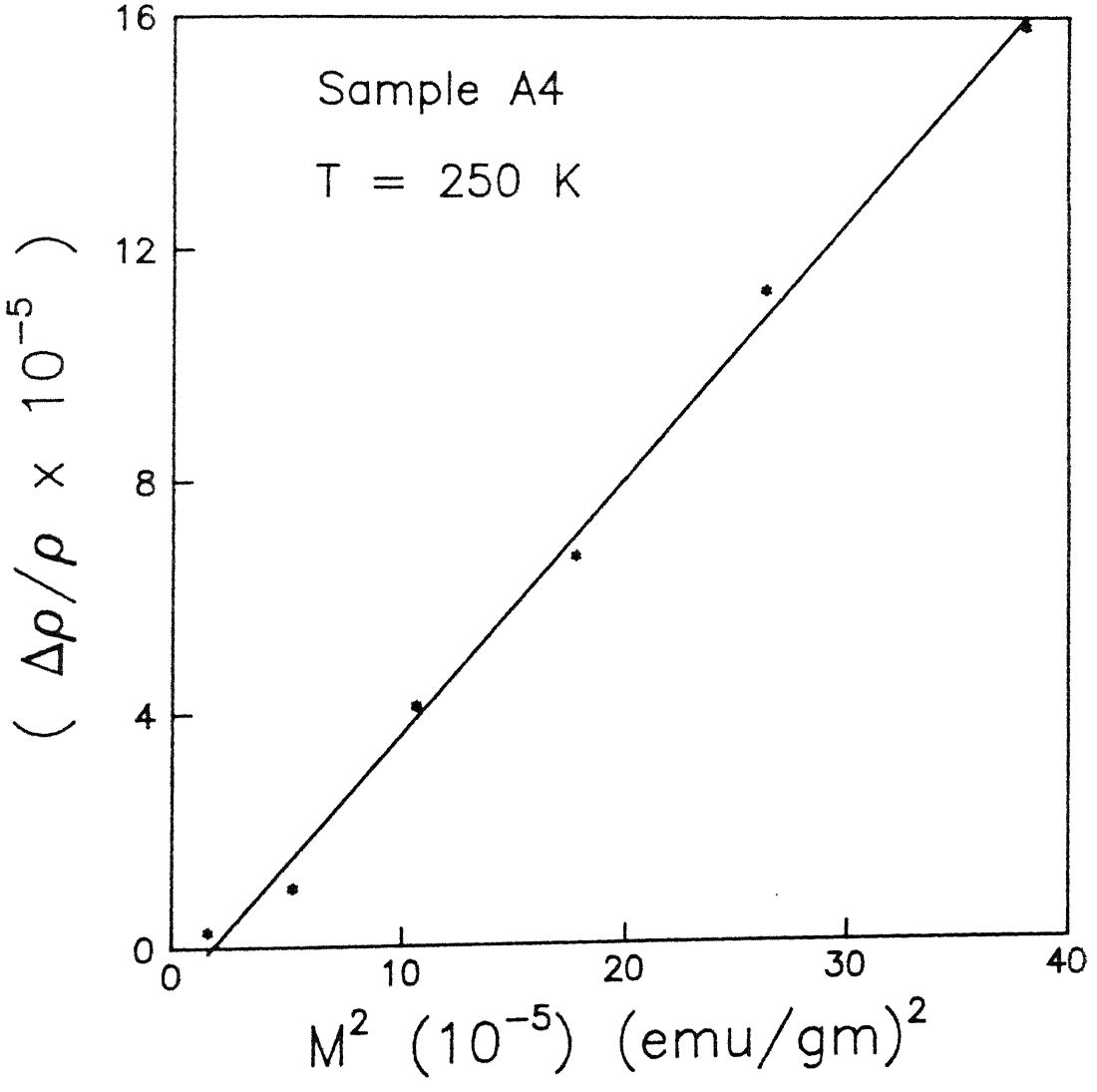

Fig. 3.16 (b) Plot of $\Delta\rho/\rho$ versus M^2 of sample A4 ($Fe_5Co_{50}Ni_2Cr_{15}B_{16}Si_{12}$) at T = 250 K, for the transverse mode.

particularly above the saturation where the change in magnetization is very small. Due to the relatively large noise, the small change in magnetization could not be reliably measured with the VSM. Therefore it is difficult to correlate further the magnetization and magnetoresistance measurements.

Magnetoresistance - Effect of Electron - Electron Interaction and Localization

The positive MR observed in A2 - A4 is discussed on the basis of the predictions of the weak-localization and interaction theories. Since the temperature dependence of the zero-field resistivity of these samples fits very well into the predictions of these models [27], it appears very reasonable to calculate their contributions to the MR.

The temperature dependence of the zero-field resistivity of these metallic glasses could be fitted to $-\sqrt{T}$ at the lowest temperatures, $-T$ at the intermediate temperatures and $-\sqrt{T}$ again at higher temperatures. The $-\sqrt{T}$ observed at the lowest temperature is ascribed to the interaction effect and the $-T$ and $-\sqrt{T}$ at intermediate and high temperatures to the localization effect. The coefficients obtained from these fits agree well with those obtained in non-magnetic samples, and the effect of ferromagnetism does not appear to alter the temperature dependence in this case. While discussing the MR we take into account the large internal field (~ 400 T [39]) in the case of ferromagnetically ordered materials. The various equations (Eqs. (1.33) - (1.44)) obtained are for systems where magnetic long-range order does not exist,

and one finds good agreements with the experimental results in such systems. When these equations are actually used to find the contribution from these effects in ferromagnetic systems, the internal field, H_{int}, has to be incorporated. The theory of Coulomb interaction by Lee and Ramakrishnan [51] predicts that the high-field MR is positive and varies as $\sqrt{H}$ (Eq. (8)). Olivier et al. [39] suggested that H, in this equation, needs to be replaced by $H_{eff} = H_{int} + H$ where H is the applied field and $H \ll H_{int}$. Then the MR can be approximated by [39]

$$\frac{\Delta\rho}{\rho} = \left[\frac{e^2}{8\pi^2} \frac{\rho}{\hbar} \right] \left[\lambda^{j=1}(F) \left[\frac{g \mu_B}{2 \hbar D H_{int}} \right]^{1/2} \right] H$$

where $$\lambda^{j=1}(F) = \frac{32}{3} \left[1 + \frac{3F}{4} - \left[1 + \frac{F}{2} \right]^{3/2} \right] F^{-1} \leq 0$$

is the interaction constant of the triplet term (j=1), and F is the bare screening parameter. The above equation shows that the MR varies linearly with the field when $H \ll H_{int}$. Using a value of $|H_{int}| \geq 50$ T, $D \simeq 3 \times 10^{-5}$ m^2/s and $|\lambda^{j=1}(F)| \simeq 8/3$ and $\rho = 124$ $\mu\Omega$ cm for sample $Fe_{75}Cr_5B_{20}$, the calculation yields $1/\rho \; d\rho/dH \leq 7.8 \times 10^{-5}$ T^{-1} [25]. The experimentally obtained value, 25.8×10^{-5} T^{-1}, differs only by a factor of 3. Maj [197] argued that the choice of $\lambda(F) \simeq 8/3$ was incorrect and, if used as a parameter, would yield a value of F>15 which is large but not unphysical. Maj suggested that the observed positive slope in $Fe_{80-x}Cr_xB_{20}$ ribbons with $5 \leq x \leq 15$ is in quantitative agreement with the theoretical predictions of Lee and Ramakrishnan [51] but not with the conclusion of Olivier et al. [39]. On the same line of argument,

as given by Maj [197], we calculate the slope and compare it with the experimentally measured value. All the three samples show similar behavior, so we choose one of them. From the temperature dependence of the resistivity we obtain $D = 3 \times 10^{-5}$ m^2/s for A3. Using $\rho = 160 \times 10^{-8}$ Ωm and $H_{int} \geq 50$ T and λ as a parameter we obtain $\Delta\rho/\rho \simeq \lambda \times 3.9 \times 10^{-5}$ T^{-1}. Suppose we take the fit to $a + bH + cH^2$, which gives the best χ^2 value at 11 K. We assume that the coefficient of the linear term originates from the electron-electron interaction; its value is found to be 33×10^{-5} T^{-1}. On equating it with the calculated value we get $\lambda \simeq 9$ from which we obtain $F > 15$. This is consistent with the value obtained by Maj [197]. The experimental values of the coefficient of the linear term for samples A2 and A4 are 22×10^{-5} and 44×10^{-5} T^{-1}, respectively and they would not change the value of λ and F drastically. This coefficient (b), however, shows a significant temperature dependence as against the observation of Olivier et al. [39] where no temperature dependence of this coefficient was observed. If H_{int} is assumed to be zero, then $\Delta\rho/\rho$ varies as $\sqrt{H}$. This behavior is observed in non-magnetic amorphous alloys. However, then the present results would be difficult to explain as $\Delta\rho/\rho$ of the samples vary linearly with H.

At higher temperatures (T>120 K), the MR is still positive and the slope is still higher. As previously noted, the coefficient of the linear term increases with temperature till the ferromagnetic T_c's of the respective samples. In the region above 20 K for these samples, the zero-field resistivity has been interpreted in terms of the localization effects. In the

non-interacting case, a positive MR is observed when the spin-orbit coupling is large (Eq. (1.37)), and the applied field $H \ll H_{so}$. If here too we replace H by $H_{eff} = H + H_{int}$, then we obtain

$$\frac{\Delta\rho}{\rho} = \alpha\,\rho\,\frac{0.605\,e^2}{8\,\pi^2\,\hbar}\left[\frac{e}{\hbar\,H_{int}}\right]^{1/2} H \quad .$$

This modification then shows that $\Delta\rho/\rho$ is positive and varies linearly with H. Taking $\alpha = 1$ [92], and $H_{int} = 50$ T, as before, and $\rho \simeq 160 \times 10^{-8}$ Ωm as the value of ρ changes by only about a percent between room temperature and 8 K, we obtain $\Delta\rho/\rho = 1.65 \times 10^{-5}\ T^{-1}$. The experimental values at 50 K, $\sim 37 \times 10^{-5}\ T^{-1}$, is very much larger. This discrepancy between the observed and the calculated results may be due to the wrong choice of the value of α. If α is taken as a parameter, as has been done by Sas et al. [198], to explain the MR behavior in Ni-Cr-B alloys, then we obtain $\alpha \simeq 20$. This value is of the same order as obtained by Sas et al [198] viz., $\alpha \simeq 5.2$. The positive MR, obtained with the introduction of Cr in paramagnetic Ni-B alloy, is explained on the basis of weak localization effects with strong spin-orbit scattering. They calculate $H_i \approx 1T$ and $H_{so} \approx 7T$. A negative term, ascribed to the magnetic effects, could also be found in these alloys. The influence of the magnetic impurities on the localization effects has been studied by a number of authors [52, 92, 198, 200]. The magnetic impurities destroy the electron interference and therefore reduce the MR due to localization. A physical picture has been put forward by Bergmann [53], who studied the influence of deposition of a layer of Fe on Mg film

and found strong deviation in the MR behavior from the theoretical one. The reduction in quantum correction to MR due to magnetic impurities destroys the phase-coherent back-scattering responsible for weak localization. This introduces an additional term, given by a characteristic field B_s, in Eq. (1.33) with

$$B_s = \frac{\hbar}{4eD\tau_s} = \frac{c\,\pi}{2eD}\, N(E_F)\, \Omega\, J^2\, S\,(S+1) \quad ,$$

where τ_s^{-1} is the spin-scattering probability, Ω is the average atomic volume, c is the atomic concentration of magnetic impurities, J is the exchange integral, $N(E_F)$ is the density of states at the Fermi level and S is the spin of the magnetic impurity.

The other contribution arises from the field and temperature dependence of the single-site magnetic scattering. The states available to the impurity spins progressively decrease with increasing field giving a magnetoresistance $(\delta\rho/\rho)_{mag}$ as calculated by Beal-Monod and Weiner [199]. This introduces a correction to Eq. (1.33) given by

$$\frac{\Delta\rho}{\rho^2} = -\frac{c\, J^2\, A'(\alpha')}{\rho^2} \quad ,$$

where c is a constant, J is the exchange interaction between the spin s of the conduction electron and the spin S of the magnetic ion,

$$A'(\alpha') = \langle S_z \rangle \left[\coth\frac{\alpha'}{2} - \frac{1}{2}\,\alpha' \frac{1}{\sinh^2\frac{\alpha'}{2}} \right]$$

and $\alpha' = g\mu_B H / k_B T$.

H is the magnetic field and $\langle S_z \rangle = s\ B_s(s\alpha)$ where B_s is the Brillouin function. This equation gives a MR which is proportional to $-B^2$ at low fields and saturates at high fields. It is observed that the introduction of as little as 20 ppm of Mn in $Mg_{70}Zn_{30}$ [200] produces a MR which is comparable to that from quantum corrections at 6 T. However, Beiri et al. [92] contest this suggestion and infer from measurements on $Cu_{50}Y_{49.5}Gd_{0.5}$ and $Cu_{50}Lu_{49.5}Gd_{0.5}$ that the theoretical estimate of the spin-scattering probability τ_s^{-1} is much larger than the experimentally observed one.

In summary, the MR, $\Delta\rho/\rho$, at all temperatures for samples A2-A4 is positive. It varies non-linearly with H. The best-fit is obtained when the data are fitted to an expression of the form $a + bH + cH^2$, where the coefficient (c) of the H^2-term is two orders of magnitude smaller than that of the linear term (b). Both b and c show temperature dependence. The coefficient (b) attains a maximum value at T_c whereas the coefficient (c) shows a minimum. The value of the MR and the slope at any given temperature are found to increase with the increase in Cr concentration. The value of b at the lowest temperature is in agreement with the prediction of the model based on Coulomb interaction if the internal magnetic field H_{int} of these materials is taken into account. However, at higher temperatures, the localization effects explain the temperature dependence of the zero-field resistivity as well. The observed slopes are much larger than those obtained by taking into account the spin-orbit coupling. The H^2- term, we find, is present

in all the Cr-containing samples and also in A1 (x=Ø) at the lowest temperature. At the lowest temperature the quadratic term in H is more pronounced. This is because the electron-magnon scattering in ferromagnets is very small at $T \ll T_c$ and so the coefficient of the H-term associated with this scattering decreases as we lower the temperature and it becomes negligible at $T < 1ØØK$. The positive coefficient, observed for $T < 5ØK$ in this alloy, is associated with the Kohler-like behavior for normal metals. The values of the coefficient of the H^2-term in all these samples are of the same sign and nearly the same magnitude ($\sim 5 \times 1Ø^{-7}$ kOe^{-2})indicating a common origin. It may be attributed to a non-magnetic origin as this value compares well with the value of this coefficient obtained in the paramagnetic region, $T > T_c$, of some of these samples. But it is not clear as to why this coefficient should decrease as temperature is increased and attain a minimum at $T \approx T_c$. The change in b at $T \approx T_c$ is not that significant so as to make the quadratic component insignificant.

Magnetoresistance of A5 and B5 : Correlation between Magnetization and Magnetoresistance

The MR measurements in both A5 and B5 show a large anisotropy in low fields characteristic of ferromagnetic domain structures. At low fields, the longitudinal MR ($\Delta\rho_{\parallel} / \rho$) is positive and the transverse one ($\Delta\rho_{\perp} / \rho$) is negative even at the lowest temperature of 11 K giving a positive value for the FAR. Figs. 3.17(a) and 3.17(b) show the ferromagnetic anisotropy of resistance (FAR) and $1/\rho(d\rho/dH)$ respectively of A5 and B5. The

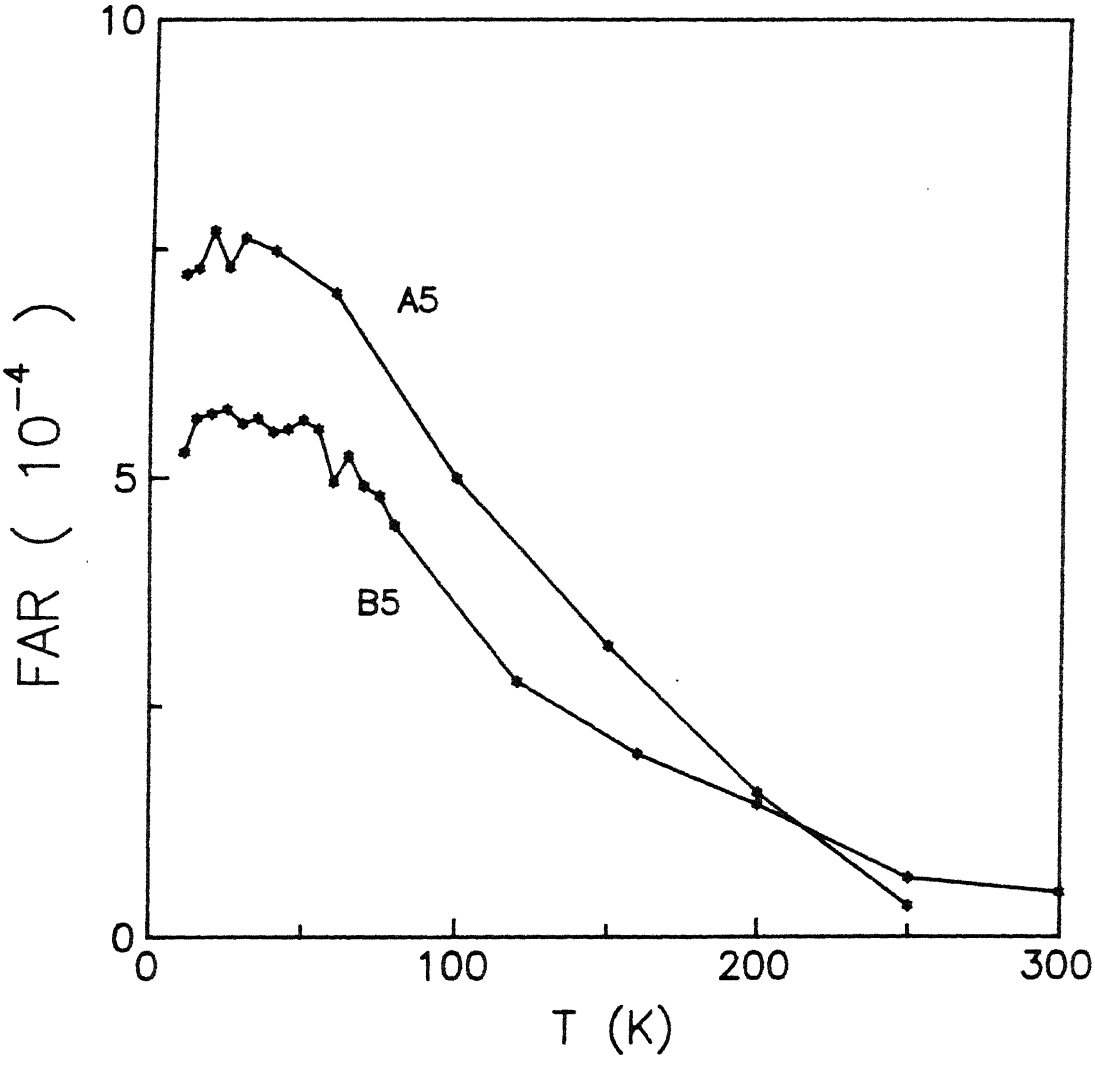

Fig. 3.17 (a) Variation of FAR with temperature of samples A5 and B5 ($Fe_5Co_{50}Mn_{17}B_{16}Si_{12}$ and $(Fe_{7.8}Co_{31.2}Ni_{24}\ Mn_{15}(BSi)_{22}$, respectively).

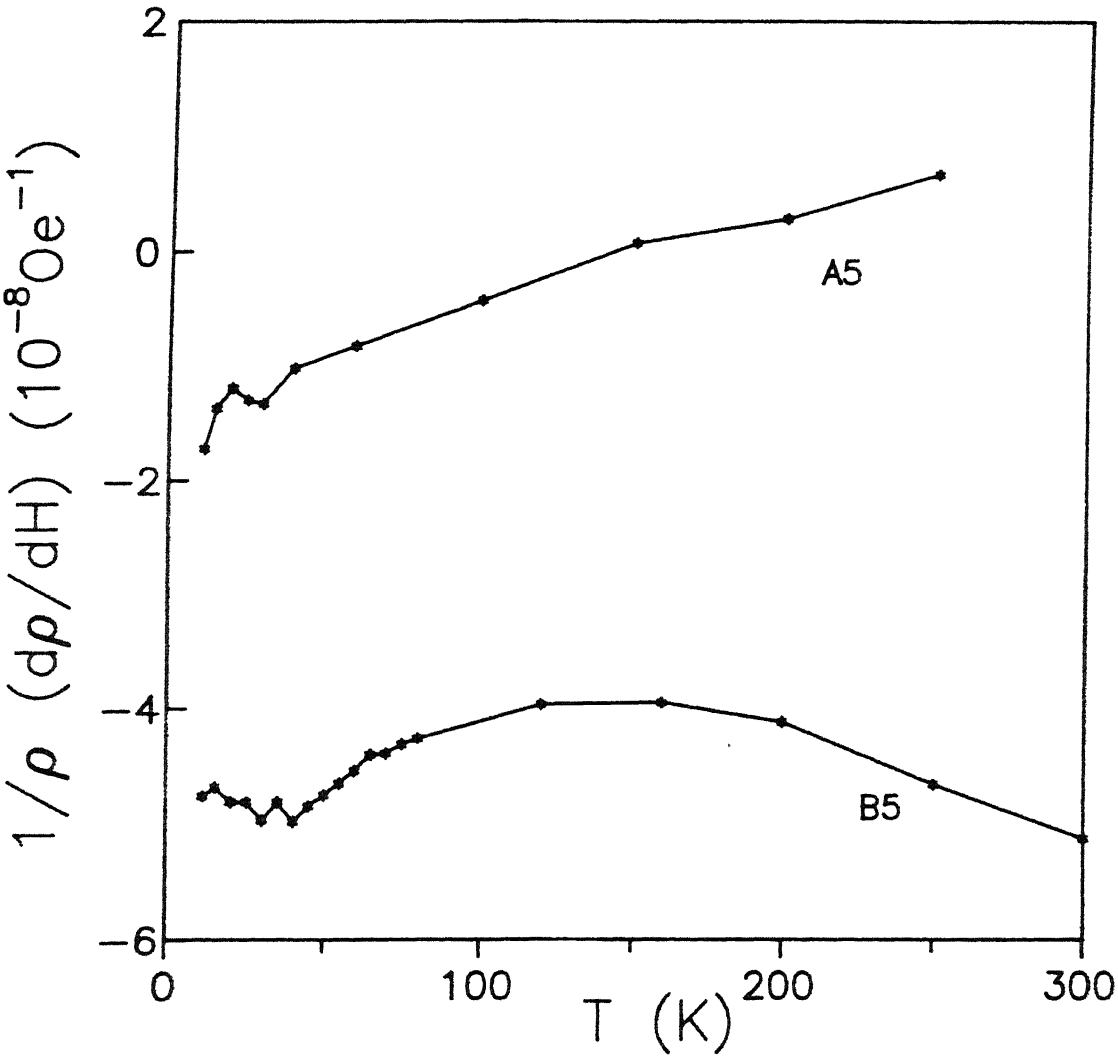

Fig. 3.17 (b) Variation of slope ($1/\rho$ $d\rho/dH$) with temperature of samples A5 and B5 ($Fe_5Co_{50}Mn_{17}B_{16}Si_{12}$ and $Fe_{7.8}Co_{31.2}Ni_{24}Mn_{15}(BSi)_{22}$, respectively), in the longitudinal mode.

magnitude of the FAR is small (Ø.Ø7%) as compared to the crystalline as well as other amorphous materials [58]. At high temperatures the FAR decreases and becomes negligible near their respective T_c's, where the magnetization disappears. At lower temperatures, however, if it were only the FM phase then the FAR should have marginally increased or if it were only the SG phase it would have dropped to zero. Contrary to this, we observe that the FAR has a tendency to decrease below 6Ø K which is also the region where there is a large drop in χ. Similar behavior in FAR is reported in FeZr system [2Ø1] albeit from low-field extrapolation. The high-field extrapolation does not yield this structure. The high-field slope ($1/\rho$ $(d\rho/dH)$), obtained from fitting the present MR data between 3 and 16 kOe to a straight line, is negative for both orientations at all temperatures below T_c for B5. The magnitude of the slope in A5 is smaller and it crosses over to small positive values as T_c is approached. The slope in the $\perp$ orientation is larger than in the $\parallel$ orientation. The large negative slopes indicate that not all spins are aligned even at 11 K. The high-field slope in conventional ferromagnets is more negative as one approaches T_c. This is caused by less electron-magnon scattering as the magnetic field quenches the magnons more effectively at higher temperatures and so this negative MR is expected to be small at low temperatures. However, B5 behaves like a conventional FM between 16Ø and 3ØØ K. There is a significant increase in the magnitude of the slope below 12Ø K. This measurement was repeated on a different piece of sample but from the same batch and the same results were obtained. The

temperature below which there is an increase in the slope correlates with the fall in χ. This result is similar to that observed in AuFe (19 at.%) alloys [96] where a minimum is observed at around 100 K in $-1/\rho$ ($d\rho/dH$) versus H plot. They argued that in the region below 100 K, the spins begin to break away from FM order and acquire random uncorrelated components which results in an increase of the high-field dc-susceptibility and hence the increase in $-1/\rho$ ($d\rho/dH$) below 100 K. Susceptibility measurements above technical saturation of the present samples also show a non-zero susceptibility at lower temperatures. In the region above T_c, the MR shows Kohler-like H^2 behavior. Thus the MR results correlate with the results of χ and dc-magnetization measurements. The presence of FAR even at 11 K indicates the existence of FM order, but it remains nearly constant (as a matter of fact, it shows a small increase with the increase of temperature) till about 60 K coinciding with the temperature below which there is a large drop in χ. This behavior is different from those exhibiting pure FM order where FAR decreases with temperature as in sample A1 (see Fig. 3.12(b)). The slope is more negative as temperature is lowered, a behavior in contrast to that seen in normal FM but which agrees with the picture of spin-freezing and the associated rise in χ (above technical saturation). Thus we are able to conclude from these results the coexistence of FM and SG phases in both the Mn-containing glasses.

3.3 Magnetization

Curie Temperature (T_C) and Magnetic Moment

The T_C's of samples A1-A5, and B5 have been measured by low-field ac susceptibility (χ_{ac}) and dc magnetization methods. The values obtained from these measurements (for some of these samples) agree within ± Ø.5 K and are between 17Ø and 4ØØ K. The highest value of 4ØØ K is obtained in sample A1 and the value of T_C decreases following the addition of Cr or Mn. Figure 3.18(a) shows the nature of decrease of the T_C. Initially the decrease of the T_C is much more rapid than the later additions of Cr. On an average, the decrease is about 8 K/at.% Cr. This trend is similar to that observed in Fe-Ni-Cr-B-Si glasses [2Ø2]. The rate of decrease of T_C is much more rapid, about 2Ø K/at.% TE (where TE = V, Mn, Cr, and Mo) in Fe-based glasses containing Cr [178] and V, Mn, Cr, and Mo [116,2Ø3]. The present value is also much smaller than the rate of decrease of about 97 K/at.% Cr observed in $Co_{80-x}Cr_xB_{20}$ glasses [116]. The sharp fall in T_C with the addition of Cr implies a loss of magnetic exchange interactions, which may be due to the antiferromagnetic coupling of Cr atoms. The complete replacement of Ni with Mn in this series (sample A5) does not, however, lower the T_C as much as observed in the case of A4 where Cr almost fully replaces Ni.

The magnetization at Ø K, M(Ø), of the samples are obtained from the extrapolation to Ø K of the M(1Ø kOe, T) data from which the magnetic moment per atom ($\bar{\mu}$) is calculated. The variation of the magnetic moment with the addition of Cr is very similar to that of T_C and is shown in Fig. 3.18(b). The decrease is rapid at

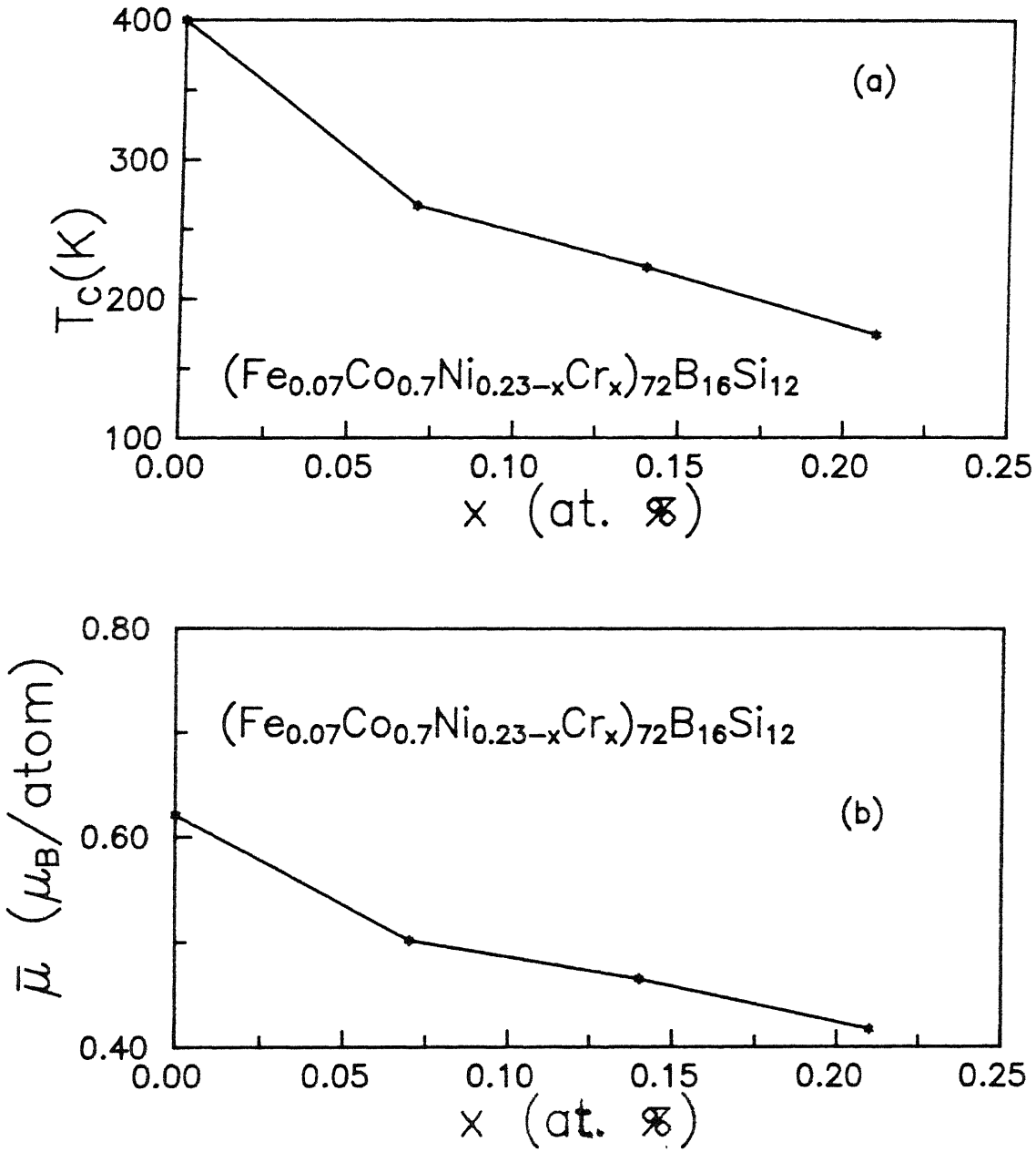

Fig. 3.18 (a) Variation of Curie temperature (T_c) with Cr concentration (x).
(b) Variation of average magnetic moment per atom ($\bar{\mu}$) with Cr concentration (x).

low concentration and is slower at higher concentrations. However, due to the lack of data points at low concentrations, not much emphasis could be laid on this observation and therefore, while calculating the dT_C/dx and $d\bar{\mu}/dx$, single straight lines passing through majority of data points are considered. The values of T_C and the magnetic moment are tabulated in Table 3.5. With the addition of Cr, the rate of fall of $\bar{\mu}$ with concentration (x) of Cr is ~ -1 μ_B/at.% Cr. If it is assumed that B and Si do not contribute to the moment of the sample and only the transition elements do and then the magnetic moment/transition element atom is calculated, there too the value of $d\mu/dx$ comes to -1 μ_B/at.% Cr. Contrary to the behavior observed in samples with Cr, the replacement of Ni with Mn raises the magnetic moment significantly. Similar behavior for the variation of the magnetic moment with Mn and Cr has been observed in $Co_{80-x}Mn_xB_{20}$ (T = Fe, V, Cr, Mn) glasses [116,140]. It is found that the magnetic moment of $Co_{80-x}T_xB_{20}$ glasses increases up to 6 at.% of Mn and then it decreases [140]. These results are explained on the basis of the idea of the virtual bound states (VBS) [116]. The increase in magnetic moment with small addition of Mn appears to be a feature encountered only in amorphous systems. Magnetic moment variation in crystalline Co-Mn system shows a monotonic decrease of the moment from 1.7 μ_B for Mn = 0 to 1.34 μ_B for Mn = 8 at.% [204].

A qualitative discussion of the above results are given on the basis of the VBS model. According to this model, a five fold-degenerate $3d_\uparrow$ virtual bound state is lifted out of the $3d_\uparrow$ band near the impurity due to its repulsive potential. If the

TABLE 3.5

Composition, Curie temperature (T_C), magnetization at Ø K (M(Ø)), spin-wave stiffness constant (D(Ø)), average magnetic moment per transition metal atom ($\bar{\mu}$), and the coefficients $B_{3/2}$ and $C_{5/2}$ (Eq. 1.2Ø) for samples A1 - A5, and B5.

	T_C (K)	D(Ø) (meV Å^2)	D(Ø)/T_C (meV Å^2/K)	$B_{3/2}$	$C_{5/2}$	$C_{5/2}/B_{3/2}$	M(Ø) emu/gm)	μ (μ_B/TM atom)
A1	4ØØ	1Ø1.5	Ø.24	Ø.48	Ø.Ø2	Ø.Ø4	59	Ø.62
A2	267	74.8	Ø.28	Ø.51	-	-	48	Ø.5Ø
A3	222.5	55.7	Ø.25	Ø.65	-	-	45	Ø.47
A4	174	46.Ø	Ø.26	Ø.66	-	-	41	Ø.42
A5	3ØØ	95.2	Ø.32	Ø.26	Ø.42	1.6Ø	77	Ø.8Ø
B5	37Ø	97.8	Ø.26	Ø.35	Ø.65	1.86	75	-
Fe	1Ø43	286	Ø.27	Ø.12	Ø.Ø4	Ø.33	-	-
Co	1394	-	Ø.25	Ø.17	-	-	-	-
Ni	631	397	Ø.63	Ø.12	Ø.15	1.25	-	-

majority-spin $3d_{\uparrow}$ VBS remains below the Fermi level (E_F), then the solute affects the moment because of the difference in populations of $3d^{\downarrow}$-band relative to that of the host. In this case, an equation of the form

$$\mu = \mu_{matrix} - Zc\mu_B \quad , \tag{3.16}$$

where Z is the valence difference between the solute and the host, is obeyed. If the potential of the solute is sufficiently repulsive, then the majority spin VBS moves above the E_F and five $3d_{\uparrow}$ electrons are transferred to $3d_{\downarrow}$ states, thereby reducing the average magnetic moment by $10\ \mu_B$ in addition to the valence difference. Thus in this approximation

$$\mu = \mu_{matrix} - (Z + 10)c\mu_B. \tag{3.17}$$

Therefore, in this case $\xi = d\mu/dc = -(Z + 10)$. The parameter $-(\xi + Z)$ is a good indicator of the position of the majority band. If $-(\xi + Z)$ is equal to zero, Eq. (3.16) is followed , or in other words, the majority $3d_{\uparrow}$ band lies below the Fermi level. If $-(\xi + Z) = 10$, then Eq. (3.17) is followed where distinct VBS appears above E_F. When $-(\xi + Z) \approx 5$, which is the case in Cr-containing samples, it is suggested that the Fermi level E_F intersects the $3d_{\uparrow}$ VBS.

In the present samples if Z is taken as ≈ -3.5 (Cr in Co-Ni system) and $\xi = -1$ then $-(\xi + Z) \approx 4.5$ which is roughly the same as obtained in $Cr_xCo_{80-x}B_{20}$ system [116]. This implies, in the above model, that the $3d_{\uparrow}$ VBS intersects the E_F and thus explains the observed fall in the magnetic moment with the addition of Cr. However, a direct calculation of Z from Eq. (3.17) yields $\left[d\mu/dx = -1 = -(Z + 10)\right]$ $Z = -9$. This result is in disagreement with the

expected value of ≈ -3.5. The increase in the moment of the alloy, on replacing Ni by Mn, shows, using the above model, that the majority-spin band is filled and below the E_F there are minority-spin holes only. Due to the non-availability of alloys with lower Mn concentration, one cannot really say if the maximum in the moment versus concentration curve has been reached or not.

Dobrzyuski et al. [136] studied the variation of magnetic moment in $(Co_{0.93-y}Ni_yFe_{0.07})_{75}B_{15}Si_{10}$ alloys. They found that with the increase in y the average magnetic moment per transition metal atom (μ_{TM}) decreased. Our sample A1 $(Fe_{0.07}Co_{0.7}Ni_{0.23})_{72}B_{16}Si_{12}$ is very near to their composition with y = 0.23. But the value of the magnetic moment and T_C reported for y = 0.23 alloy are about 0.9 μ_B and 500 K respectively and are not in good agreement with 0.62 μ_B and 400 K respectively for A1. This disagreement may probably be due to the higher content of metalloids in A1. However, if an alloy is chosen which has a $T_C \approx 400$ K, i.e., for y = 0.35, its $\mu_{TM} \approx 0.68$ is comparable to that of A1. From the Mössbauer studies on the same alloys it is reported that for alloys with $y \leq 0.4$, the magnetic moment of iron is (1.73 ± 0.03) μ_B. This is used along with the magnetization data to infer that $\mu_{Ni} = 0.12\ \mu_B$. Compton scattering and hyperfine interaction studies [205] by the same group reveal that the earlier assumption of Ni carrying zero moment is not true. Using these values, we make an attempt to calculate the magnetic moments of Co and Cr in our alloys. In A1, since $x_{Cr} = 0$, subtracting the contributions of Fe and Ni using the above values, we find the contribution of Co to be 0.67 μ_B. With the knowledge

of the moments of Fe, Co, and Ni, we calculate the moment of Cr in A2, A3, and A4. We assume in this calculation that the fall in moment with the addition of Cr is solely due to the moment of Cr and in the process the moments of Fe, Co, and Ni do not change. Under this assumption, the calculation shows that Cr has to be attributed with -1.5, -1.34 and -Ø.85 μ_B in A2, A3, and A4 respectively. The negative sign means that the moment on Cr is of opposite sign to those of Fe, Co, and Ni. From similar arguments extended to Fe-Ni-Cr-B-Si alloys [2Ø2], -4μ_B is attributed to Cr atoms. Hasegawa and Kanamori [2Ø6], based on a study of Fe-Cr system in the coherent potential approximation (CPA), show that Cr atoms carry about -Ø.75 μ_B in the low Cr concentration and then the moment progressively decreases and becomes zero at 5Ø at.% Cr. The study also shows that, under the same conditions, even the Fe moment decreases. The theoretical results are in good agreement with the neutron diffraction data. Thus our assumption that the moments in Fe, Co and Ni remain constant may not be quite justified.

Another approach of explaining the above results is on the basis of the charge-transfer model [2Ø7]. This model explains the observed decrease in magnetization by the s-p electron transfer from the metalloid atoms to the 3d bands of the transition metals. Based on this model the magnetic moment of the present alloys can be written as

$$\bar{\mu} = x\,\mu_{Fe} + y\,\mu_{Co} + z\,\mu_{Ni} + p\,\mu_{Cr} + q\,\mu_{Mn} - g\,\mu_B - h\,\mu_{Si} \quad ,$$

where x, y, z, p, q, g, and h are the concentrations of Fe, Co, Ni, Cr, Mn, B and Si respectively and μ their respective moments.

We assume that the contributions from B and Si to the total moment, to be the same as given in Ref [208]. Thus we write

$$\bar{\mu} = 0.05 \times 2.2 + 0.5 \times 1.7 + (0.17 - p) \times 0.6 + p\,\mu_{Cr} - 0.59 (0.16 \times 3 + 0.12 \times 4),$$

where p is the concentration of Cr. For p = 0, this calculation gives, $\bar{\mu} = 0.496\ \mu_B$ / atom which is in fair agreement with that obtained from the measurements on A1 ($0.5\ \mu_B$ / atom). With the addition of Cr we calculate μ_{Cr} from the above relation and find μ_{Cr} = -0.83, -0.59, and -0.45 for A2, A3, and A4 respectively. The values of the moments of Cr, obtained from this method, are also in agreement with the theoretical calculations of Hasegawa and Kanamori [206]. In the case of A5, we rewrite the above equation as

$$\bar{\mu} = 0.05 \times 2.2 + 0.15 \times 1.7 + 0.17 \times \mu_{Mn} - 0.59 (0.16 \times 3 + 0.12 \times 4) \quad .$$

If we equate the above equation with the observed value of 0.645 μ_B, we obtain $\mu_{Mn} = 1.48\ \mu_B$. This value is not in agreement with that obtained by Krishnan et el. [208] on $(Co_{0.975}Fe_{0.025})_{78}Mn_4B_{12}Si_6$ ($\mu_{Mn} = 3.7\ \mu_B$). Measurements on another sample with higher Mn concentration (Mn_8) by the same group [209], using the above simple expression leads to $\mu_{Mn} = 1.4\ \mu_B$. This suggests that the Mn moment decrease with increasing Mn content. However, it is argued [209] that this inference is wrong as NMR results establish that the moments at the Co and Mn sites are independent of the Mn content of the alloy in the range of compositions studied. The observed decrease in moment of the alloy beyond Mn_4 is attributed to the reduction in the moment of the Fe

atoms. The same study also points to another important conclusion that the Mn-Co interaction is strongly ferromagnetic and overcomes the Mn-Mn nearest neighbor antiferromagnetic interaction. If we extend this argument in the present case we are able to explain the increase in moment on substituting Ni with Mn. This also means that Mn-Co interaction is much stronger than the Ni-Co interaction. The calculated value of μ_{Mn} is in agreement with the value obtained in Co-Mn-B [141] and $(Co_{0.975}Fe_{0.025})_{74}Mn_8B_{12}Si_6$ [209] alloys. The above study brings forth the basic difference between Mn and Cr in their interactions with transition metal hosts.

Temperature Dependence of Magnetization

The magnetization data taken at H = 10 kOe are analyzed in terms of the spin-wave and other contributions to the thermal demagnetization of the samples A1-A5 and B5. The analysis is extended up to $T \simeq 0.5\ T_c$ as it is well known that in amorphous ferromagnets the range of spin-wave analysis can be extended to temperatures as high as $0.8\ T_c$. A least-squares fit method was used to differentiate between the various fits.

We find that in samples containing Cr (A2, A3, and A4), a fit to Eq. (1.19) containing both $T^{3/2}$ and $T^{5/2}$ terms yields a negative coefficient for the $T^{5/2}$ term. The negative coefficient seems to be unphysical. The χ^2 value does not change appreciably with the inclusion of the $T^{5/2}$ term. Similarly, inclusions of T^4 or $T^{7/2}$ and T^2 terms, in addition to the $T^{3/2}$, result in negative coefficients for the higher terms. This shows that M(T) of these alloys, within the experimental resolution of the present

measurements, are best described by a $T^{3/2}$ term arising from the q^2 term in the spin-wave dispersion relation and the $T^{5/2}$ term is negligibly small. Figure 3.19 shows the plot of M(T)/M(Ø) vs T/T_c of these alloys. The solid lines are the best fits to the data. The coefficient B of this term is observed to increase with the increase in Cr. The spin-wave stiffness constant D(Ø) is obtained from the coefficient B (Eq. (1.24)) and is observed to decrease with the increase in concentration of Cr. The value of $D(Ø)/T_c$ remains nearly constant at (Ø.265 ± Ø.Ø15) meV A^2 / K (Table 3.5).

In sample A1 (without Cr), inclusion of a $T^{5/2}$ term, in addition to the $T^{3/2}$, does not change the χ^2 value appreciably but gives a $T^{5/2}$ term which is of the same sign as the $T^{3/2}$ term but of magnitude $1Ø^4$ times smaller (Table 3.6). The coefficient obtained is, at least, an order of magnitude smaller than that observed in Fe-B-C alloys [128]. A comparison of the value of D(Ø), obtained from the $T^{3/2}$ term, with an alloy of similar composition [136] having a $T_c \approx 4ØØ$ K, shows that our result is in agreement with theirs of 1ØØ meV A^2. We have also attempted to observe the effect of the inclusion of other terms in the fit. The addition of another term due to single-particle excitations would involve too many parameters. So we have tried to see the effect of the other terms in place of the $T^{5/2}$ term. A very marginal improvement in χ^2 value is found when, apart from the $T^{3/2}$ term, another term due to single-particle excitations is incorporated, with $\Delta \neq Ø$ (Eq. (1.31)), i.e., $T^{3/2}\exp(-\Delta/k_BT)$. In this

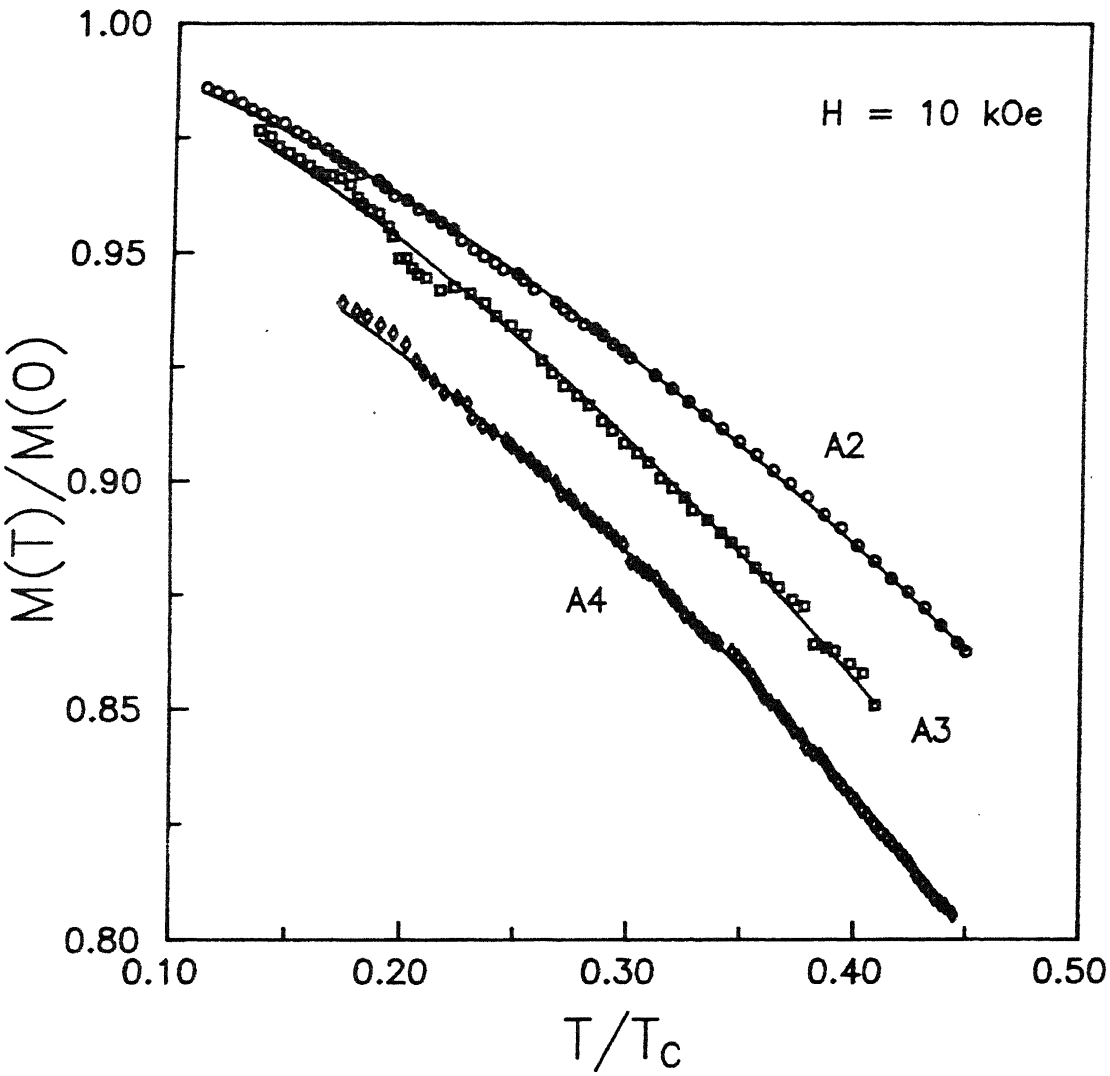

Fig. 3.19 Normalized magnetization M(T)/M(Ø) versus T/T_c of samples A2, A3, and A4 ($Fe_5Co_{50}Ni_{17-x}Cr_xB_{16}Si_{12}$, x = 5, 1Ø, and 15). The data of A4 are displaced along the vertical axis. The solid curves are fits of the experimental data to Eq. (1.19).

Table 3.6

Fit of $\Delta M/M(\emptyset)$ (= $M(T)-M(\emptyset)/M(\emptyset)$) to various equations for samples A1, A5, and B5.

(a) $-BT^{3/2}$

(b) $-BT^{3/2} - CT^{5/2}$

(c) $-BT^{3/2} - CT^{3/2} \exp(\Delta/kT)$

	B ($K^{-3/2}$)	C ($K^{-3/2}$ or $K^{-5/2}$)	Δ/k (K)	χ^2
A1				
(a)	6.1×10^{-5}			7.3×10^{-7}
(b)	6.0×10^{-5}	6.3×10^{-9}		7.2×10^{-7}
(c)	6.0×10^{-5}	2.6×10^{-5}	270	7.2×10^{-7}
A5				
(a)	8.7×10^{-5}			3.2×10^{-6}
(b)	5.1×10^{-5}	2.7×10^{-7}		4.3×10^{-7}
(c)	7.6×10^{-5}	3.3×10^{-4}	400	3.1×10^{-7}
B5				
(a)	9.1×10^{-4}			1.0×10^{-5}
(b)	5.0×10^{-5}	2.5×10^{-7}		6.0×10^{-7}
(c)	1.3×10^{-5}	1.1×10^{-4}	75	1.1×10^{-7}

analysis Δ is taken as a parameter and is obtained from the best-fit method. Inclusion of this term does not affect the coefficients of the $T^{3/2}$ term and gives a value of $\Delta \simeq 270$ K. The coefficient of the single-particle term is only a factor of 2 smaller than that of the $T^{3/2}$ term (Table 3.6). The value of Δ obtained for Ni, from the saturation magnetization data, varies between 156 and 743 K [138] and the coefficient of the term between (0.5 and 6.2) $\times$ 10^{-5} $K^{-3/2}$. Similar analysis on $Fe_xNi_{80-x}B_{18}Si_2$ alloys shows that the Stoner gap Δ varies between 20 and 60 K. We find that, in the case of A1, the choice whether the deviation from the $T^{3/2}$ term is to be attributed to the $T^{5/2}$ term or to the Stoner single-particle excitations is difficult to make from the χ^2 values alone. However, we choose the fit with the $T^{5/2}$ term as it gives consistent results for all the samples as shown below.

In contrast to the behavior observed in A1, in A5 a term in addition to the $T^{3/2}$, of the form $T^{5/2}$ decreases the χ^2 value by an order of magnitude, thus showing a clear necessity for an additional term. The coefficient of the $T^{5/2}$ is smaller than that of the $T^{3/2}$ term by a factor of 100. Figure 3.20 shows the plot of $M(T)/M(0)$ vs T/T_c of samples A1, A5, and B5. The continuous line is the best-fitted curve and the coefficients are given in Table 3.6. The lowest χ^2 is again, as in A1, for the fit with the exponential term. The value of Δ obtained in this case is 400 K and the value of the coefficient is larger by a factor of 4 than the coefficient of the spin-wave term ($T^{3/2}$). The value of $D(0)/T_c$, obtained from this fit, is in agreement with those

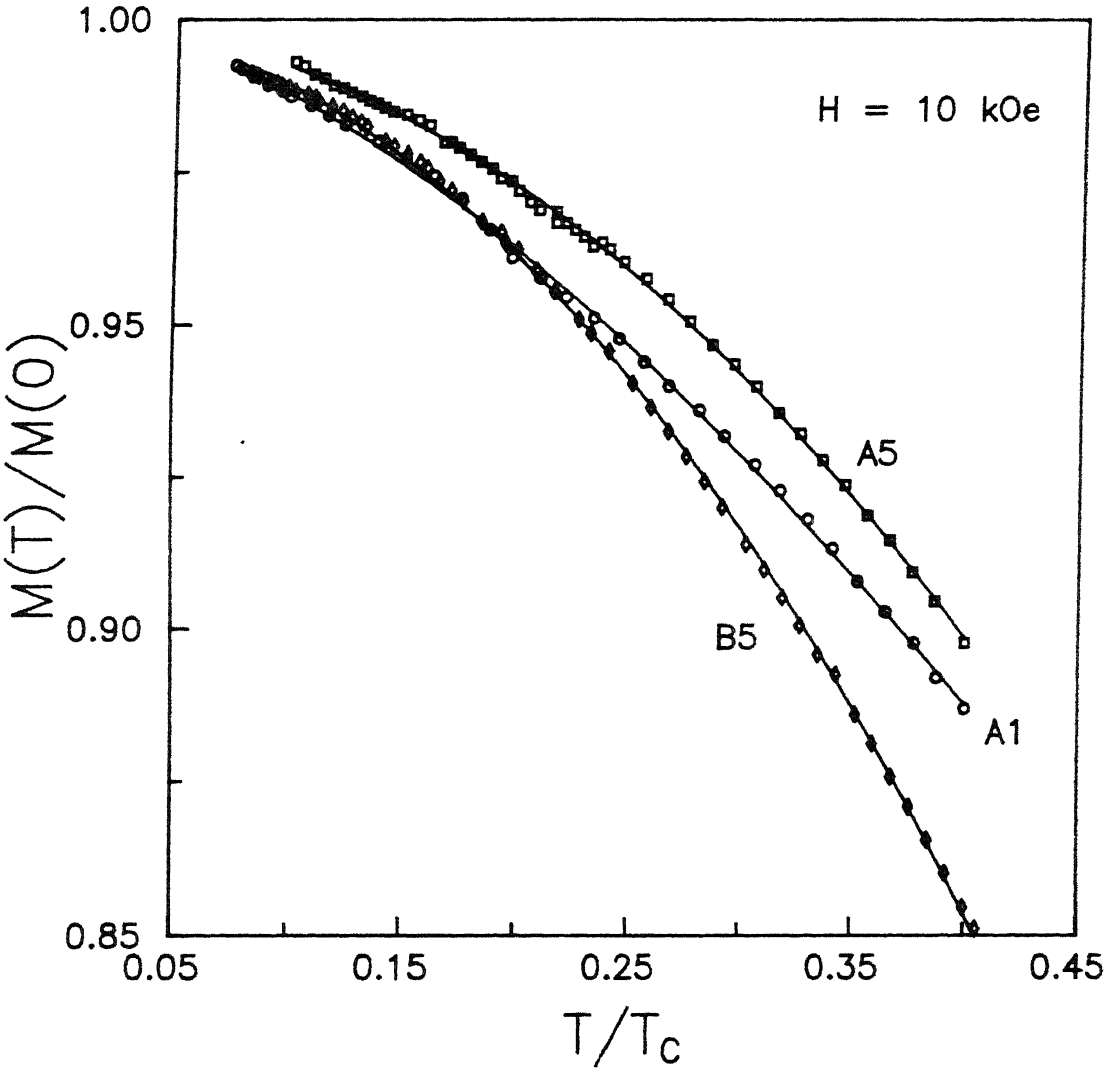

Fig. 3.20 Normalized magnetization M(T)/M(Ø) versus T/Tc of samples A1, A5, and B5 ($Fe_5Co_{50}Ni_{17}B_{16}Si_{12}$, $Fe_5Co_{50}Mn_{17}B_{16}Si_{12}$, and $(Fe_{7.8}Co_{31.2}Ni_{24}Mn_{15}(BSi)_{22}$, respectively). The solid lines are fits of the experimental data to Eq. (1.19).

obtained for samples A1 - A4. Again, as in A1, we have chosen only the $T^{5/2}$ term. The marginal improvement of χ^2 with the inclusion of the single-particle excitations may be due to more number of parameters, or it may actually be present. But in the absence of D values obtained independently from other measurements we do not interpret our data on the lines of the Stoner excitations.

Similarly, in B5 a $T^{5/2}$ term, in addition to the $T^{3/2}$, is found to be necessary to obtain a good fit. The coefficient of the additional term is two orders of magnitude smaller than that of the $T^{3/2}$ term. Here too, the exponential term when included gives the best χ^2 value. However, the value of Δ obtained is ($\sim$ 71 K) considerably smaller than those obtained for samples A1 and A5. We also find that in this sample the coefficient of the spin-wave term is small giving rise to a large value of D(Ø) and the ratio of $D(Ø)/T_c$ is also considerably larger than those in the other set of samples. Another feature, found in both the samples A5 and B5, is that a two-term fit with $A - BT^2$ gives a good fit with comparable χ^2 values. Addition of a $T^{3/2}$ term to this results in only a marginal improvement of χ^2. Puznaik et al. [21Ø] found that, in Co-rich Co-Si-B alloys, a fit of the form $A - BT^{3/2} - CT^2$ best describes their results. However, they suggested that the origin of the T^2 term is not due to the single-particle excitation. They noted that the Co-based alloys are best described as strong ferromagnets and the T^2 term in their study is associated with the small value of the mean-square dispersion Δ of the exchange integral J_{ij}.

To summarize, we find that the magnetization of (i)

Cr-containing samples (A2 - A4) is described by the $T^{3/2}$ term alone and (ii) A1, A5, and B5 also consists of a second term of the form $T^{5/2}$ in addition to the $T^{3/2}$ term.

It is seen that to compare various values of the coefficients B and C with widely varying T_c's, it is better to write them in the form of $B_{3/2} = B\ T_c^{3/2}$ and $C_{5/2} = C\ T_c^{5/2}$ (Eq.(1.2Ø)). We find that $B_{3/2}$ varies between Ø.26 and Ø.66. The value of $B_{3/2}$ varies with T_c in different ways in the Cr and Mn-containing samples. It decreases with decreasing T_c in Mn-containing samples in agreement with the observation of Kaul [131] but in Cr-containing samples it increases. Since the values are varying over such a wide range it is difficult to compare with the theoretical calculations [211] based on Heisenberg model of localized spins. Similar large variation in the values of $B_{3/2}$ is also reported in Co-B-Si alloys [212]. The theoretically calculated value for $B_{3/2}$ is Ø.587 and Ø.512 for S = 1/2 and S = 1 respectively. It was found that ferromagnetic glasses are much better described by this model than the corresponding crystalline alloys. As in other amorphous ferromagnets the value of $B_{3/2}$ is considerably large as compared to the value of about Ø.12 found in crystalline Fe, Co, and Ni.

The magnitude of $C_{5/2}$ of A5 and B5 is about an order of magnitude larger than those reported in Fe- and Ni-rich metallic glasses [127,131,135]. The theoretically predicted value is found to be Ø.156 and Ø.195 for S = 1/2 and S = 1 respectively. Since the value of C is very small, the error is also relatively large. The ratio of C/B gives the range of the exchange interaction (Eq. 1.25) $\langle r^2 \rangle^{1/2}$. It is found that in A1 the range is of the order

1A whereas in A5 and B5, it is about 7.5 A. Magnetization study on crystalline Ni-Fe-Cr alloys [144] suggest that the introduction of Cr suppresses the anharmonic term ($T^{5/2}$). We find that the coefficient of this term is very small in A1. With the substitution of Cr (A2 - A4) this coefficient may be further suppressed and this might explain the observation of only the $T^{3/2}$ term in these samples.

Figure 3.21 shows the plot of D(Ø) versus T_c. There exists a correlation between D(Ø) and T_c. D(Ø) is found to decrease with decreasing T_c. The plot shows that through the data points a straight line could be drawn which will also pass through the origin. Kaul [131] suggested that D(Ø), as a function of T_c, can be represented by an empirical relation

$$D(Ø) = D_o + m\, T_c \quad ,$$

where D_o and m are the intercept and the slope of the straight line. Extensive data on Fe-Ni amorphous alloys having T_c down to temperatures ~ 3Ø K show that $D_o \neq Ø$ [131]. It is found to be ≃ (27 ± 2) meV $Å^2$. Luborsky et al. [213] found three sets of data which give a linear dependence between D and T_c corresponding to (1) Fe-B-X (2) Fe-Ni-B-P and (3) Co-X in increasing order of D. For (1) extrapolation to zero D occurs at ~ 38Ø K, for (2) at about 2ØØ K and for (3) at about Ø K. Similar observations have also been made in Co-B-Si alloys [212]. These extrapolations, however, suffer from the drawback, as pointed out by Kaul [131], that the extrapolation are from large values of T_c ~ 4ØØ K.

For a nearest-neighbor cubic ferromagnet the Heisenberg model gives the expression for T_c as [118]

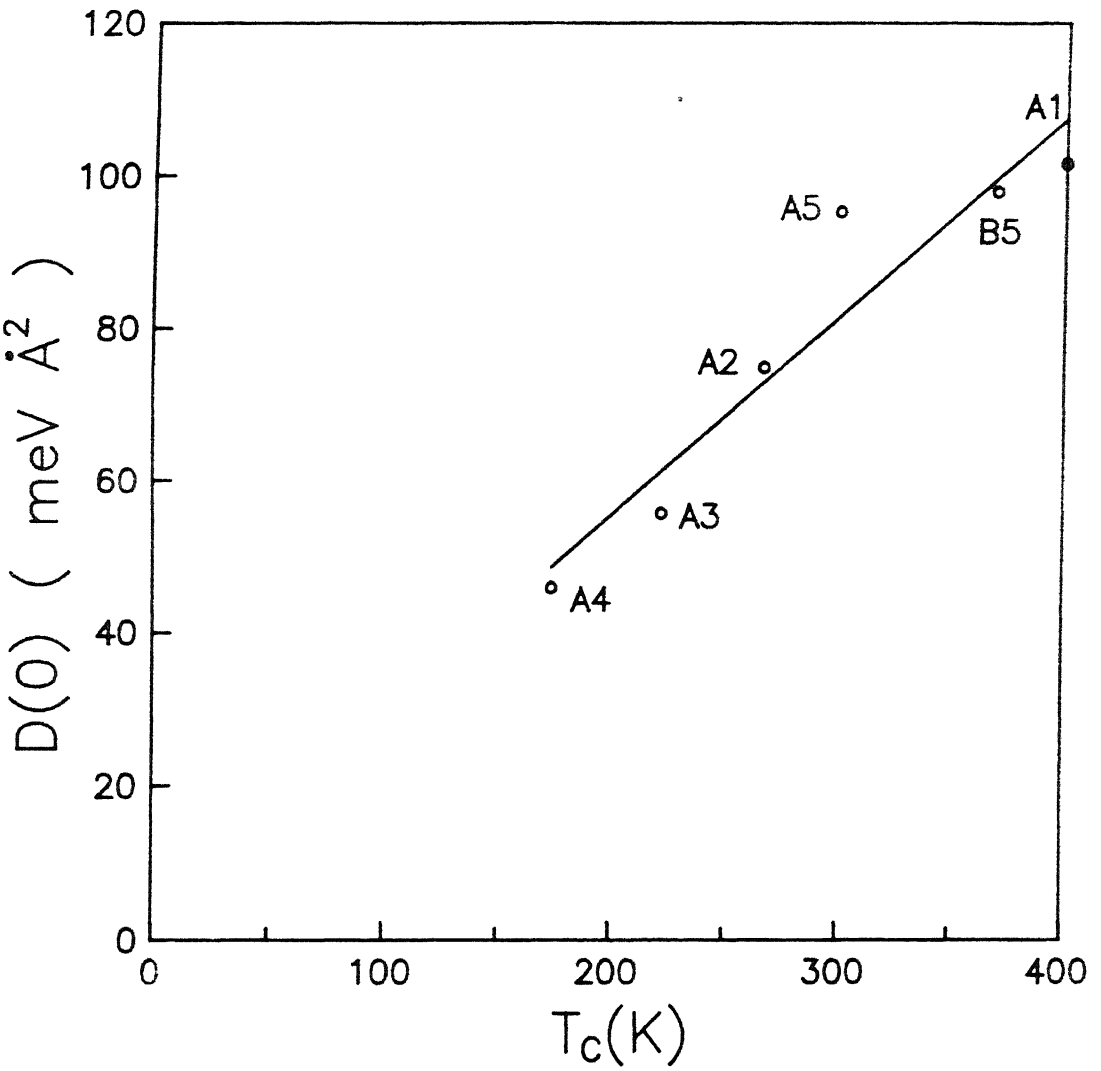

Fig. 3.21 Variation of spin-wave stiffness constant (D(Ø)) with Curie temperature (T_c).

$$T_c = [\ 2\ S\ (\ S + 1\ )\ /\ 3\ k_B\ ]\ z\ J\ ,$$

where J is the exchange coupling constant between nearest neighbor pairs, S is the localized atomic spin, and z is the number of nearest neighbors. D is related to J by

$$D = S\ z\ J\ a^2\ /\ 3\ ,$$

where a is the nearest neighbor distance. D, then, is written as

$$D = [\ k_B\ a^2\ /\ 2\ (\ S + 1\ )\ ]\ T_c\ .$$

The above expression shows that D versus T_c should be a straight line which passes through the origin. Kaul [131] calculated the values of the slope as Ø.14 and Ø.187 meV A^2 K^{-1} for S = 1 and S = 1/2 respectively using a = 2.55 A. We obtain the value of the slope ~ Ø.25 meV A^2 K^{-1} which is somewhat higher than the above values.

In summary, the Heisenberg model explains the temperature dependence of magnetization of the present series of alloys. The samples with Cr are adequately described by the $T^{3/2}$ term alone. The coefficient of this term increases with the increase in Cr. The sample without Cr and the one containing Mn show the presence of a $T^{5/2}$ term. The values of $D(Ø)/T_c$ vary between Ø.2 and Ø.3 meV A^2 K^{-1}. The plot of D(Ø) versus T_c shows that a straight line could be drawn through the data points and it also passes through the origin as predicted by the Heisenberg model.

Low-Field ac Susceptibility Measurements

The χ measurements of samples A1 to A4 show a behavior characteristic of a ferromagnet. The susceptibility rises in the PM-FM transition and then remains constant limited by the

demagnetization value as the temperature is lowered. On substituting Ni by Cr the magnitude of χ decreases and the ferromagnetic transition temperature (T_c) decreases monotonically from 395 to 180 K. The nature of χ , however, shows no change except for a small decrease of χ as the temperature is lowered. Figure 3.22 shows the plot of χ of samples A1 - A4 and summarizes the above results. On addition of Mn (A5 and B5) the PM-FM transition is observed at higher temperatures but as the temperature is lowered ($T < 120$ K) there is a large drop in χ from the demagnetization limited value (Fig. 3.23). At $T \simeq 30$ K there appears a shoulder and below 20 K the susceptibility drops further sharply. At 16 K the value of χ_{ac} is only 5% of its value at 80 K. Similar observations of a decrease in χ upon lowering of temperature have been identified with a ferromagnetic to a spin-glass transition [147,149,214,216]. This reduction in χ is interpreted as a restraint on the infinite ferromagnetic cluster response due to the freezing of finite clusters at lower temperatures [2]. An external dc magnetic field will suppress the ferromagnetic response and will modify the $\chi(T)$ behavior. In Fig. 3.24 we show the effect of various external coaxial dc fields on $\chi(T)$ for sample A5. Application of small dc magnetic fields modifies the $\chi(T)$ behavior and a peak could be seen at temperatures around 30 K. However, in the present case the application of a field as small as 13.8 Oe (Curve C) suppresses χ and it has to be magnified 10 times to see the flat peak around 50 K. Here it differs from AuFe alloys where a sharp structure could be observed at T_f even at 1.5 kOe. In the presence of external dc

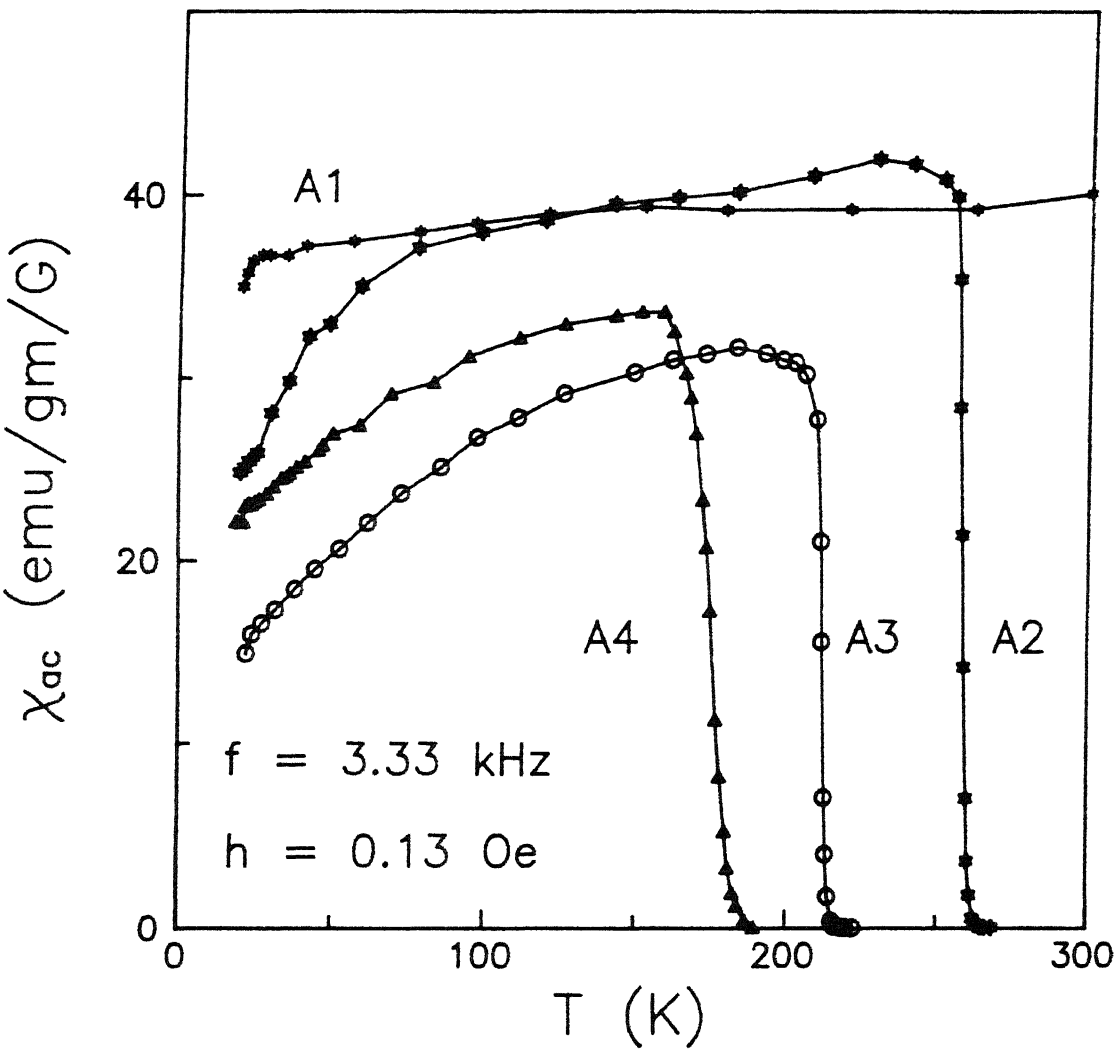

Fig. 3.22 χ_{ac} as a function of temperature for samples A1, A2, A3, and A4 ($Fe_5Co_{50}Ni_{17-x}Cr_xB_{16}Si_{12}$, x = Ø, 5, 1Ø, and 15).

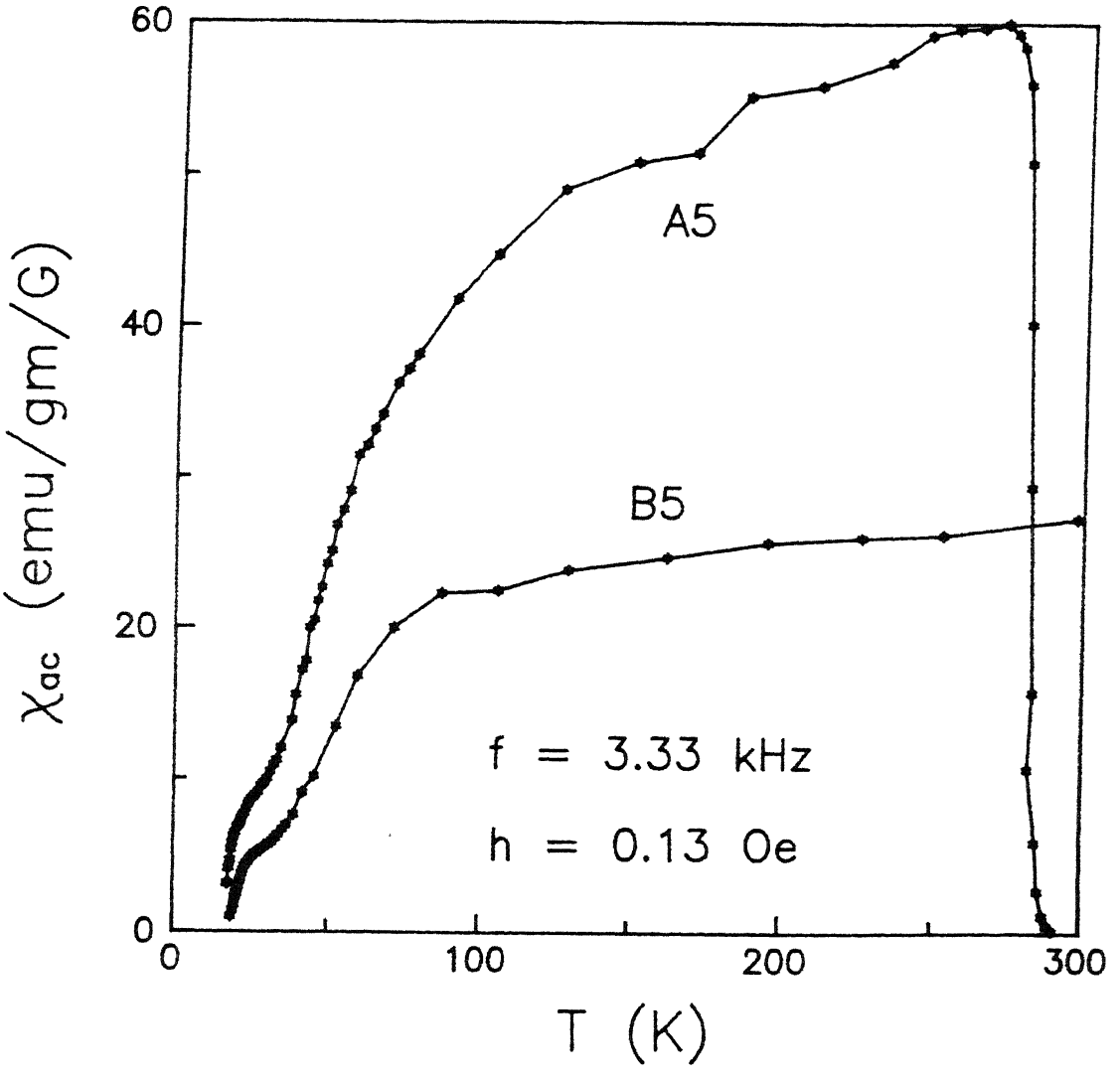

Fig. 3.23 χ_{ac} as a function of temperature for samples A5 and B5 ($Fe_5Co_{50}Mn_{17}B_{16}Si_{12}$ and $Fe_{7.8}Co_{31.2}Ni_{24}Mn_{15}(BSi)_{22}$, respectively).

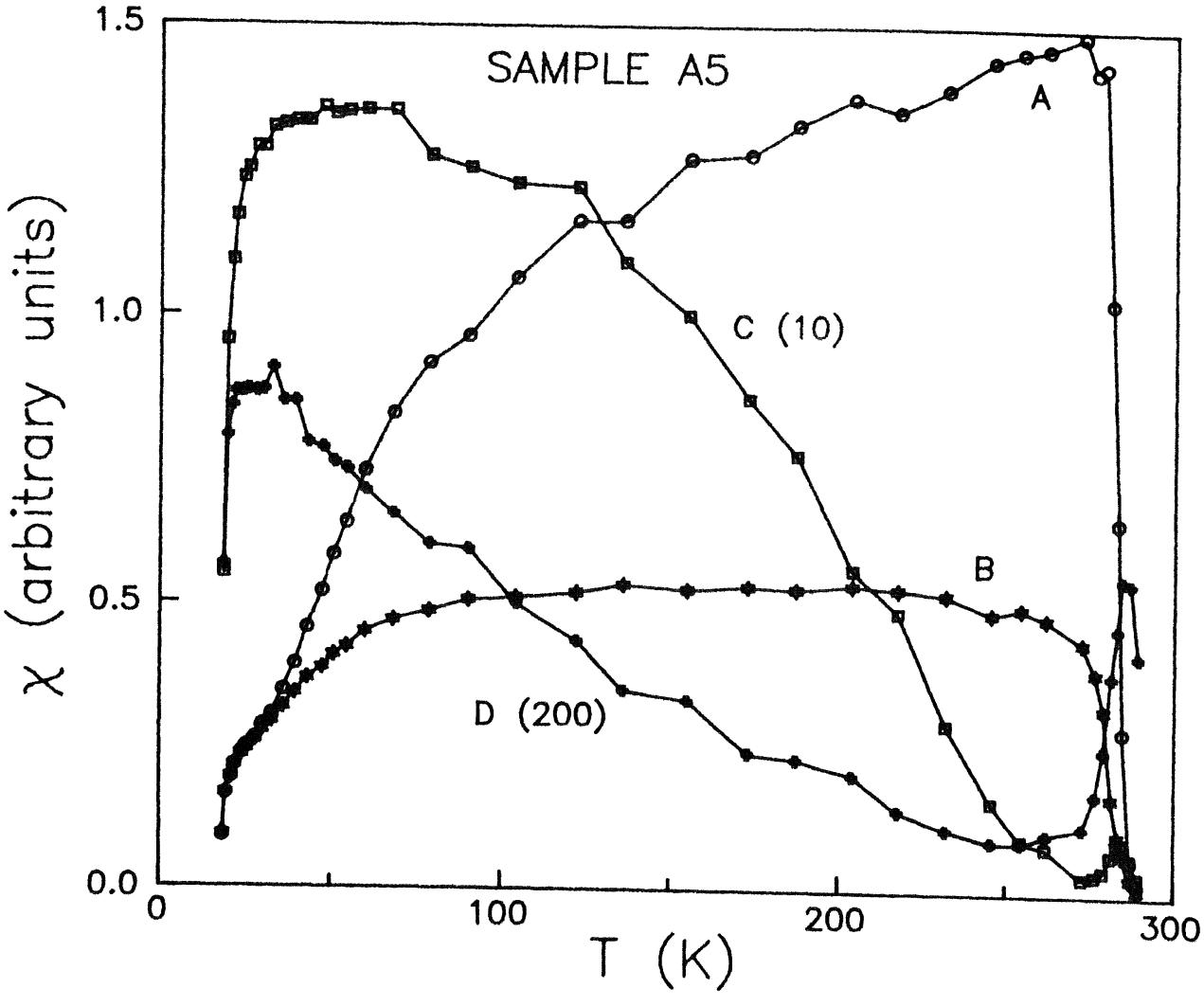

Fig. 3.24 $\chi_{ac}(T)$ of sample A5 ($Fe_5Co_{50}Mn_{17}B_{16}Si_{12}$) in various dc magnetic fields; A, H= Ø; B, H= 1.4 Oe; C, H = 14 Oe; D, H = 69 Oe. The figures in brackets are the multiplicative factor.

fields peaks in χ are known to exist near PM-FM and FM-SG transitions [142]. They are supposed to arise as a result of χ becoming zero for both large and small M. Scaling laws, which describe the peak heights against H, also hold good for the lower (FM-SG) transition as a result of which the peaks shift to lower temperatures with the increase in field. This can be observed also in our results (Fig.3.24) where the peak at 7Ø Oe (Curve D) is sharp but is at a lower temperature compared to the broad peak at 13.8 Oe. To corroborate these findings dc-magnetization measurements (Fig. 3.25) were made with a Faraday balance in 5ØØ Oe field and a distinct peak is observed at 3Ø K in the zero-field-cooled state. This temperature below which M drops, signaling the onset of the partial breakdown of long-range order, is designated as the spin-freezing temperature T_{xy}. M also exhibits a time dependence characteristic of a SG phase at 5 K in a measuring field of 1Ø Oe. The inset of Fig. 3.25 shows M against log t measured with a SQUID magnetometer. The data show that the decay of M is slower than log t and can be better described by a power law ($\propto t^{-\alpha}$). However, measurements at 19 K do not show any time dependence. Arrott-plots (not shown) at 19 K and above are linear and has a large positive intercept on the M^2-axis indicating the presence of long-range order (LRO). The results of B5 are identical to those of A5 and are not shown here. They establish that the system undergoes a PM-FM transition at a higher temperature and undergoes a second transition at T_{xy}. This phase is to be identified with the mixed-phase as envisaged in the GT model [215] where FM long-range order (large dc-susceptibility at

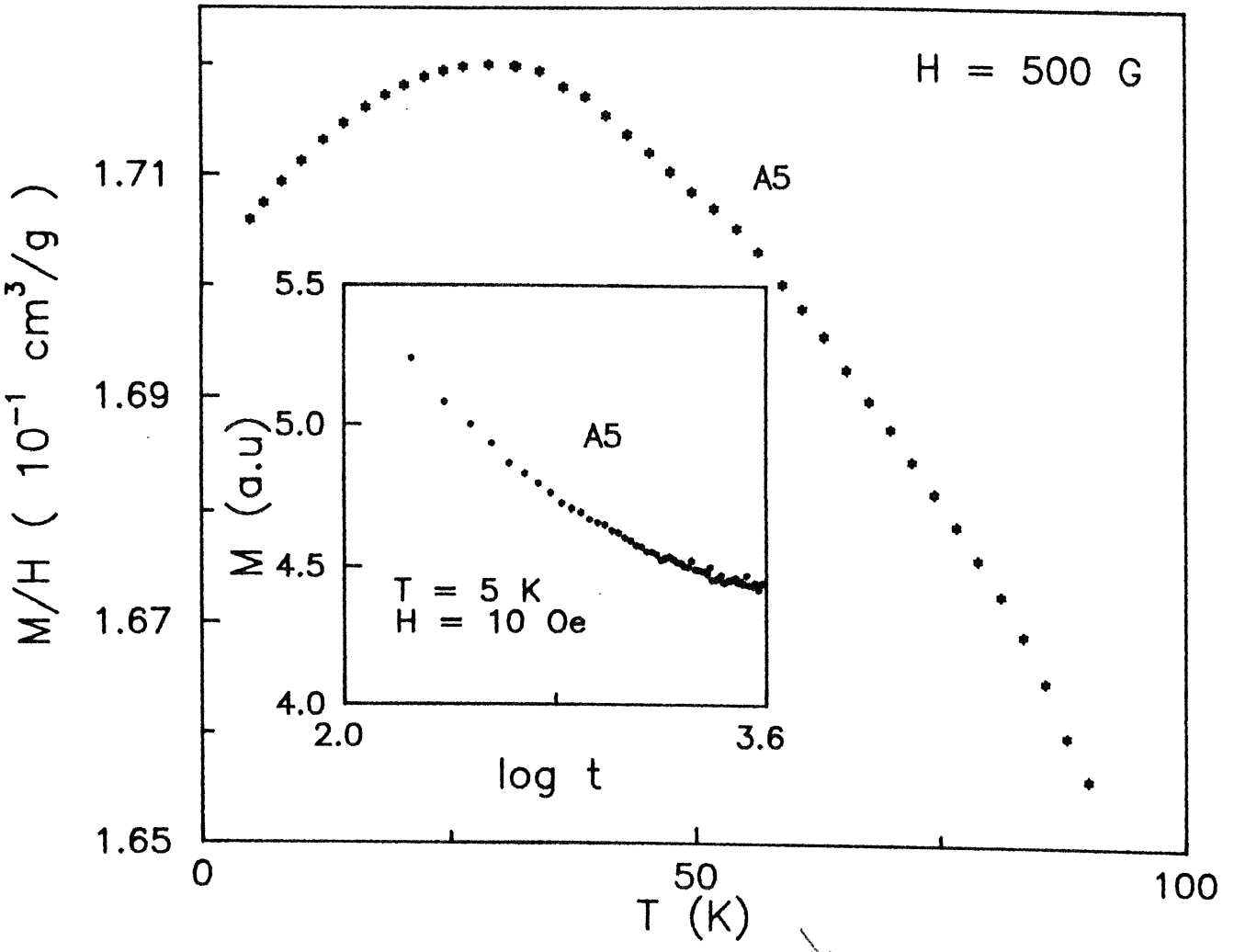

Fig. 3.25 M/H versus T of sample A5 ($Fe_5Co_{50}Mn_{17}B_{16}Si_{12}$), zero-field-cooled. Inset shows the time dependence of magnetization of A5 at 5 K in H = 10 Oe.

5ØØ Oe and Arrott plot) in z direction coexists with frozen-in transverse spin components (χ very small and time dependence of M).

From the phase diagram given by Miyazaki et al. [149] for $(Fe_{1-x}M_x)_{77}Si_{10}B_{13}$ (M = V, Cr, Mn, Ni) alloys, it is found that substitution of Fe by Mn raises T_{xy} ($\simeq$5Ø K) considerably as compared to Cr, V, and Ni. Though no explanation is put forward for this particular behavior, our results also indicate that the T_{xy} of Cr-containing samples, if any, is at a much lower temperature.

3.4 Critical Exponents

A. *Analysis*

The critical exponents describing the ferro- to paramagnetic transition are obtained from the following relations:

$$M = B\ (T - T_c)^{\beta}, \qquad \text{for } T < T_c \tag{3.18}$$

$$\chi = \Gamma\ (T - T_c)^{-\gamma}, \qquad \text{for } T > T_c \tag{3.19}$$

and $M = D\ H^{1/\delta}$ at $T = T_c$, (3.2Ø)

where B, Γ, and D are the critical amplitudes.

The three exponents among themselves are related by the scaling relation [216]

$$\beta\ \delta = \beta + \gamma\ . \tag{3.21}$$

There are several methods of obtaining the exponents from the above relations [163]. Our method of analysis is as follows: From the low-field χ_{ac} measurements, we obtain χ as a function of T for $T > T_c$. From the demagnetization corrected value of χ (demagnetization factor $\simeq$ Ø.Ø1), γ is obtained from the

Kouvel-Fisher plot [217]. In this plot, relation (2) is expressed as

$$X(T) = \chi^{-1} \left[\frac{d}{dT} \chi^{-1} \right]^{-1} = \frac{1}{\gamma_{eff}} (T - T_c) \quad .$$

The slope and the intercept of the plot of the function X(T) provides γ_{eff} and T_c respectively. This method has the advantage that a prior knowledge of T_c is not essential. A 3-point derivative of χ^{-1} is taken thus smoothing the data over a small region ($\simeq$ 100 mK). The values of γ_{eff} and T_c with the uncertainties are obtained using a least-squares fit program and are given in Table 3.7. The results of this analysis is plotted in Fig. 3.26, which shows X as a function of ε (= $(T - T_c) / T_c$), for samples A2 and A3. In this figure the data for sample A2 are displaced along the vertical axis and therefore they do not pass through the origin. However, the data for A3 are not displaced and hence they pass through the origin. A sample of Metglas 2826A (Allied Chemicals) was also measured to verify the results as its values of γ and T_c exist in the literature [218]. We obtain for sample 2826A, γ = 1.35 and T_c= 225.3 K where the range of analysis is confined to ε = $(3.15\text{-}47.5)\times10^{-3}$. The values are in good agreement with those reported. The T_c obtained by the KF method matches with that obtained by the derivative method, except for the sample A4. In A4, the T_c differs by about 7 K between these two methods.

From the dc-magnetization measurements the values of β, γ, and δ are obtained. A plot of ln M vs ln H is made at T_c. Figure 3.27 shows the plots for samples A2 and A3. The values of δ

Table 3.7

Values of β_{eff}, γ_{eff}, δ, and T_c of A2, A3, and A4.

	Method	A2	A3	A4	Heisenberg 3D [170]
T_c(K)	ACS	267.0(1)	222.3(3)	-	
	VSM	268.1(8)	222.5(7)	174.0(8)	
α^*		0.2	-0.2	-0.7	
β_{eff}	VSM	0.35(1)	0.41(1)	0.52(3)	0.365
γ_{eff}	ACS	1.19(1)	1.38(2)	-	1.387
[Range of fit]	$\varepsilon \times 10^3$	2.2-25	3.1-32	-	
γ_{eff}	VSM	1.19(2)	1.30(3)	1.73(6)	
δ	VSM	4.42(1)	4.49(5)	4.32(14)	4.803
B		38.7	44.7	57.7	
Γ^{-1}		10,000	11,600	15,800	
M(0) (emu/gm)		48.1	44.7	40.8	
$\bar{\mu}$ (μ_B/atom)		0.42	0.38	0.34	

VSM: Vibrating Sample Magnetometer; ACS: ac Susceptibility; *: Calculated from Rushbrook inequality, $\alpha = 2(1-\beta)-\gamma$; + obtained from scaling analysis; $\varepsilon = (T-T_c)/T_c$.

The numbers in brackets indicate the uncertainty in the least significant figure and are obtained from the confidence limits of the best-fitted parameters of the least-squares fit.

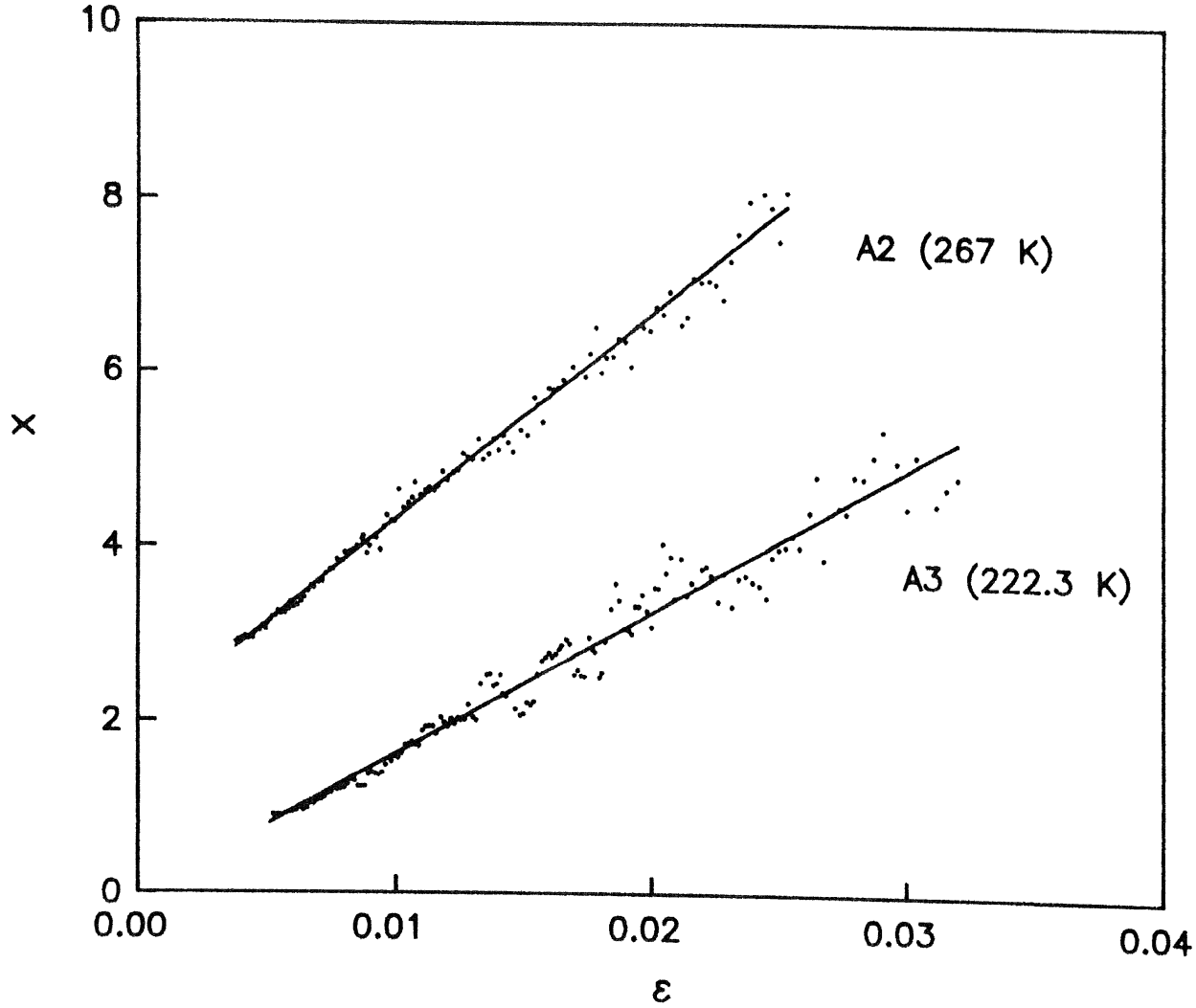

Fig. 3.26 Plot of X ($=\chi^{-1}(d\chi^{-1}/dT)^{-1}$) versus ε ($=(T-T_C)/T_C$) of A2 and A3 ($Fe_5Co_{50}Ni_{17-x}Cr_xB_{16}Si_{12}$, x = 5 and 10, respectively). The figures in bracket indicate the respective T_C. The data of A2 are displaced along the vertical axis. The continuous line is obtained from least-squares analysis.

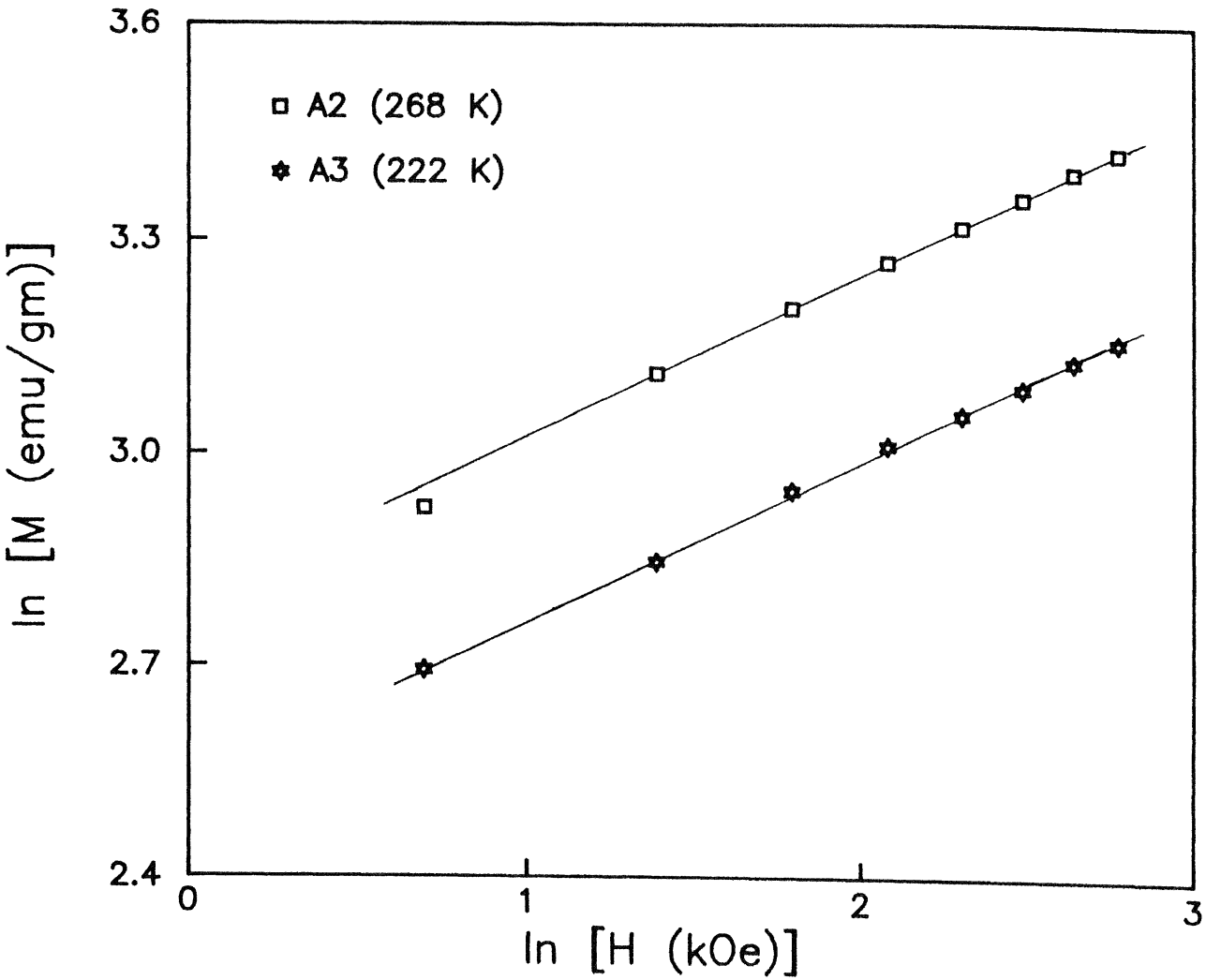

Fig. 3.27 lnM versus lnH plot near the T_c of A2 and A3 ($Fe_5Co_{50}Ni_{17-x}Cr_xB_{16}Si_{12}$, x = 5 and 10, respectively) for determining δ.

are estimated from the slopes of these straight lines. For sample A4, the slope near T_c was strongly temperature dependent. In the absence of M(H) data exactly at T_c = 174 K, δ was plotted as a function of temperature, over an interval of 8 K around T_c, from which the value of δ at 174 K was obtained. The values of δ for the three samples are given in Table 3.7. We find that δ of sample A4 ($\simeq$4.2) is slightly lower than those of A2 and A3 ($\simeq$ 4.45) and also the error in it is relatively large, which may partly be due to the extrapolation procedure adopted. To estimate M_s we consider the Arrott-Noakes equation of state [219]

$$\left[\frac{H}{M}\right]^{1/\gamma} = \left[\frac{T - T_c}{T_1}\right] + \left[\frac{M}{M_1}\right]^{1/\beta} ,$$

with the material parameters M_1 and T_1. With proper choices of β and γ, a plot of $(M)^{1/\beta}$ vs $(H/M)^{1/\gamma}$ gives a set of straight lines near T_c . The intercepts on the $M^{1/\beta}$ and $(H/M)^{1/\gamma}$ axes give M_s and χ^{-1} respectively. Using Eq. (3.21) an equivalent form of this graph (not shown) could be plotted between $M^{\delta-1}$ vs H/M. Near T_c, the data points fall on a straight line. The low-field data points deviate from the straight line. From the intercepts of the high-field data of the isotherms near T_c, extrapolated to H = Ø (H corrected for demagnetization), we obtain M_s. The Kouvel-Fisher method of analysis allows us to obtain β and T_c by rewriting Eq. (3.18) in the form

$$Y(T) = M_s \left[\frac{d}{dT} M_s\right]^{-1} = \frac{1}{\beta_{eff}} (T - T_c) .$$

The plot of Y versus T is a straight line whose intercept and slope give T_c and β respectively. However, Y versus $-\varepsilon$ is plotted in Fig. 3.28 where the data for samples A3 and A4 are displaced along the vertical axis and therefore they do not pass through the origin (unlike A2). The values of β obtained are in the range Ø.35 - Ø.52. The exponent in the range $T > T_c$ is obtained from $M^{3.5}$ vs H/M plots. The high-field intercepts on the H/M axis provides $1/\chi$ at different temperatures. Then, using the method of Kouvel and Fisher, γ and T_c are obtained. The values of γ and T_c (within 1 K) agree with those obtained from the low-field χ_{ac} measurements [Table 3.7]. The analysis has been confined to a narrow region of temperature around T_c. As we go farther away from T_c, the curvature in the plots increases to such an extent that it becomes difficult to make a linear extrapolation. Due to this restriction the region beyond the asymptotic critical regime has not been analyzed.

The magnetic equation of state is a relationship among the variables M, H, and T. Using the scaling hypothesis, this can be written as

$$\frac{M(\varepsilon,H)}{|\varepsilon|^{\beta}} = M\left[\frac{\varepsilon}{|\varepsilon|}, \frac{H}{|\varepsilon|^{\beta\delta}}\right] .$$

In terms of the variables $m \equiv |\varepsilon|^{-\beta} M(\varepsilon,H)$ and $h \equiv |\varepsilon|^{-\beta\delta} H(\varepsilon,M)$, called the scaled magnetization and scaled magnetic field respectively, the above equation can be written as

$$m = f_{\pm}(h).$$

This relation shows that m, as a function of h, falls on two

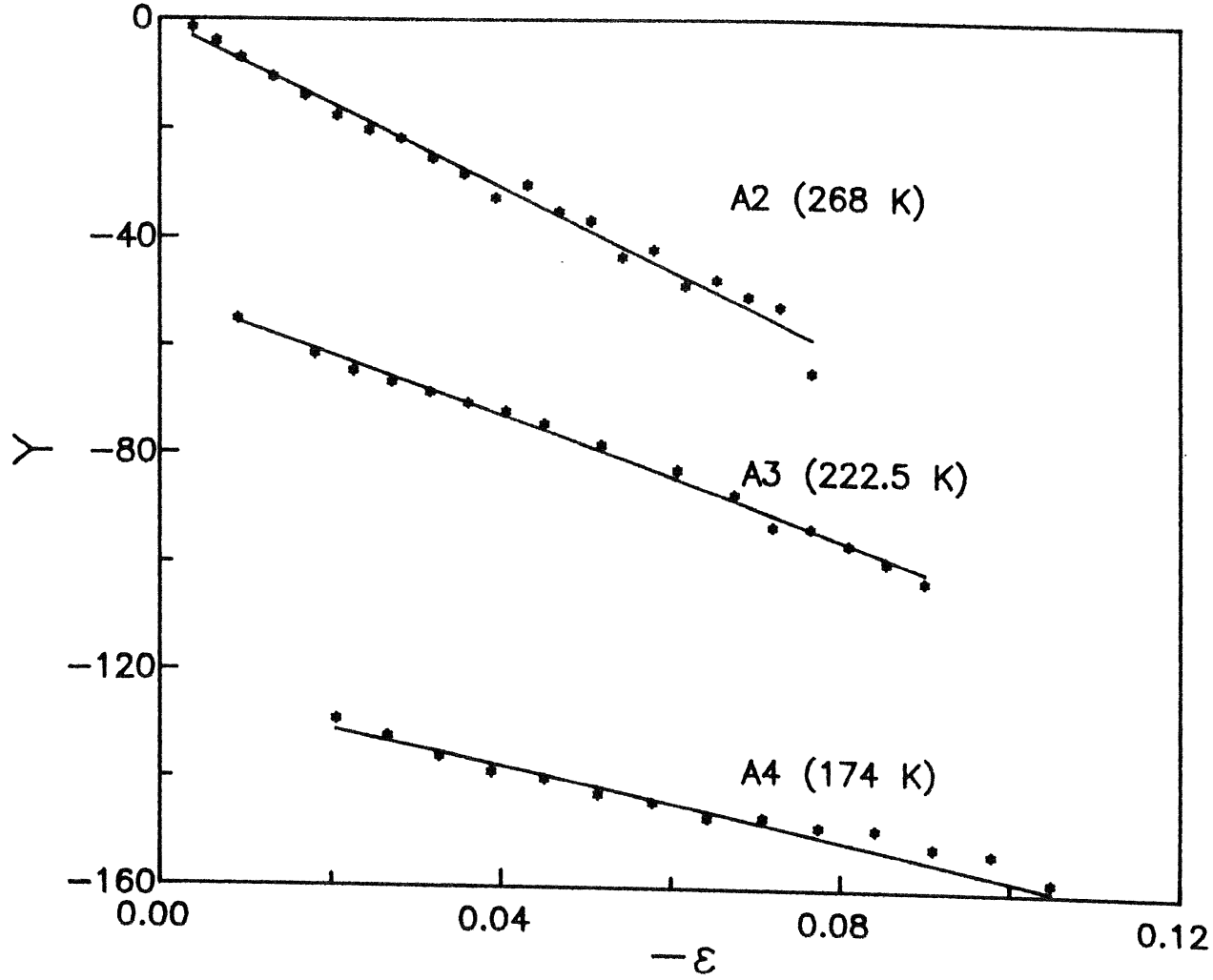

Fig. 3.28 Plot of Y ($=M_S(dM_S/dT)^{-1}$) versus ε ($=(T-T_C)/T_C$) of A2, A3, and A4 ($Fe_5Co_{50}Ni_{17-x}Cr_xB_{16}Si_{12}$, x = 5, 10, and 15, respectively). The figures in brackets indicate the respective T_C. The data of A3 and A4 are displaced along

curves: one for $T < T_c$ and the other for $T > T_c$. If the scaling relations are valid and a correct choice of β, γ, and δ are made, then in a plot of ln m vs ln h, all the data points collapse onto two branches (Figs. 3.29(a)-(c)). Due to the relatively higher uncertainty in all the exponent values of sample A4 (see Table 3.7), the plot for this sample (Fig. 3.29(c)) is not as satisfactory as those of the A2 and A3 (Figs. 3.29(a) and (b)). For large values of ln h, the data may be fitted to a straight line, the slope of which is $1/\delta$. It is still better to plot m^2 vs h/m to verify the scaling relations [163]. Figures 3.30(a)-(c) show this plot for A2, A3, and A4; the data points only above H_{ext} = 2 kOe have been shown in the figure. They also show that the scaling equations are valid over a wide region of temperature both above and below T_c. The intercepts on the axes give m_o^2 and h_o/m_o. These are related to the critical amplitudes B and Γ in the following manner:

$$B = m_o \quad , \qquad T < T_c$$

and $$\Gamma^{-1} = (h_o/m_o), \quad T > T_c \quad .$$

These values are included in Table 3.7. h_o is identified with the effective exchange interaction field.

B. *Discussion*

Table 3.7 summarizes the values of T_c, β, γ, and δ obtained for samples A2, A3, and A4. With the substitution of Ni by Cr, the T_c decreases monotonically by about 8 K/at.% Cr. The value of δ remains nearly the same for the three samples but is lower than the theoretical estimate of 4.8. It is found that this exponent

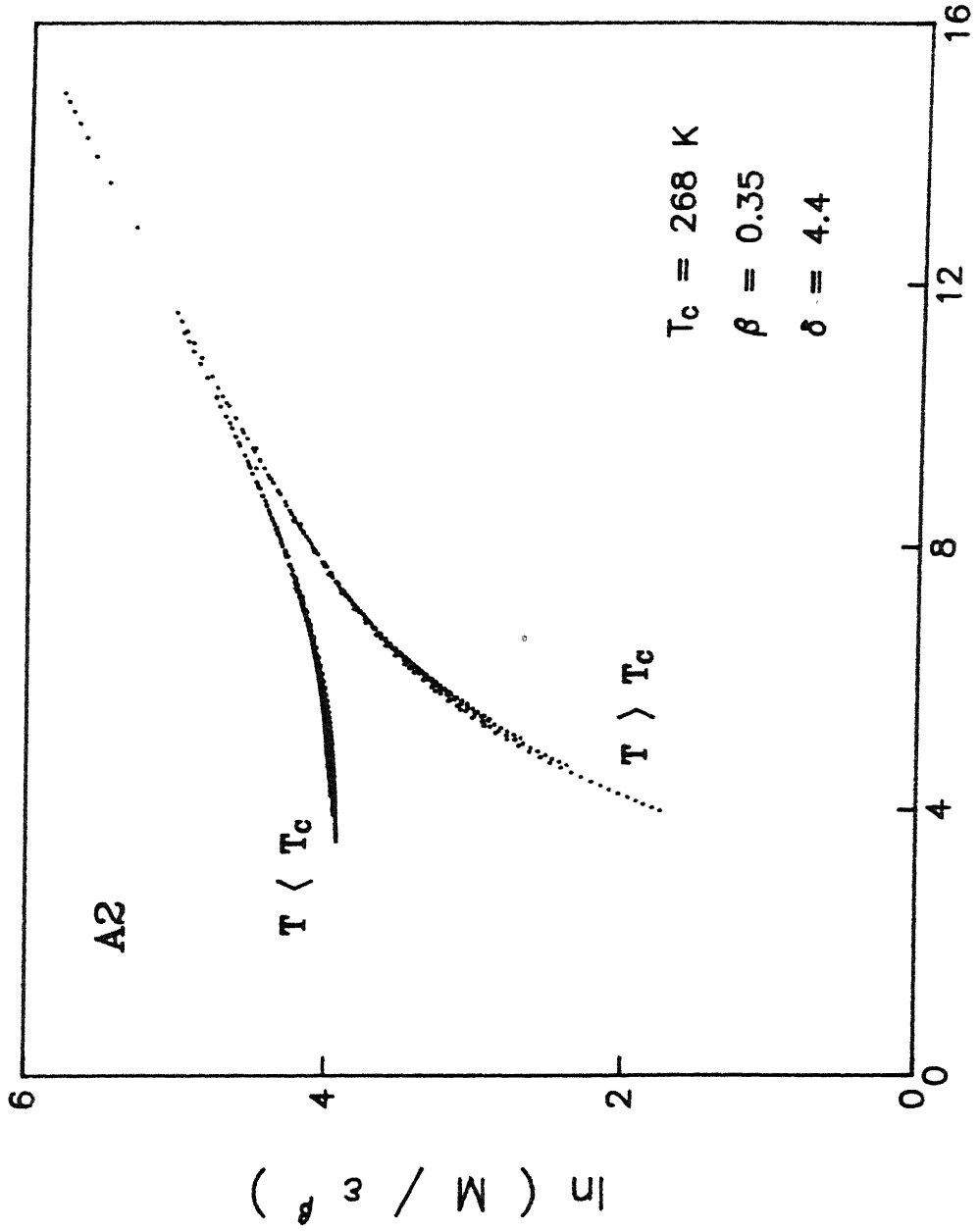

Fig. 3.29 (a) Scaling plot for A2 ($Fe_5Co_{50}Ni_{12}Cr_5B_{16}Si_{12}$).

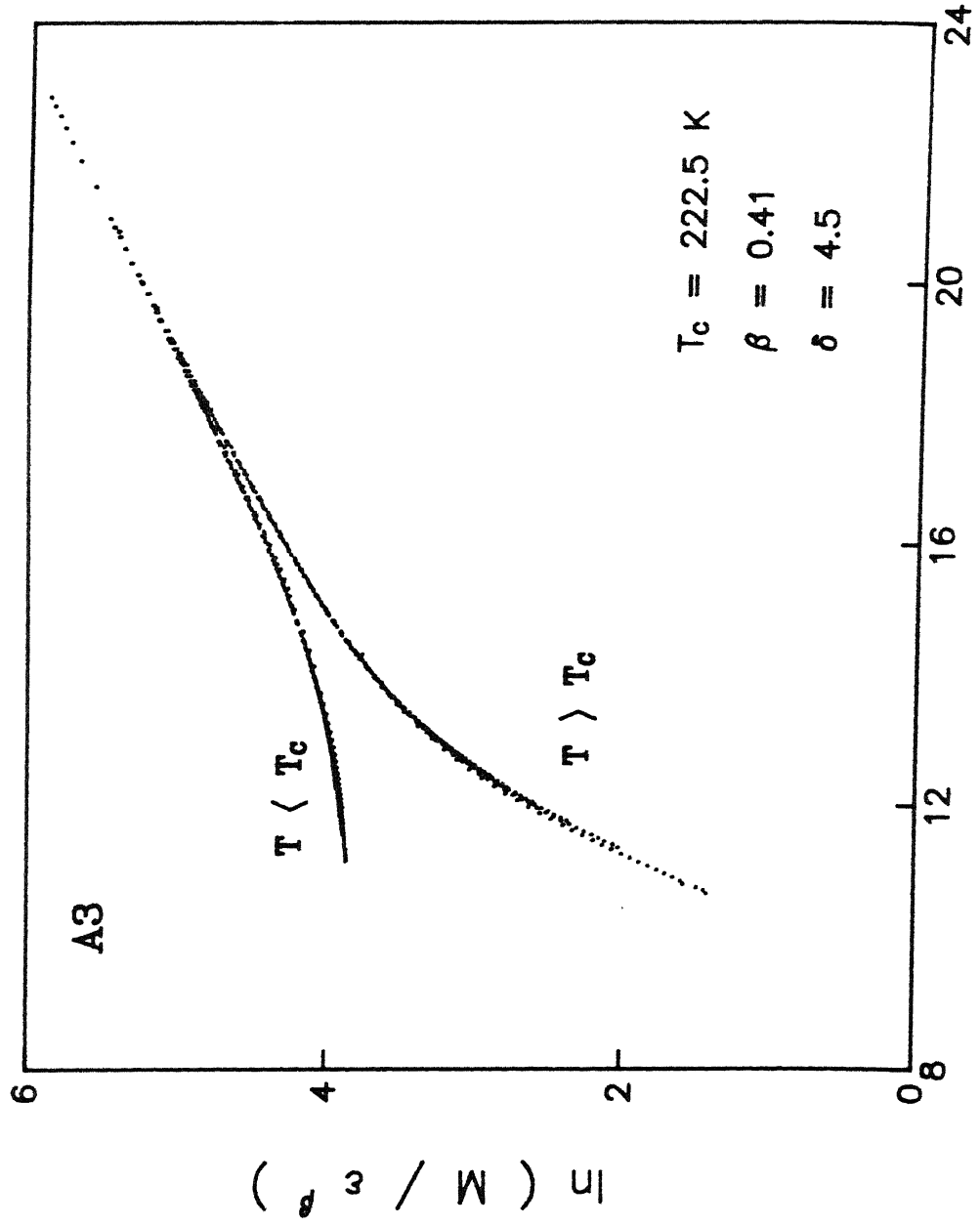

Fig. 3.29 (b) Scaling plot for A3 ($Fe_5Co_{50}Ni_7Cr_{10}B_{16}Si_{12}$).

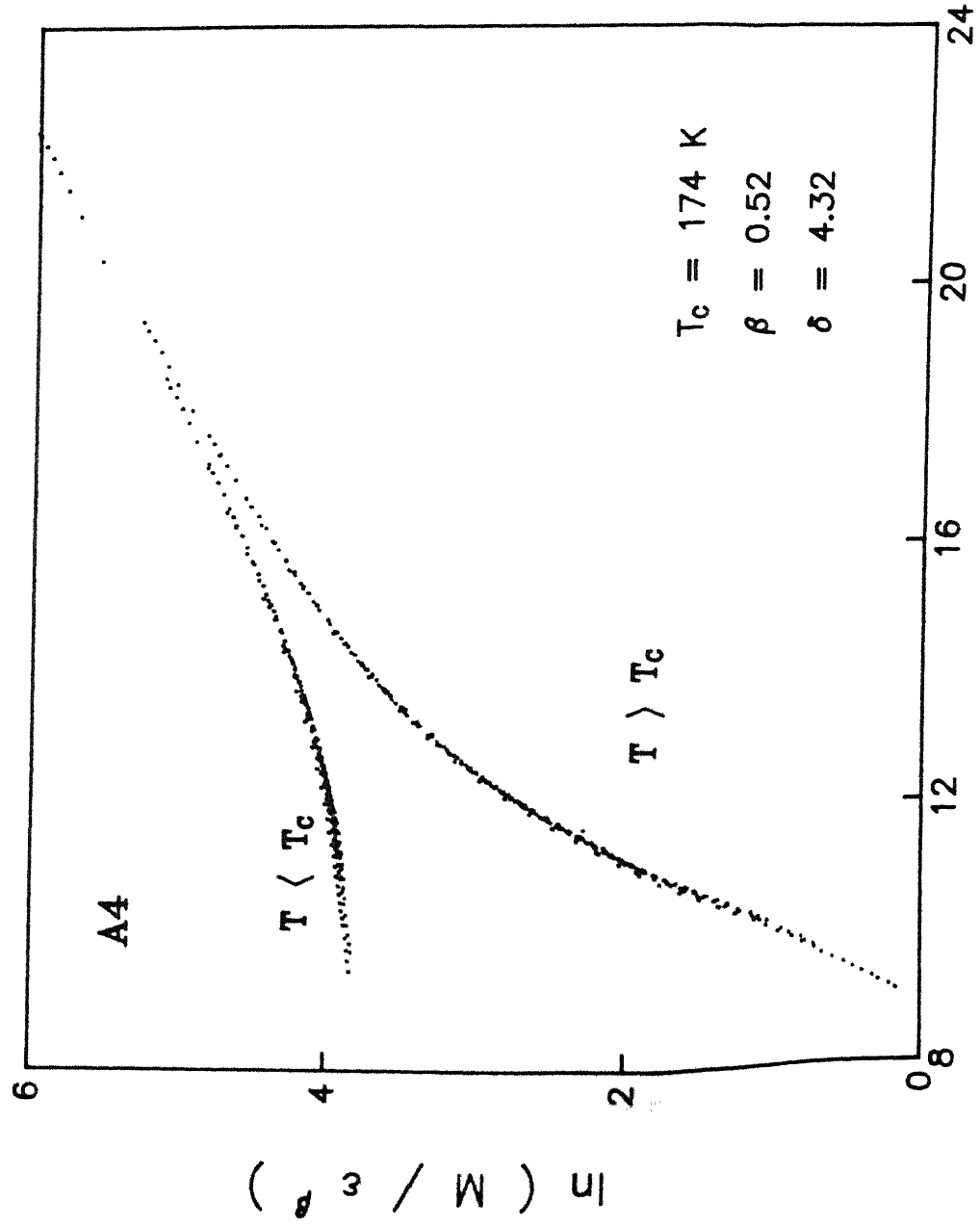

Fig. 3.29 (c) Scaling plot for A4 ($Fe_5Co_{50}Ni_2Cr_{15}B_{16}Si_{12}$).

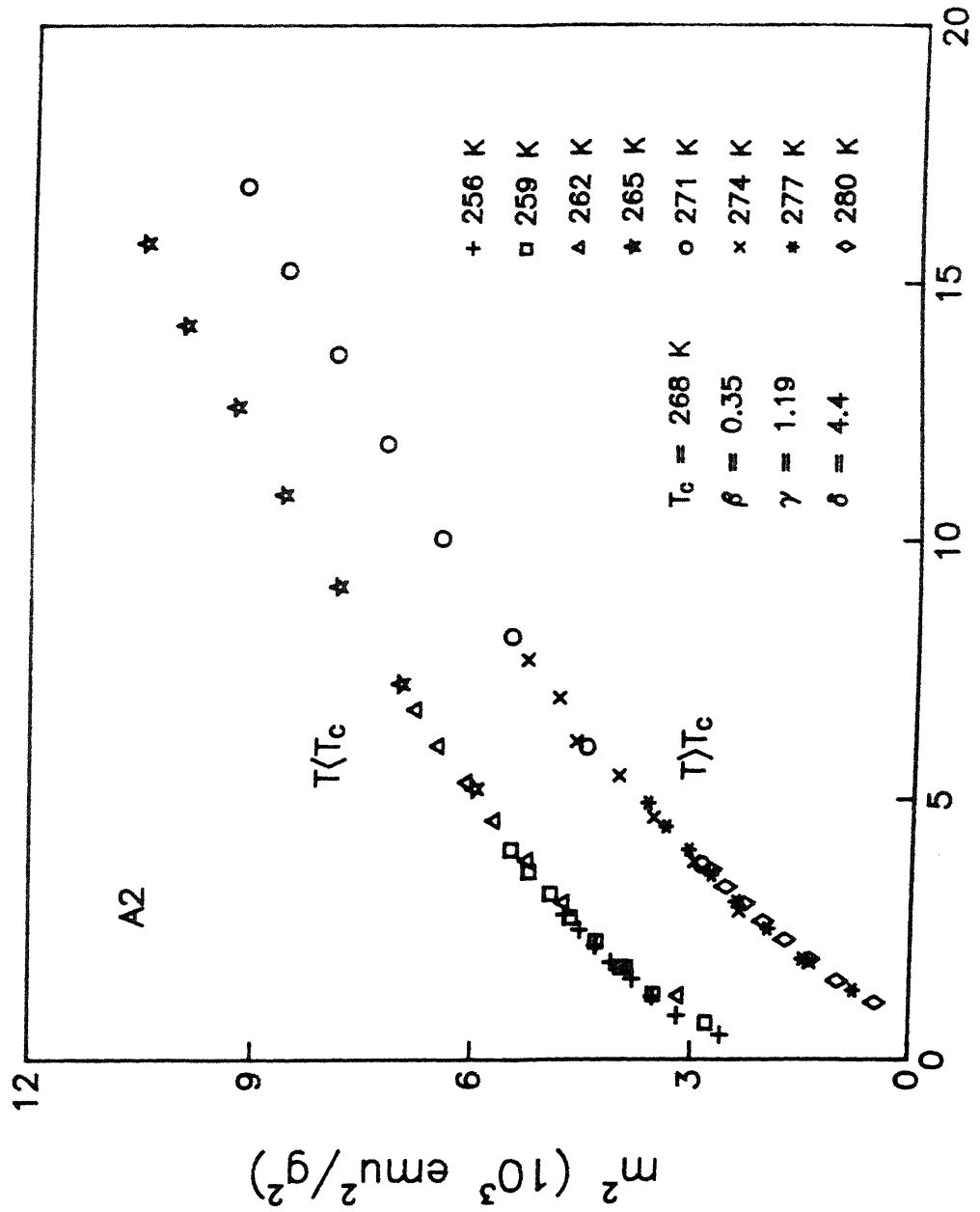

Fig. 3.30 (a) Plot of m^2 versus h/m for A2 ($Fe_5Co_{50}Ni_{12}Cr_5B_{16}Si_{12}$).

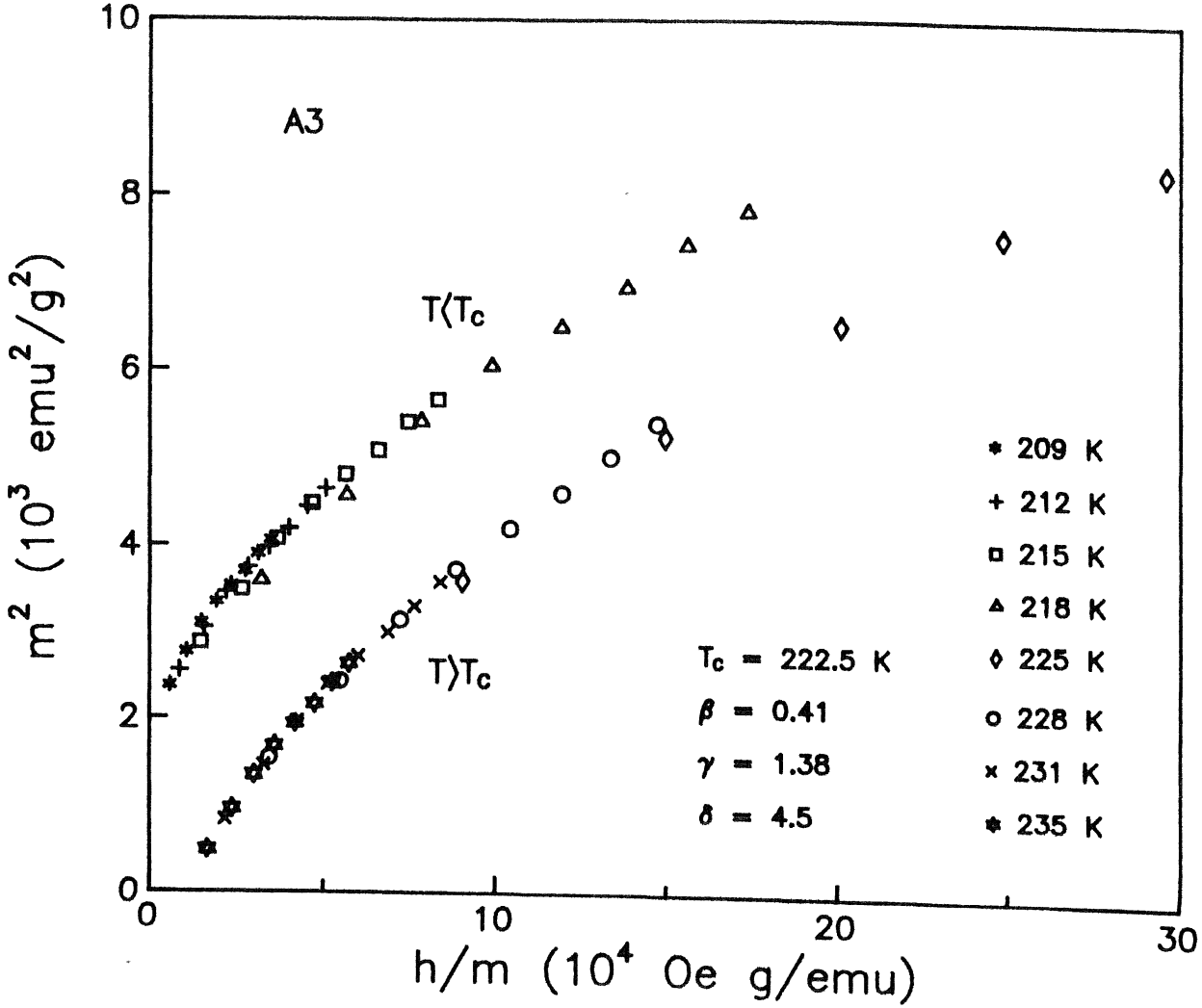

Fig. 3.30 (b) Plot of m^2 versus h/m for A3 ($Fe_5Co_{50}Ni_7Cr_{10}B_{16}Si_{12}$).

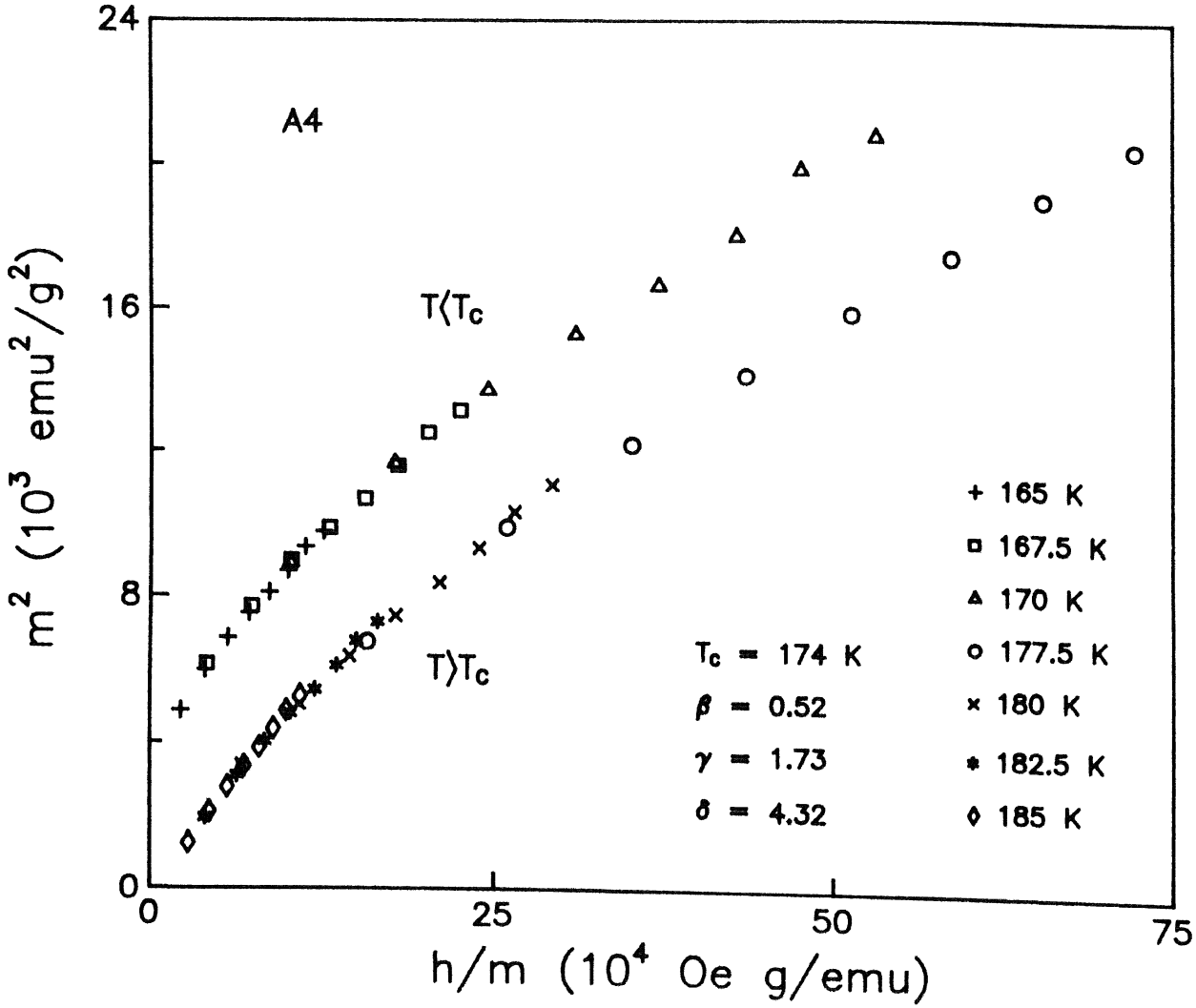

Fig. 3.30 (c) Plot of m^2 versus h/m for A4 ($Fe_5Co_{50}Ni_2Cr_{15}B_{16}Si_{12}$).

varies in the range 2.8 - 6.8 for amorphous ferromagnets [163]. β exhibits a small concentration dependence, though in the case of A2 and A3, it is closer to the Heisenberg value of Ø.365. The experimentally determined values are more in the vicinity of Ø.4Ø. But A4 has a value of β which is higher than those of A2 and A3. The value of γ is the most-often experimentally determined quantity and is normally used as an evidence for or against the various theories. The sample A2 shows an uncharacteristically low value for γ. The value for A3 matches with the 3D Heisenberg value. With further addition of Cr (A4), γ increases to $\simeq$1.73. Thus, while we observe that, with the addition of Cr, the coefficients β and γ increase beyond the uncertainties associated with them, the changes in the exponents are relatively small in the case of A2 and A3. Their values are closer to the theoretically estimated ones for homogeneous systems. For sample A4 (large Cr) the exponents β and γ are significantly larger and different from those of A2 and A3. In all these alloys the indices obey the scaling equation of state over the whole range of temperature. Assuming that the Rushbrook inequality holds good, an estimate of the value of the specific heat exponent is made. It gives α = Ø.2, -Ø.2, -Ø.7 for A2, A3, and A4 respectively.

It is observed that there exists a significant curvature in the M(H) plots for all the three samples at $T > T_c$. In the case of A4, the curvature is seen to exist even beyond $1.4T_c$. In the case of A2 and A3, the region up to only $1.15T_c$ could be studied. The non-linearity in M(H) curve, beyond T_c, is known to arise due to superparamagnetic clusters. In a structurally disordered material

there is a tendency towards the formation of localized clusters of strongly interacting moments giving rise to superparamagnetism [220]. One of the other criteria for superparamagnetic behavior is that a plot of M vs H/T should give a universal curve. In our studies, though a large curvature is observed, it does not show the universal nature. Similar behavior is also observed in other Ni-rich alloys [221] and is attributed to the formation of clusters which are not independent of temperature, and interact among themselves. One plausible explanation for the deviation of the indices in sample A4 from those of a homogeneous system could be the existence of these clusters. The presence of clusters in Cr-containing samples have been inferred from specific heat [173,222] and neutron diffraction measurements [223]. It is also found that the presence of Cr smears the transition. In addition, neutron scattering measurements on Fe-Cr and Fe-Mn based glasses [223] show that the spin-spin correlation length ξ does not diverge at T_c. In general, the influence of disorder is not observed in the true critical region, the reason being that as $T \rightarrow T_c$ there are strong correlations in the spin system and all spins within a range described by $\xi(T)$ interact cooperatively and the effect of disorder on a length scale smaller than $\xi(T)$ is reduced [171]. The effect of disorder is observed only at higher temperatures where $\xi(T)$ becomes small compared to atomic scale inhomogeneities. Thus, the non-divergence of $\xi(T)$ at T_c due to the presence of clusters may be responsible for the anomalous behavior of the exponents in A4. Alloys near $x \approx x_c$ also exhibit similar values of exponents.

From the present measurements we are able to conclude that the presence of quenched disorder does not lead to significant change in the exponents as evident from the results of A2 and A3. The exponents do not match exactly with the theoretical values but are in conformity with other experimental results. This difference in the theoretically predicted and the experimentally measured values has been discussed [163,224] and is attributed to the presence of long-range interactions in the system. We find that in sample A2 and A3 the exponents β and γ increase with the addition of Cr but the increase is relatively small. The exponents are closer to the theoretically estimated values for homogeneous systems. However, in A4 the values of the exponents β and γ are large and significantly different from those of A2 and A3 and are very similar to those observed in compositions close to the critical concentration. Recently, Houer and Wagner [225] have shown that deviations from Heisenberg values need not be limited to compositions close to the critical concentration and may be observed in materials which are further away from x_c.

3.5 High-Temperature Magnetization

The alloys studied are A1 - A4. The magnetization behavior as a function of temperature of sample A1 is shown in Fig. 3.31. The large drop in magnetization (plotted in emu) at $\approx$ 400 K indicates the ferromagnetic (FM) to paramagnetic (PM) transition temperature (T_c) of the amorphous phase. The transition is fairly sharp and the paramagnetic tail touches the zero magnetization line. This shows that the whole amorphous matrix goes into the paramagnetic

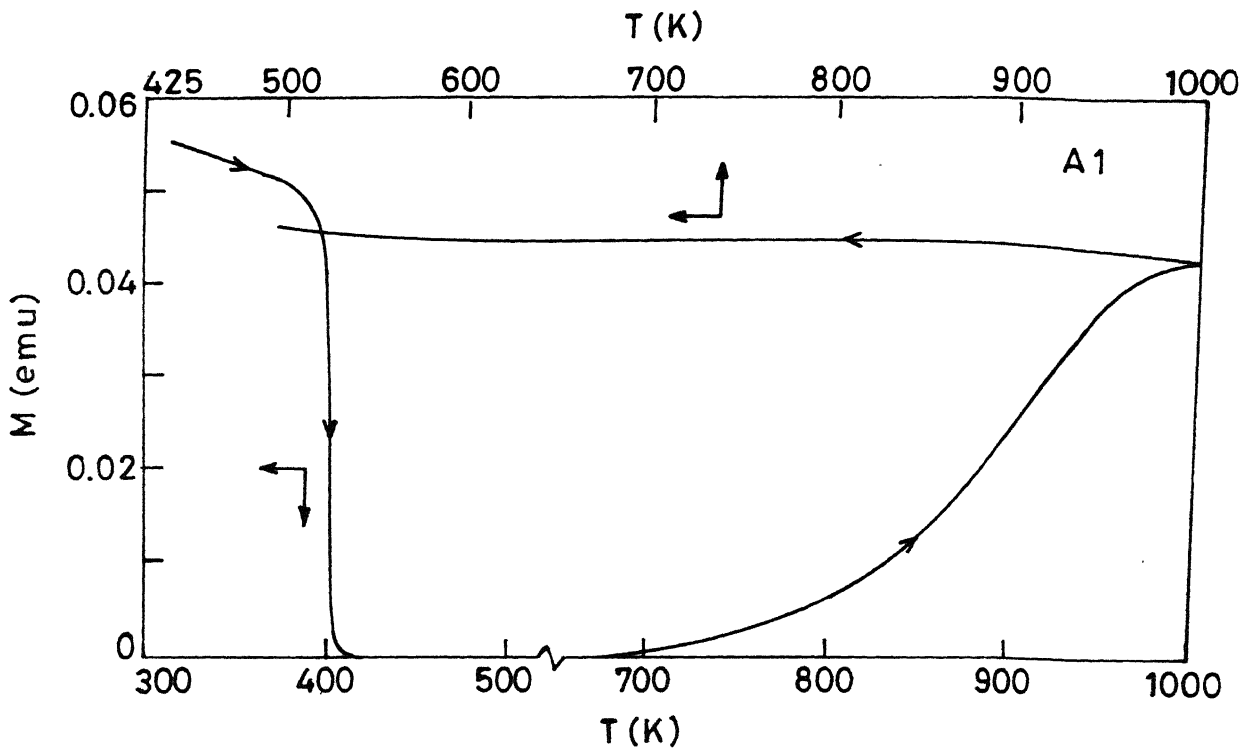

Fig. 3.31 The magnetization M as a function of temperature of sample A1 ($Fe_5Co_{50}Ni_{17}B_{16}Si_{12}$) in H = 30 Oe. The arrows indicate the heating and cooling cycles.

state and that there are no other secondary phases which have T_c at higher temperatures as observed in some FeB alloys [226]. The magnetization remains nearly constant till about 660 K, beyond which it again begins to increase. This is an indication of the growth of a crystalline phase which has a T_c at a much higher temperature. On increasing the temperature further, the magnetization increases continuously till 960 K beyond which it becomes nearly constant. The continuous increase in magnetization between 660 K and 960 K shows the growth and formation of one or more crystalline phases, which are magnetic and have T_c > 1000 K.

The crystallization temperature (T_x) is denoted here as the temperature at which the magnetization just begins to increase after the FM-PM transition (amorphous) has taken place. In this case it is 660 K. This measurement gives a much lower value for T_x than that obtained from DTA studies on similar systems. The indication of an exothermic peak in DTA studies is taken as an evidence for crystallization and by this method the T_x of $Fe_5Co_{70}(SiB)_{25}$ is obtained as 773 K [174] and for $Co_{58}Ni_{10}Fe_5B_{16}Si_{11}$ as 797 K [227]. This suggests that the reduction of the concentration of Co lowers the value of T_x significantly. The magnetic moment of the final crystallized phases here is almost as large as in the amorphous phase. On lowering the temperature the moment remains nearly constant at the 1000 K value. This is a signature of the system behaving as a strong FM. One of the characteristics of a strong FM is that the magnetization is independent of the structural details and so the moment remains the same in both the amorphous as well as the

crystalline phases [103] which is the case here.

The x-ray diffraction (XRD) patterns (Fig. 3.32) of the crystallized samples show the presence of the following phases: cubic Co, Co_2B, Co_2Si and Ni_5Si_2. Because of the complex nature of the present samples, quantitative estimation of the various phases crystallized are difficult to make from the XRD pattern alone. The presence of the various phases are identified by matching the d values with those given in the literature [228]. An attempt is made to identify the major crystallized phases from the nature of the magnetization data. The nearly constant magnetization curve between 500 and 1000 K indicates that the major crystallized phase is Co as it has a $T_c \simeq 1385$ K. This inference is in agreement with the work of Wang and Meng [227] on a similar system $Co_{58}Ni_{10}Fe_5B_{16}Si_{11}$ where, from calorimetric studies, it is concluded that at 797 K the major phase which crystallizes has the same structure as elemental Co with a different lattice parameter and the phases which crystallize at 938 K are Co, Co_2B, and Co_2Si. However, the fractions of Co_2B and Co_2Si, as compared to cubic Co, are very small because the T_c of these phases are 783 K and 857 K [229] respectively, and their presence in large quantity would have significantly altered the M(T) curve.

Figure 3.33(a) shows the M(T) curve of sample A2 (x = 5). With the addition of Cr, the T_c goes down to 260 K and the T_x increases to 700 K. The addition of Cr is known to increase T_x and decrease T_c in Fe-based metallic glasses [175]. The crystallization behavior is nearly identical to that of sample A1. The final phase is ferromagnetic as is evident from the large

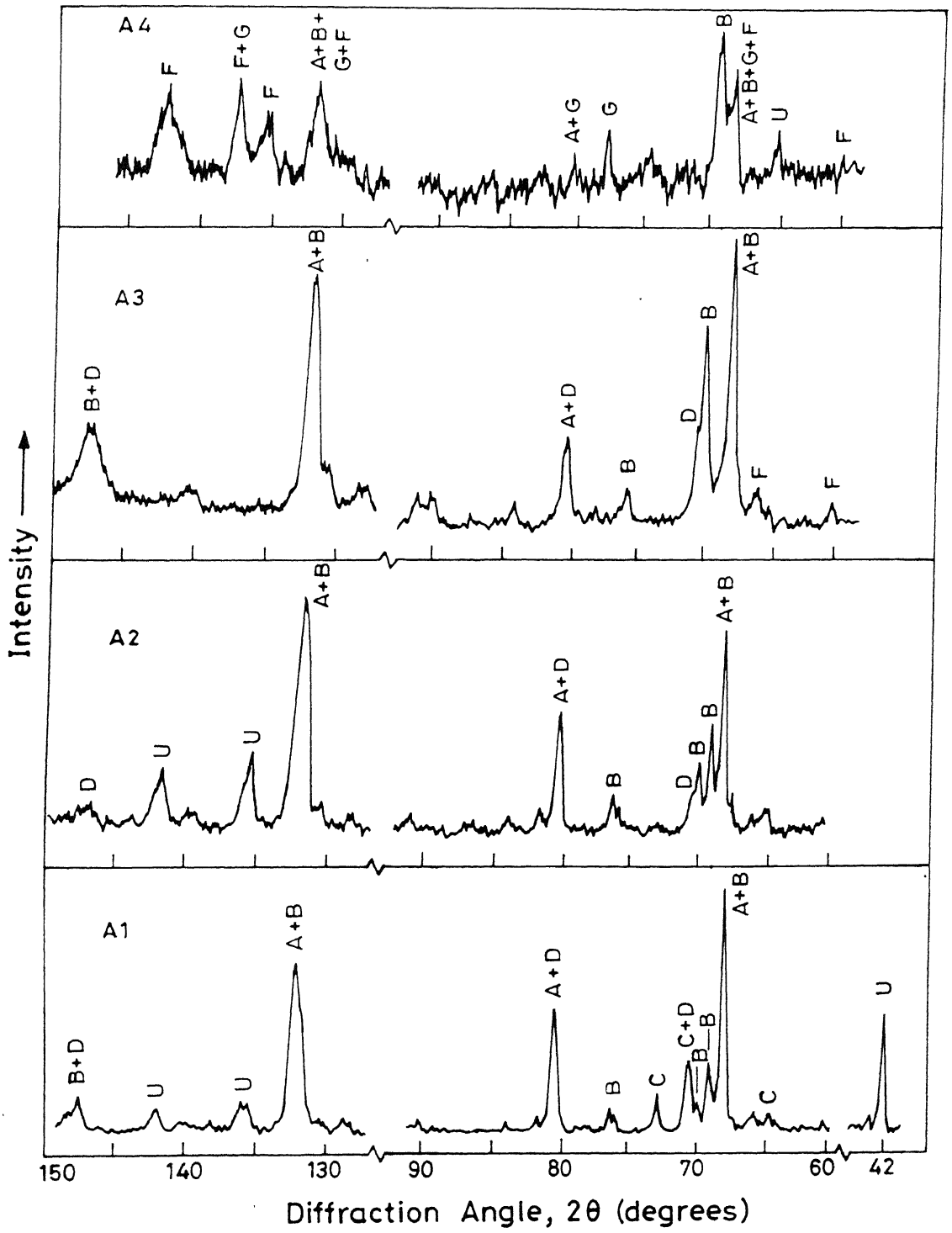

Fig. 3.32 The x-ray diffraction patternsof A1, A2, A3, and A4 ($Fe_5Co_{50}Ni_{17-x}Cr_xB_{16}Si_{12}$, x = Ø, 5, 1Ø, and 15). The lines correspond to the following identified phases. A: Cubic Co, B: Co_2Si, C: Ni_5Si_2, D: Co_2B, E: $Fe_{4.5}Ni_{18.5}B_6$, F: Cr_2B, G: Cr_3Co_5Si, U: Unidentified.

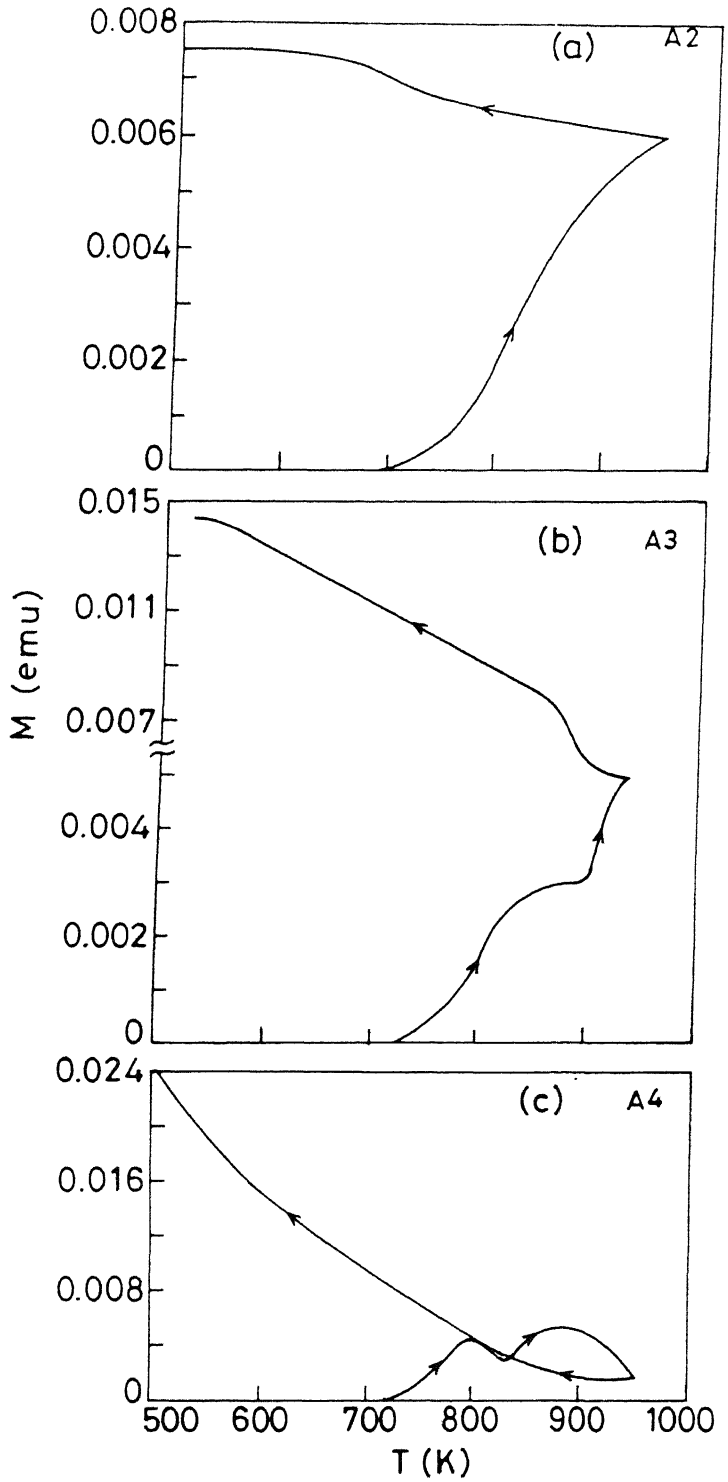

Fig. 3.33 The magnetization M as a function of temperature of samples A2, A3, and A4 ($Fe_5Co_{50}Ni_{17-x}Cr_xB_{16}Si_{12}$, x = 5, 10, and 15) in H = 30 Oe. The arrows indicate the heating and cooling cycles.

moment. The crystallized phases are identified as (from XRD) cubic Co, Co_2B, and Co_2Si. The differences between the XRD pattern of this sample and that of A1 are the absence of Ni_5Si_2 and the strong unidentified line at $2\theta = 42.1^\circ$ for A2. While heating, the change in curvature of the magnetization curve around 800 K can be identified with the growth of Co_2B phase, which becomes more distinct with further addition of Cr, as in A3 and A4. In the cooling cycle the rise at about 670 K, however, could not be associated with the T_C of the precipitated phases.

With further addition of Cr (x = 10), the magnetization behaves differently from those of A1 and A2 as shown in Fig. 3.33(b). The T_C of this sample is 222 K and the T_x is 712 K. Beyond this temperature the magnetization rises and around 800 K the change in the curvature is identified with the formation of Co_2B. Around 900 K, the magnetization becomes constant. This is because the increase due to the crystallization is compensated by the fall due to the T_C of Co_2Si. The final crystallized phase is ferromagnetic and is evident from the large value of the moment. In the cooling cycle, there is a sharp rise at 885 K. In this region M was constant during the heating cycle. The magnetization changes by a factor of about 3 between 930 and 500 K. The final phases are identified as cubic Co, Co_2Si, Co_2B, and Cr_2B. With the increase in Cr we find, from the character of the magnetization curves and the XRD patterns, that the final phase gets depleted in cubic Co and becomes richer in Co_2Si and Cr_2B. In the cooling cycle, the rise in magnetization by a factor of 3, is to be attributed to the significant amount of Co_2Si and Co_2B present in

the matrix and a small amount of paramagnetic Cr_2B.

The M(T) curve of sample A4 (x = 15) is shown in Fig. 3.33(c). This has a T_C of 180 K and a T_x of 712 K. Addition of Cr increases the T_x by about 7% from 660 K (A1) to the present value of 712 K. But we observe that in another sample where Ni is replaced, instead of Cr by Mn ($Fe_5Co_{50}Mn_{17}B_{16}Si_{12}$), the T_x goes to 900 K. The effect of Mn in increasing the T_x is much larger than that of Cr. In the heating cycle two distinct and reproducible humps could be observed in Fig. 3.33(c). These are around the same temperatures (800 and 900 K) as in A2 and A3 where they arise due to the T_C of Co_2B and Co_2Si phases. In this sample the discontinuities become more prominent and may also be associated with the formation of Co_2B and Co_2Si phases. But in contrast to samples A2 and A3, where there is an evidence of Co_2B phase in the XRD pattern, the corresponding lines are absent in the XRD pattern of this sample. In the cooling cycle, however, no such structure is observed near these temperatures. The final phase must be a paramagnetic one because the moment is only 0.0016 emu and on cooling to 500 K the moment rises by a factor of about 15. The curvature of the cooling-curve is also different from those of the earlier figures and M varies more like 1/T as in a paramagnet. The final crystalline phase consists of $Cr_3Co_5Si_2$ and Cr_2B, in addition to cubic Co and Co_2Si.

In conclusion, this study shows that the nature of the crystallized phase changes significantly with the replacement of Ni by Cr. The major phase which crystallizes in A1 is cubic Co. The nature of the magnetization curve shows that the other phases

present are small in quantity. A2 behaves in a similar manner as A1. In the cooling cycle of sample A3, distinct appearance of T_c of Co_2Si is observed. The magnetization grows continuously as the temperature is lowered. This nature of the magnetization curve is explained as due to the presence of both ferromagnetic and paramagnetic phases in nearly equal amounts. In A4, the final phase is paramagnetic and consists mostly of Cr_3Co_5Si and Co_2Si.

CHAPTER IV

CONCLUSIONS

(a) Electrical Resistivity

We have studied the electrical resistivity of a cobalt-rich ($Fe_5Co_{50}Ni_{17-x}Cr_xB_{16}Si_{12}$,x = Ø, 5, 1Ø, and 15 and $Fe_5Co_{50}Mn_{17}B_{16}Si_{12}$, designated as A1-A5) amorphous system which is ferromagnetic and at the same time shows resistivity minima at relatively high temperatures. We find that with substitution of Ni by Cr/Mn T_c decreases while T_{min} and ρ increase. The temperature dependence of the resistivity for sample A1 (x = Ø) above T_{min} and $T<T_c$, has been explained in the framework of the diffraction model, taking into account the magnetic state of the material. The magnetic term varies as T^2 and not as $T^{3/2}$ as predicted theoretically [36]. The magnetic T^2 term could be distinguished from the structural term only at high temperatures. This result is in agreement with that of Kaul et al. [16]. An evidence of the magnetic T^2 term is found at temperatures even beyond T_c, with the coefficient comparable to that at $T<T_c$.

In the region below T_{min} (x > Ø), we find that the conductivity varies as $\sqrt{T}$, T, and $\sqrt{T}$ at low, intermediate and high temperature regions respectively, arising from the electron-electron interaction and localization effects. We show here for the first time, all the three distinct regions predicted theoretically. The coefficient of the $\sqrt{T}$ term at low temperatures ((4ØØ - 1ØØØ) $(\Omega\ m)^{-1}\ K^{-1/2}$) is in agreement with the universal value of 6ØØ $(\Omega\ m)^{-1}\ K^{-1/2}$ obtained by Cochrane and Strom-Olsen

[56] for non-magnetic systems with strong electron-electron interaction. Also, the diffusion constant of electrons and the density of states at the Fermi level of these materials are calculated from the above coefficients.

The magnetic spin-disorder resistivity is found to be smaller than the electron-phonon term by a factor of about 1000. Hence we conclude that, on the basis of our analysis below T_{min} in terms of the localization theory, the resistance minima observed are of non-magnetic origin.

(b) Magnetoresistance (MR)

The MR of samples A1-A5 and B5 ($Fe_{7.8}Co_{31.2}Ni_{24}Mn_{15}(BSi)_{22}$) exhibit identical behavior in both the transverse and longitudinal directions. The ferromagnetic anisotropy of resistivity (FAR) is positive and is about an order of magnitude smaller compared to that of the Fe-B series. The magnitude of FAR decreases with the addition of Cr. A correlation between the magnetization and the FAR is obtained which shows that the FAR decreases with the average magnetic moment/atom. The high-field slope ($1/\rho\ d\rho/dH$), below T_c, of A1, A5, and B5 are negative. The negative slope in A1 is understood, in terms of the localized model, to be due to the result of reduction in the number of magnons as the field is raised. The magnon number also decreases with the decrease in the temperature and therefore in the ferromagnetic regime the magnitude of the slope is expected to decrease with the lowering of temperature which is in agreement with our observations.

The MR behavior of samples A5 and B5 indicates that the FAR

nearly becomes constant below 60 K and the magnitude of the slope ($1/\rho\ d\rho/dH$) increases below this temperature. This behavior is unlike that observed in normal ferromagnets where, as we lower the temperature, the FAR increases and the magnitude of the slope tends to zero. At $T < 60$ K, the low-field ac susceptibility also indicate a large drop from the demagnetization limited value. Both these results are interpreted as an indication for the onset of partial breakdown of long-range order. However, there exists long-range order even down to 11 K as the FAR gives a non-zero value. The time dependence of magnetization measured at 4.2 K and the low-field dc magnetization show the existence of spin-glass-like phase below 30 K. These two results together confirm that below 30 K the magnetic phase in these samples resembles the mixed phase as envisaged in the Gabay-Toulouse model where both the long-range order and the spin-glass phase coexist.

The Cr-containing samples (A2-A4) exhibit positive slope at all temperatures and their magnitudes are comparable with those of other amorphous materials. The plots of $\Delta\rho/\rho$ versus H are not strictly linear but and are best described by an equation of the form $\Delta\rho/\rho = a + bH + cH^2$. The ratio of $c/b \simeq 10^{-2}$. It is found that $\Delta\rho/\rho$ increases with the increase in Cr content. The plot of $\Delta\rho/\rho$ versus T/T_c, at a given field, show a pronounced peak at their respective T_c. This result is explained on the basis of the exchange-scattering model [88,89]. At temperatures away from T_c $\Delta\rho/\rho$ varies as M^2 as predicted by this theory. The peak in $\Delta\rho/\rho$ at $T \simeq T_c$ is associated with the increase in susceptibility at T_c. The positive slope of these has also been compared with the

predictions of the electron-electron interaction and the localization effects in the presence of the spin-orbit coupling. The expressions used in these theories are modified by replacing the applied field H by an effective field, $H_{eff} = H_{int} + H$, where H_{int} is the internal field of the ferromagnet. A reasonably good agreement is obtained between the theory and the experimental data when this correction is incorporated.

(c) Magnetization

The magnetic moment and the T_c decrease identically with the addition of Cr. The variation of the magnetic moment with the addition of Cr and Mn is discussed on the basis of various models. We find that the rate of change of magnetic moment with Cr concentration $\xi = d\mu/dx \approx -1$. The fall in μ, however, could not be described by the 'virtual bound state' model which gives $\bar{\mu} = \mu - (Z + 10)\, c\mu_B$, where Z is the valence difference between the solute and the host. We obtain Z = -9 whereas actually it is about -3.5. However, a calculation, based on the charge-transfer model, does reproduce the observed average $\bar{\mu}$ (0.5 μ_B/atom). This calculation further yields μ_{Cr} = -0.83, -0.59, and -0.45 for A2, A3, and A4, respectively. We also find that on replacing Ni with Mn, $\bar{\mu}$ increases. A similar calculation yields $\mu_{Mn} = 1.48\ \mu_B$. This result is thought to arise from strong ferromagnetic interaction between Mn and Co which overcomes the Mn-Mn nearest neighbor antiferromagnetic interaction. Spin-wave analysis is extended up to $0.5T_c$. Bloch's $T^{3/2}$ law adequately describes the temperature dependence of magnetization in Cr-containing samples. The

calculated spin-wave stiffness constant, D, decreases with the increase in Cr. In A5 and B5, additional terms of the form $T^{5/2}$ is found necessary. The results of the fit on including the Stoner single particle excitations are discussed. The value of D scales with T_c and the ratio $D/T_c \approx 0.27$ meV A^2/K. When the D(T) curve is extrapolated to $T_c = 0$, within experimental error, it is found to pass through the origin. This result is in agreement with the Heisenberg model.

(d) Critical exponents

The critical exponents β_{eff}, γ_{eff}, and δ for samples A2, A3, and A4 are obtained from ac and dc magnetization measurements. The influence of Cr on the critical exponents is studied. We find that the exponent δ remains essentially the same ($\simeq$4.45) in all the three compositions. The coefficients β_{eff} and γ_{eff}, in the case of sample A2 and A3, exhibit a relatively small concentration dependence and the observed values are closer o the theoretically estimated ones for homogeneous systems. However, with increase in Cr concentration, for sample A4, these values are larger and considerably different from those of A2 and A3. These results are ascribed to the formation of magnetic clusters with increasing addition of Cr in these alloys. The formation of magnetic clusters leads to the non-divergence of the correlation function at T_c and consequently a different set of exponent values describes the results.

(e) High-Temperature Magnetization

The crystallization study show that the nature of the crystallized phase changes significantly with the replacement of Ni by Cr. The crystallization temperature increases with the addition of Cr. The major phase which crystallizes in A1 is cubic Co. In sample A3, distinct appearance of Co_2Si is observed. In A4, the final phase is paramagnetic and consists mostly of Cr_3Co_5Si and Co_2Si.

Scope of Future Work

1. The resistivity measurements of the present samples could be done till only 8K. It was found that in the narrow temperature range 8-2Ø K the electron-electron interaction described the temperature dependence of resistivity satisfactorily. It would be of interest if this study could be extended to still lower temperatures.

2. The magnetoresistance measurements were limited to fields up to 17 kOe. This restricted the analysis of the magnetoresistance data of the Cr- and Mn-containing samples on the basis of localization and interaction theories. At high fields, $g\mu_B H \gg k_B T$, $\Delta\rho/\rho$ varies as $-\sqrt{H}$ due to localization effects. Since the present samples are ferromagnetic due to electron-magnon interaction, $\Delta\rho/\rho$ would also vary as -H. To detect the presence of localization term, i.e. to differentiate between -H and $-\sqrt{H}$ data is required over an extended region in field.

3. The Hall effect measurements are very few compared to those of other transport properties. This measurement in the present alloy system would supplement the present investigations of the zero-field resistivity and magnetoresistance.

4. The study of M(H) for the present alloys would be of interest. The law of approach to magnetic saturation is known to be affected by the structural defects of amorphous alloys.

5. Mixed phase characteristics would have been established more firmly if SQUID magnetometer was available.

REFERENCES

1. U. Mizutani, Prog. Mat. Science **28**, 97 (1983).

2. M.A. Howson and B.L. Gallagher, Phys. Rep. **170**, 265 (1988).

3. P.J. Cote and L.V. Meisel, in *Glassy Metals* I, *Topics in Applied Physics*, edited by H.-J. Güntherodt and H. Beck (Springer Verlag, Berlin, 1980), p. 141.

4. Béla Vasavari, Physica B **159**, 79 (1989).

5. J.H. Mooij, Phys. Stat. Solidi (a) **17**, 321 (1973).

6. N.F. Mott, Phil. Mag. **26**, 1249 (1972).

7. S.R. Nagel, Phys. Rev. B **16**, 1694 (1977).

8. C.C. Tseui, Phys. Rev. Lett. **57**, 1943 (1986).

9. W. Teoh, N. Teoh, and S. Arajs, in *Amorphous Magnetism II*, edited by R.A. Levy and R. Hasegawa (Plenum Press, New york, 1976), p. 327.

10. R. Hasegawa, Phys. Lett. **38** A, 5 (1972).

11. N.F. Mott, Phil. Mag. **29**, 1249 (1972).

12. J.M. Ziman, Phil. Mag. **6**, 1013 (1961).
T.E. Faber and J.M. Ziman, Phil. Mag. **11**, 153 (1965).

13. A.K. Sinha, Phys. Rev. B **1**, 4541 (1970).

14. R. Evans, D.A. Greewood, and P. Woyd, Phys. Lett. **35** A, 57 (1971).

15. P.J. Cote and L.V. Meisel, Phys. Rev. Lett. **39**, 102 (1977).

16. S.N. Kaul, W.H. Kettler, and M. Rosenberg, Phys. Rev. B **33**, 4987 (1986); ibid **35**, 7153 (1987).

17. A. Mogro-Campero and J.L. Walter, Phys. Rev. B **20**, 5030 (1979); A. Mogro-Campero, Phys. Lett. **76** A, 315 (1980).

18. N. Banerjee, R. Roy, and A.K. Majumdar, Phys. Rev. B **24**, 6801 (1980).

19. R. Roy, Ph.D. Thesis, IIT, Kanpur, 1985.

20. K. Frobose and J. Jäckle, J. Phys. F **7**, 2331 (1977).

21. T. Kasuya, Prog. Theo. Phys. **22**, 227 (1959).

22. I. Marnari, Prog. Theo. Phys. 22, 335 (1959).

23. D.A. Goodings, Phys. Rev. 132, 542 (1963).

24. G. Thummes, J. Kötzler, R. Ranganathan, and R. Krishnan, Z. Phys. B 69, 489 (1988).

25. G. Bergmann and P. Marquarat, Phys. Rev. B 17, 1355 (1978).

26. S.N. Kaul, W.H. Kettler, and M. Rosenberg, Phys. Rev. B 35, 7153 (1987).

27. A. Das and A.K. Majumdar, Phys. Rev. B 43, 6042 (1990).

28. E. Babic, Z. Marohnic, M. Ocko, A. Hamzic, K. Saulo, and B. Dirac, J. Magn. Magn. Mater. 15, 934 (1980).

29. W.H. Kettler and M. Rosenberg, Phys. Rev. B 39, 12142 (1989); J. Phys. F 17, L209 (1987).

30. W. Kettler, R. Werahardt, J. Appl. Phys. 53, 8248 (1982).

31. Rita Singhal and A.K. Majumdar, Phys. Rev. B 44, 2673 (1991).

32. L. Fernández-Barquin, J. Rodriguez-Fernández, and J.C. Gómez-sal, J. Magn. Magn. Mater. 83, 357 (1990).

33. M. Ishiki, Y. Fukuda, and K. Igaki, J. Phys. F 14, 3007 (1984).

34. S.N. Kaul, Solid State Commun. 15, 1821 (1974).

35. J.M. Baranaiaran, J.C. Gómez-sal, J. Rodriguez, R.J. López, Sánchez, and O.V. Nidsen, Phys. Stat. Solidi (a) 99, 243 (1987).

36. R. Richter, M. Wolf, and F. Goedsche, Phys. Stat. Solidi (b) 95, 473 (1979).

37. J. Kondo, in *Solid State Physics*, edited by F. Seitz, D. Turnbull, and H. Elveriech (Academic press, New York, 1969), 23, p. 183.

38. R.W. Cochrane, R. Harris, J.O. Storm-Olsen, and M.J. Juckermann, Phys. Rev. Lett. 35, 676 (1975).

39. M. Olivier, J.O. Storm-Olsen, and Z. Altuonian, Phys. Rev. B 35, 333 (1987).

40. David G. Onn, Y. Obi, and L.Q. Wang, J. Appl. Phys. 53, 7762 (1982).

41. K.V. Rao, H. Gudmundsson, H.U. Astrom, and H.S. Chen, J. Appl. Phys. 50, 1592 (1979).

42. R.W. Cochrane, J.O. Storm-Olson, Physica 86-88 B, 779 (1977).

43. S.J. Poon, J. Durand, and M. Yung, Solid State Commun. 22, 475 (1977).

44. T.E. Sharon and C.C. Tsuei, Phys. Rev. B 5, 1047 (1972).

45. C.L. Chien, Phys. Rev. B 19, 81 (1979).

46. E. Weisen, A. Handstein, J. Schneider, and K. Zaveta, Phys. Stat. Solidi A 66, 607 (1981).

47. G.S. Grest and S.R. Nagel, Phys. Rev. B 19, 3571 (1981).

48. N.F. Mott, Adv. Phys. 16, 49 (1961).

49. N.F. Mott and E.A. Davis, *Electronic Processes in Non-crystalline Materials* (Clarendon, Oxford, 1979).

50. P.W. Anderson, Phys. Rev. 102, 1008 (1958).

51. P.A. Lee and T.V. Ramakrishnan, Rev. Mod. Phys. 57, 287 (1985); Phys. Rev. B 26, 4009 (1982).

52. B.L. Altshuler and A.G. Aronov, in *Electron-Electron Interactions in Disordered Systems*, edited by A.L. Elfros and M. Pollak (Elsevier Science Publications, 1985).

53. G. Bergmann, Phys. Rep. 107, 1 (1984).

54. Ö. Rapp, S.M. Bhagat, and H. Gudmundson, Solid State Commun. 42, 741 (1982).

55. E. Babic, A. Hamzic, and M.Miljak, LT-17, *Proceedings of Int. Conf. on Low Temp. Physics* (North Holland, Amsterdam, 1984), p. 367.

56. R.W. Cochrane and J.O. Storm-Olsen, Phys. Rev. B 29, 1088.

57. J. Smit, Physica 16, 612 (1951).

58. A.K. Nigam and A.K. Majumdar, Physica B + C 95, 385 (1978).

59. J. Yamasaki, H. Fukunaga and K. Narita, J. Appl. Phys. 52, 2202 (1981).

60. I.A. Campbell, A. Fert and O. Jaoul, J. Phys. C 3, S95 (1970).

61. I.A. Campbell, J. Phys. F 4, 481 (1974); J.N.F. Dorleign, Philips Res. Rep. 31, 287 (1976).

62. Y.D. Yao, S. Arajs, and S.T. Lin, J. Appl. Phys. 53, 2258 (1982).

63. M. Naka, R.Kern, and U Gonser, J. Appl. Phys. 52, 1448 (1981).

64. Ratanamala Roy and A.K. Majumdar, Phys. Rev. B 31, 2033 (1985).

65. S.N. Kaul and M. Rosenberg, Phys. Rev. B 27, 5698 (1983).

66. M. Inagaki, M. Suzuki, Y. Iwama, and U. Mizutani, Jpn. J. Phys. 25, 1514 (1986).

67. O. Jaoul and I.A. Campbell, J. Phys. F 5, C69 (1975).

68. A.P. Malozemoff, Phys. Rev. B 34, 1853 (1986).

69. L. Berger, Physica 30, 1141 (1964).

70. L. Berger and S.A. Friedberg, Phys. Rev. B 105, 670 (1968).

71. A.P. Malozemoff, Phys. Rev. B 32, 6080 (1985).

72. Y.Z. Wang, F.M. Yang, Y.S. Wu, M.Y. Feng, and W.S Zhan, J. Magn. Magn. Mater. 31-34, 1473 (1983).

73. Girish Chandra, A.K. Nigam, V. Srinivas, Shiva Prasad, S N. Shiringi, R. Krishnan, and G. Rajaram, Mat. Sci. Engg. 99, 211 (1988).

74. Yang Fu-Mui, Wu Yong-Sheng, Wang Yi-Zhong, Zhai Xi-Chao, Lin Zhi-Yi, and Pan Shiao-Thur, in *High Field Magnetism* , edited by M. Date (North Holland, Amsterdam, 1983), p. 121.

75. J.R. Long, G.C. Hadjipanayis, and D.J. Sellmyer, J. Appl. Phys. 53, 8240 (1982).

76. P. Czarnecki and G. Fritzkoulskin, Phys. Stat. Solidi (a) 76, K93 (1983).

77. H. Gudmundsson, H.J. Hannesson, and H.U. Astrom, J. Appl. Phys. 57, 3523 (1985).

78. G. Rajaram, Shiv Prasad, Girish Chandra, A.K. Nigam, V. Srinivas, S.N. Shiringi, and R. Krishnan, J. Magn. Magn. Mater. 74, 113 (1988).

79. A. Das and A.K. Majumdar, J. Appl. Phys. 70, 6323 (1991).

80. S.K. Jen and S.M. Yang, J. Appl. Phys. 63, 4303 (1982).

81. R.R. Hake, M.G. Karkut, and S. Aryaineyad, Solid State Commun. 35, 709 (1980).

82. S.D. Genniro, Phys. Rev. B 26, 5957 (1982).

83. S. Ven Molsan, R.J. Gambino, and J.M.D. Coey, J. Appl. Phys. 52, 2193 (1980).

84. P. Czarnecki, B. Idzikowski, and A. Wrzeciono, Physica B **155**, 273 (1989).

85. P. Czarnecki, Phys. Stat. Solidi (b) **147**, 1547 (1988).

86. D. Dahlberg, K.V. Rao. and K. Fukamichi, J. Appl. Phys. **55**, 1948 (1984).

87. R. Crook, E.D. Dahlberg, and K.V. Rao, in *Rapidly Quenched Metals, Vol. I*, edited by S. Steel and H. Warliamont (North Holland, Amsterdam, 1985), p. 1239.

88. R. Asomoza, A. Fert, I.A. Campbell, and R. Mager, J. Phys. F **7**, 2327 (1977); ibid **9**, 349 (1979).

89. A.K. Bhatacharjee and B. Coqblin, J. Phys. F **8**, L221 (1978).

90. B.L. Altushuler, A.G. Aronov, A.I. Larkin, and D.E. Khaselniski, Sov. Phys.-JETP **54**, 511 (1981).

91. Arisato Kawabata, J. Phys. Soc. Japan **49**, 628 (1980).

92. J.B. Bieri, A. Fert, G. Crenzet, and A. Schuhl, J. Phys. F **16**, 2099 (1986).

93. M.A. Howson and D. Greig, J. Phys. F **13**, L155 (1983).

94. S.B. Roy, A.K. Nigam, Girish Chandra, and A.K. Majumdar, J. Phys. **18**, 2675 (1988).

95. M. Gabay and G. Toulouse, Phys. Rev. Lett. **47**, 201 (1981).

96. A. Hamzic and I.A. Campbell, J. Phys. Lett. **42**, L309 (1981).

97. S. Senoussi and Y. Oner, J. Magn. Magn. Mater. **40**, 12 (1983).

98. D. Raskin and C.H. Smith, in *Amorphous Metallic Alloys*, edited by F.E. Luborsky (Butterworths Monographs in Materials London, 1983), p. 381.

99. H.S. Chen, Rep. Prog. Phys. **43**, 353 (1980).

100. J. Durand, in *Glassy Metals II*, Topic in Applied Physics, edited by H. Beck and H.G. Guentherodt (Springer-Verlag, Berlin, 1983), p. 343.

101. K. Moorjani and J.M.D. Coey, *Magnetic Glasses* (Elseiver Science Publishers, Amsterdam, 1984), p. 1.

102. R.C. O'Handley, in *Amophous Metallic Alloys*, edited by F.E. Luborsky (Butterworths Monographs in Materials, London, 1983), p. 257.

103. T. Egami, Rep. Prog. Phys. **47**, 1601 (1984).

104. R. Hasegawa and R. Ray, J. Appl. Phys. **50**, 1586 (1979).

105. N. Kazama, M. Kameda, and T. Masumoto, AIP Conf. Proc. **34**, 307 (1976).

106. R. Hasegawa, R.C. O'Handley, and L.I. Mendelshon , AIP Conf. Proc. **34**, 298 (1976).

107. P. Mangin, M. Piéench, G. Marchal, and C. Janot, J. Phys. F **8**, 2085 (1978).

108. W. Felsch, Z. Phys. **219**, 280 (1969).

109. H.S. Chen, R.C. Sherwood, and E.M. Gyorgy, IEEE Trans., MAG-**13**, 1538 (1977).

110. M. Mitera, M. Naka, T. Masumoto, M. Kazama, and K. Watanabe, Phys. Status Solidi (a) **49**, K163 (1978).

111. T. Mizoguchi, T. Yamachin, H. Miyajima, in *Amorphous Magnetism* I, edited by H.O. Hooper and M. de. Graff (Plenum Press, New York, 1973), p. 325.

112. K. Yamachi and T. Mizoguchi, J. Phys. Soc. Japan, **39**, 541 (1975).

113. N.F. Mott, Proc. Phys. Soc. London **47**, 571 (1935); J.C. Slater, Phys. Rev. **49**, 537 (1936); L. Pauling, Phys. Rev. **54**, 899 (1938).

114. A. Malozemoff, A.R. Williams, and V.L. Moruzzi, Phys. Rev. B **29**, 1620 (1984) and the references cited therein.

115. R.C. O'Handley, Solid State Commun. **38**, 703 (1981).

116. J. Friedel, Nuovo Cimento, Suppl. to vol. III, 287 (1958).

117. A.R. Williams, V.L. Moruzzi, A.P. Malozemoff and K. Terakura, IEEE Trans. Magn. MAG-**19**, 1983 (1983).

118. F. Keffer, in *Encyclopedia of Physics Vol. XVIII*, edited by H.P. Wign (Springer, Berlin, 1966), part 2, p. 1.

119. F. Bloch, Z. Phys. **61**, 206 (1930).

120. C. Herring and C. Kittel, Phys. Rev. **81**, 869 (1951).

121. J.D. Axe, L. Passel, and C.C. Tseui, AIP Conf. Proc. **24**, 119 (1975).

122. J.D. Axe, G. Shirane, T. Mizoguchi, and K. Yamaguchi, Phys. Rev. **15**, 2763 (1972).

123. H.A. Mook, N. Wakabayasmi, and D. Paul, Phys. Rev. Lett. **34**, 1Ø29 (1975).

124. J.J. Rhyne, R.W. Lynn, F.E. Luborsky, and J.L. Walter, J. Appl. Phys. **50**, 1583 (1979).

125. R.J. Birgenean, J.A. Tarvin, G. Shirane, E.M. Gyorgy, R.C. Sherwood, H.S. Chen, and C.L. Chien, Phys. Rev. B **18**, 2192 (1978).

126. Y. Ishikawa, K. Yamada, K. Tazima, and K. Fukamichi, J. Phys. Soc. Japan **50**, 1958 (1981).

127. A.K. Majumdar, V. Oestreich, and D. Weschenfelder, Phys. Rev. B **27**, 5618 (1983).

128. A.W. Simpson, quoted in C.L. Chien and R. Hasegawa, Phys. Rev. B **16**, 215 (1977).

129. C.L. Chien and R. Hasegawa, Phys. Rev. B **16**, 215 (1977).

13Ø. S.N. Kaul, Phys. Rev. B **24**, 655Ø (1981).

131. S.N. Kaul, Phys. Rev. B **27**, 5761 (1981).

132. B.E. Argyle, S.H. Charap, and E.W. Pugh, Phys. Rev. **132**, 2Ø51 (1963).

133. S.M. Bhagat, M.L. Spano and K.V. Rao, J. Appl. Phys. **50**, 2115 (1977).

134. O. Beckman, E. Figueroa, K. Gramm, L. Ludgreen, K.V. Rao, and H.S. Chen, Physica Scr. **25**, 726 (1982).

135. R. Puzanik and W. Dmowski, J. Phys. F **17**, 1437 (1987).

136. L. Dobrzyuski, K. Szymanski, J. Waliszewski, A. Malinowski, A. Wisniewski, M. Baran, and J. Latuszkiewicz, J. Magn. Magn. Mater. **88**, 23 (199Ø).

137. J. Mathon and E.P. Wohlfarth, Proc. Royal Soc. A **302**, 4Ø9 (1968).

138. E.D. Thomson, E.P. Wohlfarth, and A.C. Bryan, Proc. Phys. Soc. **83**, 59 (1964).

139. E. Babic, Z. Marohnic, and E.P. Wohlfarth, Phys. Lett. **95** A, 335 (1983).

14Ø. R.C. O´Handley and M.O. Sullivan, J. Appl. Phys. **52**, 1841 (1981).

141. Y. Obi, H. Marita, and H. Fujimoni, IEEE Trans. Magn. **MAG-16**, 1132 (198Ø).

142. G.L. Whittle, A.M. Stewart, and A.B. Kaiser, Phys. Stat. Solidi (a) **97**, 199 (1986).

143. A.T. Aldred, Phys. Rev. B **14**, 219 (1976).

144. A.K. Gangopadhyay, R.K. Ray, and A.K. Majumdar, Phys. Rev. B **30**, 6693 (1984).

145. S.N. Piramanayagam, S.N. Shringi, Shiva Prasad, A.K. Nigam, Girish Chandra, R. Krishnan, and V.R.V. Ramanan, Solid State Commun. **76**, 93 (199Ø).

146. Y. Yeshurun, K.V. Rao, M.B. Salamon, and H.S. Chen, Solid State Commun. **38**, 371 (1981).

147. J.A. Geohegan and S.M. Bhagat, J. Magn. Magn. Mater. **25**, 17 (1981).

148. Y. Yeshurun, K.V. Rao, M.B. Salamon, and H.S. Chen, Phys. Rev. B **24**, 1536 (1981).

149. T. Miyazaki, I. Okamoto, Y. Ando, and M. Takahshi, Phys. Rev. B **18**, 16Ø1 (1988).

15Ø. S.H. Barke, R. Cywiaski, J.R. Davis, and B.D. Rainford, J. Phys. **13**, 441 (1983).

151. B.R. Coles, B.V.B. Sarkissian, and R.H. Taylor, Phil. Mag. B **37**, 489 (1978).

152. R.G. Ailken, T.D. Chemang, J.S. Kouvel, and H. Hurdequint, J. Magn. Magn. Mater. **30**, L1 (1982).

153. A.K. Majumadar and P.v. Blanckenhagen, Phys. Rev. B **29**, 4Ø79 (1984).

154. L.M. Kistler and S.M. Bhagat, J. Phys. C **15**, L929 (1982).

155. V. Manves, R.A. Brand, W. Kenne, and R. Marx, Solid State Commun. **48**, 811 (1983).

156. H. Maletta, G. Aeppli, and S.M. Shapino, J. Magn. Magn. Mater. **31-34**, 1367 (1983).

157. K. Westerholt and H. Bach, J. Phys. F **12**, 1227 (1982).

158. A. Burton, C. Chanssi, J. Odin, R. Rammal, J. Souletive, J.L. Tholence, R. Tournier, F. Holtzberg, and S. Ven Moluvar, J. Appl. Phys. **52**, 1763 (1981).

159. R.A. Cowley, G. Shirane, R. J. Birgenen, E.C. Sevensson, and H.J. Guggenheim, Phys. Rev. B **22**, 4412 (198Ø).

16Ø. M. Alba, J. Hamman, and M. Negeus, J. Phys. C **15**, 5441 (1982); J.L. Dormann, A. Safi, V. Cagan, and M. Negeus, Phys.

Stat. Solidi (b) **31**, 573 (1985).

161. S.F. Edwards and P.W. Anderson., J. Phys. F **5**, 965 (1975).

162. D. Sherrington and S. Kirkpatrick, Phys. Rev. Lett. **35**, 1792 (1975).

163. S.N. Kaul, J. Magn. Magn. Mater. **53**, 5 (1985).

164. M.E. Fisher, Phys. Rev. **176**, 257 (1968).

165. A.B. Harris, J. Phys. C **7**, 1671 (1974).

166. G. Grinstein and A. Luther, Phys. Rev. B **13**, 1329 (1976).

167. A. Weinrib and B.I. Halperin, Phys. Rev. B **27**, 413 (1983).

168. G. Sobotta, J. Magn. Magn. Mater. **28**, 1 (1982); Solid State Commun. **43**, 875 (1982).

169. S.N. Kaul, Phys. Rev. B **38**, 9178 (1988).

170. J.C. Le Guillon and J. Zinn-Justin, Phys. Rev. Lett. **39**, 95 (1977).

171. M. Fähnle, G. Herzer, H. Krönmuller, R. Meyer, M. Saile, and T. Egami, J. Magn. Magn. Mater. **38**, 240 (1983).

172. M. Olivier, J.O. Strom-Olsen, Z. Altounian, and G. Williams, J. Appl. Phys. **53**, 769 (1982); M.A. Manheimer, S. M. Bhagat, and H.S. Chen, J. Magn. Magn. Mater. **38**, 147 (1983); P. Hargraves and R.A. Dunlap, J. Magn. Magn. Mater. **75**, 378 (1988) ; A.T. Aldred and J.S. Kouvel, Physica B **86-88**, 329 (1977); U. Güntzel and K. Westerholt, Phys. Rev. B **41**, 740 (1990).

173. I. Ikeda and Y. Ishikawa, J. Phys. Soc. Japan **49**, 950 (1980).

174. I.B. Kekalo, A.N. Zhdanov, and V.Yu. Tsvetokov, Phys. Met. Metallography **59**, 76 (1985).

175. Hans Jorgen Vind Nielsen, J. Magn. Magn. Mater. **12**, 187 (1979).

176. C. Hargitai, M. Hossó, I. Nagy, T. Tarnóczi, and C. Kopasz, J. Magn. Magn. Mater. **41**, 97 (1984).

177. G. Busch and H.-J. Guntherodt, in *Solid State Physics*, edited by H. Ehrenreich, F. Seitz, and D. Turnbull (Academic, New York, 1974), **29**, p. 235.

178. J.M. Ziman, *Principles of Theory of Solids* (Cambridge University Press, Cambridge, 1972), p. 64.

179. J.S. Dugdale, Contemp. Phys. **28**, 547 (1987).

180. G. Bergmann, Phys. Rev. B **28**, 2914 (1983).

181. E. Abrahams, P.W. Anderson, D.C. Licciardello, and T.V. Ramakrishnan, Phys. Rev. Lett. **42**, 673 (1979).

182. M.A. Howson, J. Phys. F **14**, L25 (1984).

183. B.L. Altshuler and A.G. Aronov, Solid State Commun. **30**, 115 (1979).

184. F.J. Dyson. Phys. Rev. **102**, 1217 (1956); **102**, 1230 (1956).

185. J.A. Copeland and H.A. Gersch, Phys. Rev. **143**, 236 (1966).

186. T. Izuyama and R. Kubo, J. Appl. Phys. **35**, 1074 (1964).

187. A. Banerjee, Ph.D. Thesis, IIT Kanpur (1990).

188. A. Banerjee, A.K. Rastogi, Manoj Kumar, A. Das, A. Mitera, and A.K. Majumdar, J. Phys. E **22**, 230 (1989).

189. M.A. Howson and D. Greig, Phys. Rev. B **30**, 4805 (1984).

190. M.A. Howson and D. Greig, J. Phys. F **16**, 989 (1986).

191. L.V. Meisel and P.J. Cote, Phys. Rev. B **16**, 2978 (1977).

192. J.M. Gonzalez, M. Vazquez, and J.L. Vincent, J. Magn. Magn. Mater. **54-57**, 261 (1986).

193. A. Veider, J.A. Badurek, R. Grossinger, and H. Kronmuller, J. Magn. Magn. Mater. **60**, 182 (1986).

194. R. Kern, M. Naka, U. Gonser, H. Fujimori, and I. Okamoto, J. Magn. Magn. Mater. **31-34**, 1471 (1983).

195. O. Jaoul, I.A. Campbell, and A. Fert, J. Magn. Magn. Mater. **5**, 23 (1977).

196. G. Bohnke, N. Croitoriu, M. Rosenberg, and M. Sostarich, IEEE Trans. Magn. **14**, 955 (1978).

197. The value $1/\rho\ d\rho/dH \leq 2.4 \times 10^{-5}\ T^{-1}$ calculated by Olivier et al. [17] is erroneous. The value quoted here has been shown by W. Maj, Phys. Rev. B **44**, 2387 (1991).

198. B. Sas, J. M. Broto, N. de Courtenay, and A. Fert, Solid State Commun. **66**, 777 (1988).

199. M. T. Beal-Monod and R.A. Weiner, Phys. Rev. **171**, 170 (1968).

200. D.V. Baxter, R. Riechter, M.L. Trudean, R. W. Cochrane, and J.O. Strom-Olsen, J. Phys. (France) **50**, 1673 (1989).

201. H. Ma, Z. Wang, H.P. Kunkel, J. Appl. Phys. **67**, 5964 (1990).

202. R. Krishnan, M. Daneygier, and M. Tarhouni, J. Appl. Phys. **53**, 7768 (1982).

203. E.M.T. Velu, P. Rongier, and R. Krishnan, J. Magn. Magn. Mater. **54-57**, 265 (1986).

204. J.S. Kouvel, J. Phys. Chem. Solids **16**, 107 (1960).

205. L. Dobrzynski, K. Szymanski, T. Waliszewski, A. Malinowski, M. Baran, and J. Latuszkiwicz, J. Magn. Magn. Mater. **99**, 222 (1991).

206. H. Hasegawa and J. Kanamori, J. Phys. Soc. Japan **33**, 1607 (1972).

207. F.E. Lubrosky, in *Ferromagnetic Materials*, edited by E.P. Wohlfarth (North-Holland, Amsterdam, 1980), **1**, p. 451.

208. R. Krishnan, K. LeDang, P. Veillet, and V.R.V. Ramanan, J. Appl. Phys. **57**, 1394 (1985).

209. R. Krishnan, K. LeDang, V.R.V. Ramanan, and P. Veillet, J. Magn. Magn. Mater. **54-57**, 263 (1986).

210. R. Puznaik, H. Szymczak, and E. Fawcett, IEEE Trans. Magn. **MAG-24**, 1767 (1988).

211. U. Krey, Z. Physik B **31**, 247 (1978).

212. M. Maszkiewicz, J. Appl. Phys. **53**, 7765 (1982).

213. F.E. Lubrosky, J.L. Walter, H.H. Liebermann, and E.P. Wohlfarth, J. MAgn. Magn. Mater. **15-18**, 1351 (1980).

214. B.H. Verbeck and J.A. Mydosh, J. Phys. F **8**, L109 (1978).

215. G.J. Nieuwenhuys, B.H. Verbeck, and J.A. Mydosh, J. Appl. Phys. **50**, 1685 (1979).

216. E.W. Stanley, *Introduction to Phase Transitions and Critical Phenomena* (Clarendon, Oxford, 1971).

217. J.S. Kouvel and M.E. Fisher, Phys. Rev. **136**, A1626 (1964).

218. See sample No. 2 of Ref. 1. Other reports (see e.g., P. Gaunt, S.C. Ho, G. Williams, and R.W. Cochrane, Phys. Rev. B **23**, 251 (1981)) of measurements on this sample give T_c = 249 K, but essentially the same $\gamma(T_c)$.

219. A. Arrott and J.E. Noakes, Phys. Rev. Lett. **19**, 786 (1967).

220. R. Hasegawa, J. Appl. Phys. **41**, 4096 (1970).

221. S.N. Kaul, Phys. Rev. B **23**, 1205 (1981).

222. K. Yamada, Y. Ishikawa, Y. Endoh, and T. Masumoto, Solid State Commun. **16**, 1335 (1975).

223. G. Aeppli, S.M. Shapiro, R.J. Birgeneau, and H.S. Chen, Phys. Rev. B **28**, 5161 (1983).

224. M. Seeger and H. Krönmuller, J. Magn. Magn. Mater. **28**, 393 (1989).

225. H.-O. Houer and D. Wagner, Phys. Rev. B **40**, 2502 (1989).

226. Ratanamala Roy and A.K. Majumdar, J. Magn. Magn. Mater. **25**, 83 (1981).

227. Y. Wang and C. Meng, J. Non-Cryst. Solids **54**, (1983) 187.

228. Powder Diffraction File - Inorganic (International Center for Diffraction Data, USA), Sets **4**, **15-19**, and **25**.

229. Max Hansen, *Constitution of Binary Alloys* (McGraw Hill, New York, 1958), p. 503.